THE UNIVERSITY OF QUEENSLAND

AUSTRALIA

Imaging basal forebrain dysfunction in Alzheimer's disease

Georg Martin Johannes Kerbler

(MSc)

A thesis submitted for the degree of Doctor of Philosophy at

The University of Queensland in 2014

Queensland Brain Institute

Abstract

The basal forebrain, a grey matter region located in the medial and ventral aspects of the mammalian brain, consists of highly heterogeneous populations of cells including, but not limited to: cholinergic, GABAergic, glutamatergic and calbindin-positive neurons. The function of the basal forebrain has been linked to mediating reward-related behaviours, attention and, more recently, learning and memory in humans. In healthy aging, the basal forebrain undergoes slow, progressive degeneration over time. However in conditions such as Down-syndrome, Alzheimer's disease and Parkinson's disease this degenerative process is highly increased; why the basal forebrain is particularly vulnerable to neurodegeneration is unclear.

Here we show that degeneration of the basal forebrain in Alzheimer's disease occurs very early, even in patients diagnosed with a prodromal stage of the disease, called amnestic mild cognitive impairment. By imaging and measuring the basal forebrain volume non-invasively through magnetic resonance imaging (MRI) in humans, the state of an individual's basal forebrain can be assessed and might be predictive of future disease progression.

We found that subjects with a basal forebrain volume below a certain cut-off value were at a 7 times higher risk of having a worse diagnosis within ~18 months. In addition, basal forebrain degeneration correlates with the two major hallmarks of Alzheimer's disease pathology: amyloid beta and tau protein burden in the brain in living subjects. During the development of Alzheimer's disease, degeneration of the basal forebrain follows a distinct posterior-to-anterior pattern, and the volume of posterior basal forebrain nuclei is correlated to amyloid beta level in asymptomatic subjects, whereas the volume of anterior basal forebrain nuclei is correlated to amyloid beta level in subjects suffering from amnestic mild cognitive impairment and Alzheimer's disease.

Furthermore, a strong correlation exists between basal forebrain atrophy, particularly of the posterior volume, and tau burden in brain regions that are typically affected by tau pathology and which are also anatomically connected to the posterior basal forebrain. In addition, we found that a weaker correlation exists between basal forebrain atrophy and amyloid burden, as compared to the correlation between basal forebrain atrophy and tau burden. Also, tau and basal forebrain atrophy were associated with cognitive measures in Alzheimer's disease subjects and controls, whereas amyloid burden was not. Our findings therefore support the idea that Aβ accumulation is a necessary but insufficient cause for

progression to AD, with secondary, downstream or parallel events being required to trigger tau aggregation and BF degeneration, which then directly underpin cognitive decline. Based on these findings we suggest that an evaluation of basal forebrain atrophy should be included into routine MRI diagnostic procedures aimed at assessing the likelihood of development of dementia in elderly subjects.

We further show, through selective ablation of a single population of cells (cholinergic neurons) of the basal forebrain in mice, that such subtle cell death in this region – similar to very early basal forebrain degeneration - does not affect the basal forebrain volume itself, but that MRI methods can still detect alterations in the diffusion of water molecules. This technique of diffusion MRI might offer an even more sensitive diagnostic method for Alzheimer's disease risk.

In order to conduct studies investigating degeneration of basal forebrain neurons in mice reliably and in greater detail in the future (through a combination of histological and MRI analysis), we are in the process of developing an average volume of the cholinergic nuclei of the basal forebrain from histological segmentation of three mice. The volumes are registered to MR images of the same mice and can therefore be used as a guide and reference by other researchers aiming to study basal forebrain pathology using mouse models recapitulating diseases such as Alzheimer's disease and Parkinson's disease.

The work of this thesis will help to better understand the development of Alzheimer's disease, further establish the role of basal forebrain dysfunction as a hallmark of Alzheimer's disease pathology, and provide another important step towards an early diagnosis of this condition.

Declaration by author

This thesis is composed of my original work, and contains no material previously published or written by another person except where due reference has been made in the text. I have clearly stated the contribution by others to jointly authored works that I have included in my thesis.

I have clearly stated the contribution of others to my thesis as a whole, including statistical assistance, survey design, data analysis, significant technical procedures, professional editorial advice, and any other original research work used or reported in my thesis. The content of my thesis is the result of work I have carried out since the commencement of my research higher degree candidature and does not include a substantial part of work that has been submitted to qualify for the award of any other degree or diploma in any university or other tertiary institution. I have clearly stated which parts of my thesis, if any, have been submitted to qualify for another award.

I acknowledge that an electronic copy of my thesis must be lodged with the University Library and, subject to the General Award Rules of The University of Queensland, immediately made available for research and study in accordance with the *Copyright Act 1968*.

I acknowledge that copyright of all material contained in my thesis resides with the copyright holder(s) of that material. Where appropriate I have obtained copyright permission from the copyright holder to reproduce material in this thesis.

Publications during candidature

Papers

Published

GM Kerbler, AS Hamlin, K Pannek, ND Kurniawan, MD Keller, SE Rose, EJ Coulson. (2013) Diffusion-weighted magnetic resonance imaging detection of basal forebrain cholinergic degeneration in a mouse model. *Neuroimage*, 66C: 133-141

GM Kerbler, J Fripp, C Rowe, VL Villemagne, O Salvado, S Rose, EJ Coulson. (2014) Basal forebrain atrophy correlates with amyloid β burden in Alzheimer's disease. *Neuroimage Clinical*, DOI: http://dx.doi.org/10.1016/j.nicl.2014.11.015

Submitted

GM Kerbler, J Fripp, S Rose, M Fodero-Tavoletti, S Furumoto, C Rowe, N Okamura, EJ Coulson and VL Villemagne. (2014) Cortical tau pathology is linked to basal forebrain degeneration in Alzheimer's disease. *In preparation for submission* to *Nature Neuroscience*

GM Kerbler, Z Nedelska, J Fripp, J Laczo, M Vyhnalek, J Lisy, AS Hamlin, S Rose, J Hort and EJ Coulson. (2014) The basal forebrain contributes to cue-based spatial navigation performance in Alzheimer's disease. *Under submission* in *Brain Structure and Function*

Each of the above papers is incorporated as an individual chapter in this thesis.

Conference abstracts (* denotes presenter)

GM Kerbler*, J Fripp, C Rowe, VL Villemagne, O Salvado, S Rose, EJ Coulson. (2013) Basal forebrain atrophy is associated with Aβ burden in Alzheimer's disease. Oral presentation at Society for Neuroscience annual meeting, November 9-13 2013, San Diego, USA

GM Kerbler, J Fripp, C Rowe, VL Villemagne, O Salvado, EJ Coulson & S Rose*. (2013) Longitudinal evaluation of basal forebrain atrophy and its association to Aβ burden and hippocampal volume in Alzheimer's disease. Oral presentation at Alzheimer's Association International Conference, July 13-18 2013, Boston, USA

GM Kerbler, AS Hamlin, K Pannek, ND Kurniawan, MD Keller, SE Rose, EJ Coulson*. (2011) Diffusion-weighted magnetic resonance imaging detection of basal forebrain cholinergic degeneration in a mouse model of Alzheimer's disease. Poster presentation at Gordon Conference: Neurotrophic Factors, June 5-10 2011, Newport, USA

GM Kerbler*, AS Hamlin, ND Kurniawan, MD Keller, IM Brereton, EJ Coulson. (2011) Imaging the loss of cholinergic basal forebrain neurons in a mouse model of Alzheimer's disease by tractography. Poster presentation at The International Conference on Alzheimer's and Parkinson's Diseases, March 9-14 2011, Barcelona, Spain

GM Kerbler*, AS Hamlin, ND Kurniawan, MD Keller, IM Brereton, EJ Coulson. (2011) Imaging the loss of cholinergic basal forebrain neurons in a mouse model of Alzheimer's disease by tractography. Poster presentation at the Brain Symposium 2010, Brisbane, Australia

Publications included in this thesis

Chapter 2:

GM Kerbler, J Fripp, C Rowe, VL Villemagne, O Salvado, S Rose, EJ Coulson. (2014) Basal forebrain atrophy correlates with amyloid β burden in Alzheimer's disease. *Neuroimage Clinical*, DOI: http://dx.doi.org/10.1016/j.nicl.2014.11.015

Contributor	Statement of contribution
GM Kerbler (Candidate)	Conceived study (20%) Designed experiments (70%) Performed experiments (70%) Wrote paper (70%)
J Fripp	Conceived study (5%) Designed experiments (20%) Performed experiments (15%) Wrote paper (5%)
CC Rowe	Wrote paper (1%)
VL Villemagne	Performed experiments (15%) Wrote paper (4%)
O Salvado	Wrote paper (1%)
S Rose	Conceived study (15%) Designed experiments (5%) Wrote paper (4%)
EJ Coulson	Conceived study (60%) Designed experiments (5%) Wrote paper (15%)

Chapter 3:

GM Kerbler, J Fripp, S Rose, M Fodero-Tavoletti, S Furumoto, C Rowe, N Okamura, EJ Coulson and VL Villemagne. (2014) Cortical tau pathology is linked to basal forebrain degeneration in Alzheimer's disease. *In preparation for submission* to *Nature Neuroscience*

Contributor	Statement of contribution
GM Kerbler (Candidate)	Conceived study (70%) Designed experiments (55%)

	Performed experiments (50%) Wrote paper (70%)
J Fripp	Performed experiments (5%)
S Rose	Conceived study (10%)
M Fodero-Tavoletti	Designed experiments (10%) Performed experiments (15%)
S Furumoto	Designed experiments (10%) Performed experiments (10%)
CC Rowe	Wrote paper (1%)
N Okamura	Designed experiments (10%) Performed experiments (10%)
EJ Coulson	Wrote paper (14%)
VL Villemagne	Conceived study (20%) Designed experiments (15%) Performed experiments (10%) Wrote paper (15%)

Chapter 4:

GM Kerbler, Z Nedelska, J Fripp, J Laczo, M Vyhnalek, J Lisy, AS Hamlin, S Rose, J Hort and EJ Coulson. (2014) The basal forebrain contributes to cue-based spatial navigation performance in Alzheimer's disease. *Under submission* in *Brain Structure and Function*

Contributor	Statement of contribution
GM Kerbler (Candidate)	Conceived study (20%) Designed experiments (50%) Performed experiments (55%) Wrote paper (79%)
Z Nedelska	Designed experiments (10%) Performed experiments (10%) Wrote paper (10%)
J Fripp	Performed experiments (10%)
J Laczo	Conceived study (5%)
Vhynalek M	Designed experiments (20%) Performed experiments (15%)
J Lisy	Designed experiments (10%)

	Performed experiments (10%)
AS Hamlin	Conceived study (5%)
S Rose	Wrote paper (1%)
J Hort	Conceived study (5%) Designed experiments (10%)
EJ Coulson	Conceived study (65%) Wrote paper (10%)

Chapter 5:

GM Kerbler, AS Hamlin, K Pannek, ND Kurniawan, MD Keller, SE Rose, EJ Coulson. (2013) Diffusion-weighted magnetic resonance imaging detection of basal forebrain cholinergic degeneration in a mouse model. *Neuroimage*, 66C: 133-141

Contributor	Statement of contribution
GM Kerbler (Candidate)	Conceived study (30%) Designed experiments (65%) Performed experiments (75%) Wrote paper (69%)
AS Hamlin	Conceived study (10%) Designed experiments (10%) Performed experiments (20%) Wrote paper (2%)
K Pannek	Designed experiments (10%) Wrote paper (10%)
ND Kurniawan	Designed experiments (5%)
MD Keller	Performed experiments (5%)
SE Rose	Conceived study (10%) Wrote paper (5%)
EJ Coulson	Conceived study (50%) Designed experiments (10%) Wrote paper (14%)

Contributions by others

1. Method of processing human MRI data supplied by J Fripp.
2. PET imaging data supplied by VL Villemagne, M Fodero-Tavoletti, N Okamura, S Furumoto.
3. Subject data obtained from the Australian Imaging Biomarkers and Lifestyle Flagship Study of Aging (http://www.aibl.csiro.au/) and the Alzheimer's Disease Neuroimaging Initiative (ADNI) study (adni.loni.usc.edu)
4. MRI and spatial navigation data supplied by Z Nedelska, J Laczo, M Vyhnalek, J Lisy, J Hort.
5. Animal surgeries performed by AS Hamlin.

Statement of parts of the thesis submitted to qualify for the award of another degree

None

Acknowledgements

This research was supported by a Smart State National and International Research Alliances Program (NIRAP) grant and an ANZ Trustees PhD Scholarship for Medical Research.

First I want to thank my PhD supervisor Dr. Elizabeth Coulson for giving me freedom in my work, stimulating discussions, being positive and encouraging me and guiding me through this long journey.
Thank you to my co-supervisor Dr. Stephen Rose, for enabling me to branch out into the world of clinical and translational research, for stimulating and honest discussions and for your jokes that broke up the late-night tractography sessions.

Thank you to all the great researchers and people I had the pleasure to do this project with, especially Jurgen Fripp, Kerstin Pannek, Victor Villemagne, Adam Hamlin, Zuzana Nedelska and Steven Yang.

I would like to thank all the past and present lab members of the Coulson lab for creating such a fun working atmosphere in the lab, and for uncountable coffee breaks: Toni Turnbull, Zoran Boskovic, Dr. Sune Skeldal, Aanchal Sharma, Dr. Alex Sykes, Dr. Linda May, Sophie Hill, Dr. Fabienne Alonso, Nick Palstra, Bree Rumballe, Lulu Camara, Dr. Dusan Matusica and Dr. Lei Qian.

I would also like to thank Rowan Tweedale for feedback with papers and this thesis and Daniel Matthews and Luke Hammond for microscopy support.

Thank you to my family, for always being there for me and giving me unconditional support and love.

To all my friends, thank you for your support, laughter and, just being wonderful.

Finally, thank you Lily, for giving me inspiration and motivation every day to be the best person I possibly can be. You are truly amazing and I look up to you, even though you're smaller than me (so far).

Keywords

basal forebrain, Alzheimer's disease, neurodegeneration, imaging, amyloid beta, tau, MRI, PET, neuron network, biomarker

Australian and New Zealand Standard Research Classifications (ANZSRC)

ANZSRC code: 110902, Cellular Nervous System, 100%

Fields of Research (FoR) Classification

FoR code: 1109, Neurosciences, 100%

Table of Contents

List of Figures and Tables

Figures

Tables

List of Abbreviations

Aβ	amyloid beta
ADNI	Alzheimer's Disease Neuroimaging Initiative
AIBL	Australian Imaging Biomarkers and Lifestyle Flagship Study of Ageing
APP	amyloid precursor protein
CSF	cerebrospinal fluid
CDR	clinical dementia rating
CDR SoB	clinical dementia rating sum of boxes
ChAT	choline acetyl transferase
EEG	electroencephalography
GABA	gamma-aminobutyric acid
GABAT	gamma-aminobutyric acid transferase
GAD	glutamic acid decarboxylase
LTP	long-term potentiation
MRI	magnetic resonance imaging
MMSE	mini-mental state examination
NFT	neurofibrillary tangle
p75NTR	p75 neurotrophin receptor
PET	positron emission tomography
PiB	Pittsburgh compound B
PSEN1	presenilin 1
PSEN2	presenilin 2
REM	rapid eye movement
ROI	region of interest
Trk	tyrosine kinase
VAChT	vesicular acetylcholine transporter

Chapter 1: Project rationale

1.1 Introduction

The cholinergic system in the human brain was discovered as one of the initial defective neurotransmitter systems in Alzheimer's disease. Once the major source of acetylcholine in the brain, namely the cholinergic basal forebrain neurons, was identified (Whitehouse et al., 1981), a long quest to study their development, architecture, and function in health as well as dysfunction in disease began. At the same time, the so-called "cholinergic hypothesis" was born (Bartus et al., 1982), which postulated that loss of cholinergic basal forebrain neurons in aging and Alzheimer's disease was a major contributor to the cognitive dysfunction observed in these subjects. A vast body of evidence accumulated over several decades of research starting from the early 1960s until today proving that the basal forebrain system is one of the most complex, functionally diverse but also vulnerable neurotransmitter systems in the brain.

Motivated by the goal of finding the cause of Alzheimer's disease and a cure for this condition several classes of drugs aimed at improving basal forebrain neuronal function and rescuing the death of cholinergic neurons were developed or are currently being developed. While the simplicity of the original form of the "cholinergic hypothesis" of Alzheimer's disease is captivating, many aspects of this pathophysiological oversimplification have been disputed and questioned even by its initial discoverers and especially in light of recent evidence (Bartus, 2000; Baxter and Bucci, 2013; Burns et al., 1997; Contestabile, 2011), such as the poor efficacy of cholinergic drugs, the finding that only mild cognitive effects are caused by cholinergic lesions in animal models and the fact that frank cholinergic cell loss only occurs in late stage Alzheimer's disease. However there is no doubt that the initial dysfunction of cholinergic neurons, and hence dysfunction of the basal forebrain neuronal system overall, represents a central and early event in Alzheimer's disease aetiology. Therefore studies of basal forebrain degeneration and its relationship to the major events in disease progression can give crucial insights in Alzheimer's disease pathogenesis.

Even though extensive research has been conducted studying the pathophysiology of the basal forebrain in Alzheimer's disease, even today, it remains to be determined whether there is a relationship between degeneration of the basal forebrain and the accumulation of amyloid plaques as well as tau neurofibrillary tangles (the major pathological hallmarks

of Alzheimer's disease) in the human brain *in vivo*. New advances in the imaging field now enable this potential interaction to be studied. Such methods in the future could also be applied to measure deterioration of connections of the basal forebrain network, and therefore give clues to how these factors manifest during the development of Alzheimer's disease. Furthermore, imaging techniques have the potential to contribute invaluable non-invasively acquired information that can aid in the diagnosis of neurological conditions including Alzheimer's disease and its prodromal conditions.

The aim of this thesis was to develop imaging methods to quantify basal forebrain neurons and their projections in mouse models of, and humans diagnosed with, Alzheimer's disease, and its prodromal stages. These methods were also used to study the relationship between basal forebrain degeneration, amyloid and tau accumulation and cognition during the development of Alzheimer's disease.

1.2 Alzheimer's disease

Alzheimer's disease is the most common form of aging dementia. Worldwide, the number of people with this condition is predicted to reach 66 million by 2030 and 115 million by 2050 (Sui et al., 2014). The prevailing hypothesis of the cause of Alzheimer's disease is that the brain overproduces or fails to degrade an endogenously produced peptide known as amyloid beta (Hardy and Selkoe, 2002). Recent evidence has shown that soluble amyloid beta is toxic, causing inhibition of synaptic activity as well as neurodegeneration.

Further aggregation of amyloid beta leads to extracellular deposits known as amyloid plaques, a histological hallmark of Alzheimer's disease from which the pathological diagnosis of the condition arose (Hardy and Selkoe, 2002; Masters and Beyreuther, 1991). Another hallmark of the disease is the aggregation of the microtubule-associated protein tau. The normal biological function of tau is to bind and stabilize microtubules in neurons but in Alzheimer's disease, tau becomes hyperphosphorylated at multiple phosphorylation sites. This renders the protein unable to associate with microtubules and subsequently tau molecules aggregate and form intracellular inclusions termed neurofibrillary tangles (NFTs).

Genetic screens have not been able to identify tau mutations in Alzheimer's disease patients but there are a number of mutations that are known risk factors for conditions such as progressive supranuclear palsy and corticobasal degeneration. These mutations affect tau function either at the transcriptional level, causing a shift in the level of

expression of different tau isoforms, or at the protein level, increasing the propensity of tau to form aggregates (Goedert and Jakes, 2005). In contrast, several mutations affecting the protein cascade responsible for the production of amyloid beta have been found to be present in patients with early onset Alzheimer's disease. The amyloid precursor protein (APP) is cleaved by the enzymatic complexes beta secretase and gamma secretase to produce amyloid beta. Presenilin 1 (PSEN1) and presenilin 2 (PSEN2) are functional components of the gamma secretase complex and mutations in APP, PSEN1 and PSEN2 genes are known risk factors for early onset Alzheimer's disease. The majority of mutations identified in these genes cause an increased production of the 42 amino acid long amyloid beta peptide ($A\beta_{42}$) vs. the 40 amino acid long ($A\beta_{40}$) version. Although this does not affect total amyloid beta levels, it has been shown that in comparison to $A\beta_{40}$, $A\beta_{42}$ is more prone to aggregate and this may play a role in inducing Alzheimer's disease (Bertram et al., 2010; Citron et al., 1997).
In Alzheimer's disease, cells within the basal forebrain might be particularly vulnerable to neurodegeneration, such as caused by the formation of protein aggregates consisting of Aβ and/or tau (Mufson et al., 2014; Vana et al., 2011).

1.3 Cell types in the basal forebrain

In general, the cellular architecture of the basal forebrain is highly complex and there appears to be no uniform distribution pattern of different cell types across its rostrocaudal extent. The basal forebrain is made up of a variety of cell types expressing different neurotransmitters and/or neurochemicals and neuropeptides. These include cholinergic, GABAergic and glutamatergic neurons, calcium binding protein (e.g. parvalbumin, calbindin, calretinin, secretagogin) -expressing neurons as well as neuropeptide (e.g. neuropeptide-Y, somatostatin, galanin) -expressing neurons. Cholinergic, GABAergic and glutamatergic neurons in the basal forebrain share common projection targets to cortical and subcortical areas (Gritti et al., 2003; Henny and Jones, 2008; Hur and Zaborszky, 2005; Zaborszky et al., 1999).

In addition to the heterogeneous neurochemical profile of basal forebrain cells, electrophysiological studies have shown differences in the membrane potential between cholinergic and non-cholinergic cells, as well as between cholinergic cells depending on their location within the basal forebrain (Unal et al., 2012). For example early firing cholinergic neurons might be more important contributors of phasic changes in cortical

acetylcholine release associated with attentional functions, whereas late firing cholinergic cells are more involved in tonic acetylcholine release mediating general arousal effects.

The most well studied cells of the basal forebrain are the cholinergic neurons, as their degeneration was found to be the underlying factor causing a decrease in brain acetylcholine levels in Alzheimer's disease patients (Whitehouse et al., 1981). Cholinergic neurons are found in all nuclei of the basal forebrain and the distribution of cholinergic cells does not appear to follow classically defined boundaries of nuclei (Zaborszky et al., 2008). These neurons express the neurotrophin receptors TrkA and p75NTR and nearly all (>95%) of the p75NTR-expressing neurons are also ChAT-positive (Mesulam et al., 1983a). In addition calbindin-D(28K) has been shown to be present in 72% of all ChAT-positive basal forebrain neurons (Geula et al., 2003). Even though cholinergic neurons are located throughout the whole extent of the basal forebrain, relative cell numbers vary greatly between basal forebrain nuclei. It has been shown that, in the human brain, the nucleus basalis of Meynert is largely composed of cholinergic neurons (90%), as compared to Ch1/medial septum (10%), Ch2/horizontal diagonal band (70%) and Ch3/vertical diagonal band (1%) areas (Mesulam et al., 1983a). However more recent work in rodents (Gritti et al., 2006; Zaborszky et al., 2005) has found that only a small population (~5%) of all neurons in the basal forebrain have the ability to synthesize acetylcholine, whereas 35% of neurons are GABAergic and 90% of all neurons synthesize glutamate. Moreover, the distribution of cholinergic-, calretinin-, calbindin- and parvalbumin-positive cells is not random. Indeed Zaborszky et al. (2005) found that the cell composition of clusters in the basal forebrain is regionally specific. For example, in the extended amygdala mostly calbindin-positive cells are present whereas the substantia innominata is rich in calbindin- and calretinin-positive cells.

The basal forebrain is a cytoarchitectonically complex structure and different nomenclatures have been proposed. Mesulam et al. (1983) suggested a nomenclature according to target projection areas. However this nomenclature was not straightforward due to the lack of specific landmarks and recently a revised version of the original nomenclature was recently introduced (Zaborszky et al., 2008). New computational tools to analyse the clustering of cell populations in structures (Nadasdy et al., 2010) will provide helpful insight into the complicated organizational pattern of the basal forebrain, and detailed neuroanatomical tracer studies are now shedding new light into the functional organization of basal forebrain cells with respect of their projection targets (Zaborszky et al., 2013).

1.4 The role of the basal forebrain in Alzheimer's disease

The basal forebrain degenerates in Alzheimer's disease (Mufson, 2003; Mufson et al., 2008; Schliebs and Arendt, 2011; Whitehouse et al., 1981) and the number of cholinergic neurons within this region is severely reduced (Contestabile, 2011; Whitehouse et al., 1981), which is believed to play a role in the cognitive dysfunction that occurrs in Alzheimer's disease (Bartus, 2000; Bartus et al., 1982; Perry et al., 1978). To treat this dysfunction and to alleviate cognitive symptoms of Alzheimer's disease a drug class called acetylcholine esterase inhibitors was developed. Acetylcholine esterase inhibitors inhibit the degrading enzyme of acetylcholine, acetylcholine esterase, in the synaptic cleft, thereby prolonging acetylcholine availability. Acetylcholine esterase inhibitors are efficacious for mild to moderate Alzheimer's disease and have been shown to slightly improve attention and executive functions, communication, expressive language and mood stability; however the time period over which they exert their effect is relatively short (Martinez et al., 2009; Pepeu and Giovannini, 2009).

Results on the effect of acetylcholine esterase inhibitors have been conflicting, with a recent study investigating long-term treatment using donepezil, rivistagmine and galantamine in patients with mild cognitive impairment showing no beneficial effect of these drugs to either reduce the risk or delay the onset of Alzheimer's disease (Raschetti et al., 2007). Therefore it is evident that acetylcholine esterase inhibitors only have limited potential to treat cognitive dysfunction in Alzheimer's disease and application in prodromal stages of the disease are not disease modifying i.e. do not prevent development of the condition. Thus there is a clear need for the development of new therapeutics that have the potential to alleviate neuronal degeneration in the basal forebrain, with one possibility being the application of molecules targeting neurotrophin receptors present on cholinergic basal forebrain neurons (Longo and Massa, 2013) which have been shown to rescue degeneration and improve cognition in an Alzheimer's mouse model (Knowles et al., 2013).

1.4.1 Cholinergic neurons

Cholinergic neurons degenerate in late-stage Alzheimer's disease but there is no loss of cholinergic neurons in mild cognitive impairment (a prodromal stage of the disease) or early/mild Alzheimer's disease (Contestabile, 2011; Gilmor et al., 1999) and no reduction in cortical levels of choline acetyl transferase (ChAT; the synthesizing enzyme of

acetylcholine expressed by cholinergic basal forebrain neurons) was found in patients with mild cognitive impairment or mild Alzheimer's disease, whereas a severe reduction in cortical ChAT and the number of cholinergic basal forebrain neurons was found in late stage Alzheimer's disease subjects (Contestabile, 2011; Davis et al., 1999; DeKosky et al., 2002; Gilmor et al., 1999; Mufson, 2003; Tiraboschi et al., 2000). In addition there was no significant reduction of the vesicular acetylcholine transporter (VAChT) in the basal forebrain in mild cognitive impairment and mild Alzheimer's disease patients compared to controls (Gilmor et al., 1999). The fact that significant cholinergic neuronal loss is only present at later stages of the disease became clear when reliable ways to categorize Alzheimer's disease patients as belonging to either mild, moderate or late-stage categories were developed - with the help of cognitive tests such as the mini-mental state examination (MMSE).

When post-mortem brain samples of the midfrontal area of patients with mild Alzheimer's disease (MMSE=20), moderate Alzheimer's disease (MMSE=10 to 19) and severe Alzheimer's disease (MMSE=1 to 9) were stained for synaptophysin, a marker used to assess synaptic density, and ChAT, both markers were found to undergo asynchronous changes. Whereas synaptophysin reduction was most pronounced in patients with moderate Alzheimer's disease, a significant decline in ChAT was only observed in patients with severe Alzheimer's disease, and neither synaptophysin nor ChAT was reduced in patients with mild Alzheimer's disease (Davis et al., 1999; Tiraboschi et al., 2000). Thus dysfunction occurs prior to synaptic loss and cholinergic neuron loss, which manifest during later stages of the disease. This finding has been further confirmed in various other cortical regions (superior frontal, inferior parietal, superior temporal and anterior cingulate) and the hippocampus (DeKosky et al., 2002).

In contrast, ChAT activity has been shown to be increased in the hippocampus and superior frontal cortex of mild cognitively impaired subjects compared to controls (DeKosky et al., 2002), which might point towards a compensatory upregulation of ChAT activity in basal forebrain neurons in response to the onset of Alzheimer's disease. In the case of the hippocampus it was hypothesized that early depletion of the entorhinal-hippocampal connection, which has been shown to occur in mild cognitive impairment (DeKosky et al., 2002; Ikonomovic et al., 2003), could lead to increased sprouting of the septohippocampal connection (Stanfield and Cowan, 1982), producing an increase in ChAT within the hippocampus (Contestabile, 2011).

ChAT-positive neurons are present in all nuclei of the basal forebrain and also express the neurotrophin receptors p75 neurotrophin receptor (p75NTR) and tyrosine kinase A (TrkA), which bind nerve growth factor (NGF) and this process is involved in survival of cholinergic basal forebrain neurons. It has been shown that there is significant reduction in the expression of p75NTR and TrkA in basal forebrain neurons in Alzheimer's disease patients compared to controls (Mufson et al., 2000; Mufson et al., 2002). Interestingly, in the same tissue samples of mild cognitively impaired subjects who displayed no reduction in cholinergic neuron number (Gilmor et al., 1999), a significant reduction of p75NTR- and TrkA- expression was found which was comparable to the reduction in Alzheimer's disease patients (Mufson et al., 2000; Mufson et al., 2002). Reductions in neuronal expression of p75NTR and TrkA in the nucleus basalis of Meynert of Alzheimer's disease and mild cognitively impaired subjects relative to controls were 56% (Alzheimer's disease) and 46% (mild cognitive impairment) and 43% (Alzheimer's disease) and 38% (mild cognitive impairment) for TrkA- and p75NTR- positive neurons respectively, and neuron numbers were also correlated with measures of cognitive function (Mufson et al., 2000; Mufson et al., 2002). These alterations in p75NTR and TrkA levels might indicate a severe neurotrophic defect and simultaneous dysfunction of cholinergic neurons before the occurrence of frank cell loss (Mufson, 2003). In line with this it was shown that the mRNA levels of TrkB and TrkC were also significantly reduced in Alzheimer's disease patients, with changes in the mRNA levels of synaptic proteins, protein phosphatases and amyloid-related proteins (Mufson, 2003).

It has also been shown that cholinergic basal forebrain neurons undergo degenerative changes when exposed to amyloid beta (Sotthibundhu et al., 2008). Furthermore through *in vitro* and *in vivo* experiments, p75NTR has been suggested to mediate this degeneration by directly interacting with amyloid beta (Knowles et al., 2009). Additional *in vitro* and *in vivo* evidence implicates amyloid beta in depression of acetylcholine synthesis and release, inhibition of long-term potentiation (LTP) through disturbance of cholinergic transmission, and impairment of muscarinic acetylcholine receptor signalling and therefore interference with function of at least one of the prominent cell types present in the basal forebrain (Auld et al., 2002; Yan and Feng, 2004). However, whether basal forebrain pathology is related to amyloid accumulation in humans *in vivo*, remains unknown. Cholinergic neurons have also been shown to exhibit NFT pathology. It is known from human post-mortem tissue studies that basal forebrain neurons develop some of the earliest pathological tau alterations described in Braak stage I (Braak et al., 2006). Even in individuals under 30 years of age, abnormally phosphorylated tau protein was found in

basal forebrain neurons (Braak and Del Tredici, 2011b). Recent studies have also documented the presence of pretangle tau oligomers in cholinergic basal forebrain neurons during the development of Alzheimer's disease (Mufson et al., 2014; Vana et al., 2011). Interestingly, an increase in early tau pathological markers coincided with a decrease in p75NTR staining and these changes correlated with Alzheimer's disease neuropathology and cognitive decline (Vana et al., 2011). Again, however, the relationship between basal forebrain degeneration and aggregation of tau tangles in living subjects has not been explored.

1.4.2 GABAergic and calbindin-positive neurons

A study by Geula et al. (2003) demonstrated a significant age-related loss of calbindin-D(28K) immunoreactivity in cholinergic basal forebrain neurons. Individuals over the age of 65 showed a 61% reduction of calbindin-D(28K)-positive cholinergic neurons compared to those under the age of 65, suggesting a significant age-related loss of expression of calbindin-D(28K), whereas no changes in ChAT or p75NTR immunoreactivity were observed. This dramatic loss of calbindin-D(28K) from cholinergic neurons presented in the same pattern in Alzheimer's disease patients and was more pronounced in the posterior part of the basal forebrain as compared to the anterior part. Cholinergic neurons lacking calbindin-D(28K) are not able to buffer high intracellular Ca^{2+} levels effectively and thus are more likely to be vulnerable to pathological processes occurring in Alzheimer's disease such as mitochondrial damage.

The GABAergic system in the brain was considered to be relatively spared in Alzheimer's disease but this view is currently being challenged. Through immunostaining of the main enzymes of the GABAergic system, glutamate decarboxylase 65 (GAD65), GAD67 and GABA transferase (GABAT), Schwab and colleagues (2013) demonstrated that these are present in the neocortex, hippocampus, basal ganglia and cerebellum in humans. GAD65 and GAD67 were found in neuropil granules, axons and neurons whereas GABAT was found in neurons and glial cells. In Alzheimer's disease, the authors found a severe reduction of GAD65 immunostaining in the middle temporal gyrus, hippocampus and putamen accompanied by a similar reduction in GAD65 protein levels as determined by western blotting. This GABAergic deficit is likely to contribute to Alzheimer's disease pathogenesis but it remains to be determined whether it occurs in GABAergic basal forebrain neurons and therefore possibly contributes to the deterioration of basal forebrain function in mild cognitive impairment and Alzheimer's disease. As well as cholinergic and

GABAergic neurons many other cell types exist in the basal forebrain; however changes in these populations have not been reported and so whether they also play roles in the deterioration of the basal forebrain in Alzheimer's disease remains poorly understood.

1.5 Anatomy of the basal forebrain

Some of the nuclei of the basal forebrain have already been mentioned in the above sections; however this part of the thesis will provide a complete list of all the grey matter structures included in the basal forebrain and will further explain how these nuclei are situated along the medial and ventral parts of the human forebrain.

The basal forebrain comprises the medial septum, vertical and horizontal diagonal bands of Broca, nucleus basalis of Meynert, magnocellular preoptic nucleus, substantia innominata, ventral pallidum, extended amygdala and the interstitial nucleus of the posterior limb of the anterior commissure. With regards to the human brain, the magnocellular preoptic nucleus is often included as part of the horizontal diagonal band of Broca whereas the substantia innominata, ventral pallidum, extended amygdala and interstitial nucleus of the posterior limb of the anterior commissure are often included as part of the nucleus basalis of Meynert. Different cell types within the basal forebrain are mostly dispersed across nuclei and therefore there are no clearly visible anatomical boundaries separating these nuclei, and it is viewed overall as a continuum (Schwaber et al., 1987; Zaborszky et al., 2005).

The medial septum is the most rostral nucleus situated between the lateral ventricles extending from the level of the genu of the corpus callosum to the level of the fornix. The medial septum merges rostroventrally with the vertical diagonal band of Broca. The horizontal diagonal band of Broca follows on from the ventral part of the vertical diagonal band of Broca and is then rostroventrally connected to the magnocellular preoptic nucleus. The Medial septum and diagonal band nucleus are eventually separated by the anterior commissure crossing the midline, with the medial septum lying dorsally and the diagonal domain located ventral to the anterior commissure. The substantia innominata extends ventrolaterally from the magnocellular preoptic nucleus and this structure has often been included as part of, or used as a synonym for, the nucleus basalis of Meynert; however recently parts of this complex have been attributed to other anatomical systems as a result of tracer studies (Zaborszky et al., 2008). The parts often included in the substantia innominata/nucleus basalis of Meynert complex are the ventral pallidum, extended

amygdala and interstitial nucleus of the posterior limb of the anterior commissure. The ventral part of the globus pallidus, or ventral pallidum, is situated rostral to the substantia innominata, whereas the caudal part of the substantia innominata is referred to as the extended amygdala, which is defined as the cell bridges extending from the centromedial amygdala to the bed nucleus of the stria terminalis (Zaborszky et al., 2008).

Dorsolateral to the ventral pallidum and ventrolateral to the caudate putamen lies the interstitial nucleus of the posterior limb of the anterior commissure, which extends dorsally to the level of the anterior commissure (Heimer, 2000; Heimer et al., 1991; Riedel et al., 2002; Zaborszky et al., 2008). The overall anatomy of the basal forebrain is highly complex and for the purpose of the magnetic resonance imaging (MRI) investigations of the basal forebrain area in this thesis we performed measurements of the whole area, or anterior and posterior areas separately. The definitions of the anterior and posterior areas (chapter 3, 4, 5) were guided by a recent study showing that degeneration of these areas might occur at different stages in Alzheimer's disease (Grothe et al., 2010). In that study it was found that all volumetric changes in mild cognitively impaired patients compared to controls were restricted to the posterior part of the basal forebrain, corresponding to the nucleus basalis of Meynert. Furthermore these anterior and posterior basal forebrain areas also differ in their projection targets.

1.6 Efferents and afferents of basal forebrain neurons

One of the major aims of this thesis was to study basal forebrain degeneration in Alzheimer's disease and how this relates to amyloid and tau accumulation as well as cognitive impairment. As the basal forebrain sends projections to many brain areas and receives input from many others (see below), it is very likely that toxic protein aggregates present in these brain areas come in close contact with basal forebrain neurons and therefore possibly exert direct neurodegenerative effects on these neurons. On the other hand, degeneration of basal forebrain neurons, and the resulting diminished support of neurotransmitters such as acetylcholine to target brain areas, is likely to contribute to the cognitive deterioration in Alzheimer's disease patients. In order to interpret these effects on basal forebrain neurons, one has to be aware of the general anatomy of the efferent and afferent connections of basal forebrain neurons. A diagram showing the major efferent projections of the basal forebrain is given (Fig. 1.1).

1.6.1 Efferent projections

Neurons in the medial septum and vertical diagonal band of Broca of the basal forebrain project to the hippocampus via the fornix and neurons in the horizontal diagonal band of Broca and magnocellular preoptic nucleus project to the olfactory bulb, piriform and entorhinal cortices. Furthermore neurons in the nucleus basalis of Meynert, substantia innominata, ventral pallidum, extended amygdala and interstitial nucleus of the posterior limb of the anterior commissure regions project to the amygdala and the entire neocortex (Amaral and Kurz, 1985; Armstrong et al., 1983; Carlsen et al., 1985; Gaykema et al., 1990; Lamour et al., 1984; Luiten et al., 1987; Mesulam et al., 1983a; Mesulam et al., 1983b; Nyakas et al., 1987; Rye et al., 1984; Sofroniew et al., 1982; Sofroniew et al., 1987; Wainer et al., 1985; Woolf et al., 1984; Woolf et al., 1986; Zaborszky et al., 1986). The general organization of cortically projecting neurons in the basal forebrain follows a rough medio-lateral and antero-posterior topography (Mesulam et al., 1983; Zaborszky et al., 2008). In the primate brain, the cortically projecting cholinergic neurons are therefore further divided into distinct subnuclei (Mesulam et al., 1983). Accordingly, medial cortical areas e.g. cingulate cortex receive projections from the cholinergic anteromedial (Ch4am) nucleus, whereas ventral orbital, frontal, and parietal regions and the amygdala receive projections from the anterolateral nucleus (Ch4al). The intermediate cholinergic nucleus (Ch4i) projects to the lateral frontal, parietal, peristriate and temporal regions and the posterior cholinergic nucleus (Ch4p) projects to superior temporal lobe and the temporal pole. It was thought that basal forebrain neurons innervate the cortex “diffusely”; however recently it was shown that cholinergic and noncholinergic neurons do not project to the frontal cortex in a diffuse manner, but are rather organized into groups of neurons projecting to the same target region (Zaborszky et al., 2013). Moreover the degree to which these “groups” of neurons overlap in the basal forebrain space might depend on the extent of the interconnectivity of the target projection areas. The authors propose that this organization therefore facilitates modulation of, for example, groups of interconnected but nonadjacent cortical regions by the basal forebrain neurons in a parallel manner. Cortical cholinergic innervation is present in all cortical layers but it has been shown to be most dense in layer V-VI of the motor cortex, layer III-IV in the primary sensory cortices and in layer II-III of the association areas (Mesulam et al., 1992; Mrzljak et al., 1995). Even though most studies investigating basalocortical innveration were focused on cholinergic neurons, it is becoming increasingly evident that basal forebrain efferents to pyramidal cells in the cortex and cortical interneurons arise not only from cholinergic but also

GABAergic and glutamatergic basal forebrain neurons (Zaborszky et al., 1999; Gritti et al., 2003; Hur and Zaborszky, 2005; Henny and Jones, 2008), and all neuronal types appear to have similar functional roles in regulating cortical activity (Hassani et al., 2009).

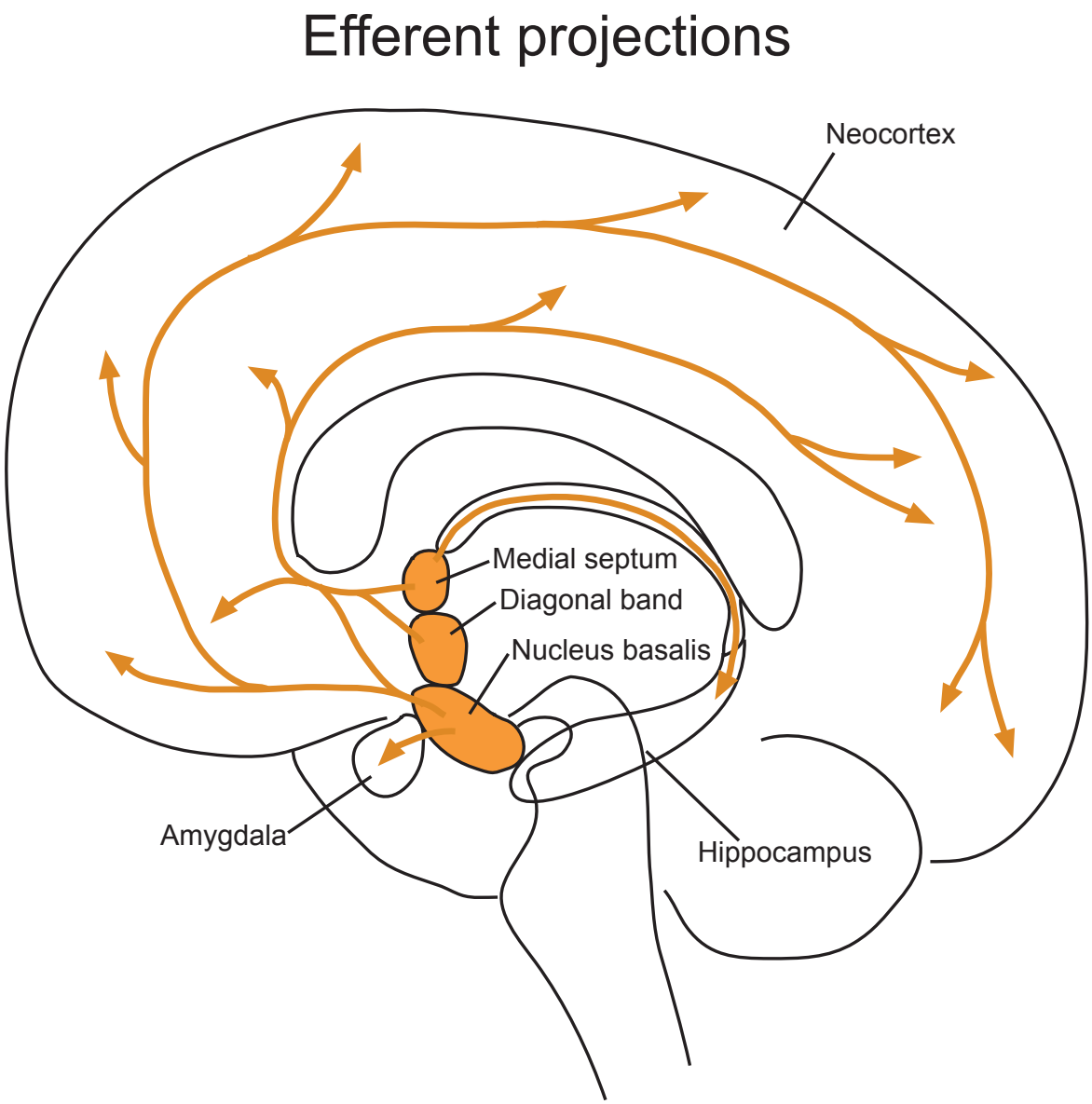

Figure 1.1: Major connections of the basal forebrain efferent neuronal projection system in the human brain.

The main nuclei of the basal forebrain (medial septum, diagonal band, nucleus basalis of Meynert) and their respective projections are shown. Cholinergic, GABAergic and glutamatergic basal forebrain neurons project along the illustrated pathways.

In addition, orexin/hypocretin-expressing neurons in the hypothalamus receive input from cholinergic and GABAergic neurons located in the medial septum, vertical diagonal band of Broca, horizontal diagonal band of Broca and magnocellular preoptic nucleus areas, which might be an important anatomical connection involved in consolidation of wakefulness (Sakurai et al., 2005).

1.6.2 Afferent projections

The basal forebrain receives afferent projections from many areas in the brain, including the brainstem, amygdala, substantia nigra, ventral tegmental area, striatum, hippocampus and prefrontal cortex (Zaborszky et al., 1999). In the brainstem, the locus coeruleus (Zaborszky et al., 1993), the medial parabrachial nucleus, the pedunculopontine nucleus, the dorsal raphe nucleus, the lateral and ventral tegmental area and the supramammillary nucleus project to the substantia innominata and magnocellular preoptic nucleus areas of the basal forebrain as revealed by tracer studies; however most of these connections still require confirmation at the ultrastructural level (Hallanger and Wainer, 1988; Jones and Cuello, 1989; Martinez-Murillo et al., 1989; Semba et al., 1988; Vertes, 1988). Brainstem afferents have been shown to be adrenergic and form synapses onto cholinergic neurons (Hajszan and Zaborszky, 2002), whereas dopaminergic neurons from the ventral tegmental area mainly connect to parvalbumin- and somatostatin- positive cells in the basal forebrain (Gaykema and Zaborszky, 1996; Zaborszky and Duque, 2003).

Neuronal input from the mesopontine tegmentum is cholinergic (Semba, 2000) and a small proportion of afferents from the dorsal raphe nucleus are serotonergic and dopaminergic neurons (Khateb et al., 1993). Projections from the basolateral amygdala form synapses onto either cholinergic or noncholinergic basal forebrain neurons in the ventral pallidum and parts of the substantia innominata; however the central amygdala sends efferents only to noncholinergic basal forebrain neurons of the substantia innominata (Jolkkonen et al., 2002; Zaborszky et al., 1984). Hypothalamic orexin/hypocretin-positive afferents onto basal forebrain neurons are organized in a topographical manner, whereby lateral hypothalamic neurons project to lateral nuclei of the basal forebrain such as the ventral pallidum and substantia innominata, and the medial hypothalamic neurons project to medial nuclei, including the medial septum, vertical diagonal band of Broca and horizontal diagonal band of Broca (Cullinan and Zaborszky, 1991). Cells in the medial septum and vertical diagonal band of Broca receive reciprocal projections from the hippocampal

formation, and the prefrontal cortex projects to noncholinergic neurons in the basal forebrain (Zaborszky et al., 1997).

1.7 Basal forebrain function

The basal forebrain is involved in controlling cerebral blood flow, cortical activity and plasticity, and the sleep-wake cycle, as well as the modulation of cognitive functions such as attention, learning, spatial and working memory, information encoding, sensory-motor gating and memory consolidation (Schliebs and Arendt, 2006).

1.7.1 Cognitive functions

Even though the role of the cholinergic neurons in learning and memory is uncertain (McKinney and Jacksonville, 2005), there is no doubt that the basal forebrain as a functional unit is crucial for cognitive processes in the brain. Since the initial discovery of the loss of cholinergic neurons in Alzheimer's disease, these cells have been implicated in attention, learning and memory (Schliebs and Arendt, 2011). Pharmacological application of anticholinergic drugs in young adults cause cognitive disturbances in these subjects, whereas administration of enhancers of the cholinergic system have beneficial (albeit minor) effects on cognition in patients suffering from Alzheimer's disease (Schliebs and Arendt, 2006). Nonspecific lesions of basal forebrain nuclei have consistently shown cognitive impairments in animals using either excitotoxins (Markowska et al., 1990; Page et al., 1991; Robbins et al., 1989), which induced nonspecific basal forebrain cell loss, or specific toxins at high concentration or damaging injection protocols, which also resulted in nonspecific cell death (Baxter and Bucci, 2013; Lehmann et al., 2003).

However application of immunotoxins, which selectively ablated cholinergic neurons in the anterior and/or posterior basal forebrain areas, resulted in almost no effects on learning and memory (Berger-Sweeney et al., 1994; Torres et al., 1994; Wenk et al., 1994). Other studies that achieved selective lesioning of cholinergic neurons in animal models demonstrated that they play a role in attention as well as working memory (Baxter and Bucci, 2013; Bucci et al., 1998; Chudasama et al., 2004; Moreau et al., 2008). The absence of severe cognitive deficits after selective lesioning of cholinergic neurons also initiated studies focused on exploring the functions of noncholinergic neurons such as GABAergic neurons and glutamatergic neurons of the basal forebrain. Selective lesioning of GABAergic neurons caused a deficit in spatial working memory in animals in one study

(Pang et al., 2011) and did not impact spatial reference memory in another study (Radley et al., 2009). Simultaneous lesion of cholinergic neurons and application of GABAergic compounds caused similar spatial working memory deficits (Pang and Nocera, 1999). Furthermore both GABAergic and cholinergic neurons were implicated in regulating hippocampal theta rhythm (Yoder and Pang, 2005), as well as regulating proactive interference (De Rosa et al., 2004; Pang et al., 2011). Most neurons in the basal forebrain (90%), including the cholinergic and GABAergic populations also produce and release glutamate (Gritti et al., 2006); therefore investigating the sole role of glutamate in the basal forebrain is difficult and this still remains to be determined.

Interestingly, some studies have explored more specific functions of cholinergic neurons, such as the importance of the septohippocampal cholinergic projection neurons for plasticity of hippocampal place cells (Ikonen et al., 2002) or the temporal profile of prefrontal cortical acetylcholine release upon cue detection (Parikh et al., 2007). It has been proposed that acetylcholine released by basal forebrain neurons into the cortex increases the amplitude and signal-to-noise ratio of evoked sensory responses, thereby selectively amplifying certain inputs while suppressing others (Parikh et al., 2007). Acetylcholine has also been shown to trigger different types of hippocampal plasticity depending on the spatiotemporal properties of its release (Gu and Yakel, 2011). When acetylcholine was released onto Schaffer collateral cells either 100ms or 10ms before Schaffer collateral activation, either LTP or short-term depression via alpha7-nictotinic acetylcholine receptor activation was induced. When acetylcholine activation followed Schaffer collateral cell activation by a 10ms delay, LTP was induced through muscarinic acetylcholine receptor activation. Application of amyloid beta abolished these different types of acetylcholine-induced hippocampal plasticity (Gu and Yakel, 2011).

In the prefrontal cortex, tonic acetylcholine release can cause persistent firing of pyramidal neurons, a characteristic that has been connected to working memory functions (Dembrow et al., 2010). Recent imaging studies indicate that basal forebrain volume, in particular the volume of the nucleus basalis of Meynert, is also correlated to general intelligence (Wolf et al., 2014), and the medial septum/vertical diagonal band of Broca volumes might be associated with human recognition memory accuracy (Butler et al., 2012).
One aim of the current work was to study the involvement of the basal forebrain in specific types of navigation in humans, namely idiothetic – navigation in relation to oneself – and allothetic – navigation in relation to external cues – and to determine whether basal forebrain degeneration in Alzheimer's disease affects either navigation type.

1.7.2 The sleep-wake cycle

Cholinergic, GABAergic and glutamatergic neurons in the basal forebrain function together in order to regulate cortical activity in awake or slow-wave and rapid eye movement (REM) sleep states (Hassani et al., 2009) and activation of cholinergic neurons has been shown to initiate transitions between these states (Han et al., 2014). In general, the electrical discharge profiles of the different neuronal subtypes in the basal forebrain are similar in awake and sleep states, but cholinergic neuronal discharge combined with release of acetylcholine is maximal only during awake and REM sleep states (Jones, 2004; Marrosu et al., 1995) whereas GABAergic and glutamatergic neurons discharge in all states. Likewise, antagonists of acetylcholine receptors induce changes in awake and REM sleep states, but not slow-wave sleep, whereas non-specific lesions in the basal forebrain have effects on all three sleep states (Jones et al., 2004). Cholinergic, GABAergic and glutamatergic neurons in the basal forebrain are also associated with gamma, delta and theta electroencephalography (EEG) activity in a complex manner, where different subgroups of neurons have been shown to be correlated with different types of EEG activity (Hassani et al., 2009).

1.7.3 Regulation of blood flow in the brain

Both GABAergic and cholinergic neurons in the basal forebrain have been shown to stimulate blood flow and vasodilation in several cortical and subcortical areas (e.g. hippocampus, amygdala) in rodents in a complex manner (Barbelivien et al., 1999a; Barbelivien et al., 1999b; Sato et al., 2004). Separate injections of carbachol (a cholinergic agonist) and GABA into the substantia innominata generated significant increases in brain regional blood flow of target projection areas of cholinergic and GABAergic neurons, whereas simultaneous injections of carbachol and GABA into the substantia innominata resulted in a small increase in blood flow. In contrast, simultaneous injection of picrotoxin (a GABA receptor antagonist) and carbachol did not induce any changes in cerebral blood flow (Barbelivien et al., 1999b). Acetylcholine esterase inhibitors have shown beneficial effects in patients suffering from vascular dementia, the second most common type of dementia (Roman, 2005). Furthermore it has been suggested that vascular pathology, such as arterial hypertension, sustained hypoperfusion and ischaemic cerebrovascular disease, occurring in vascular dementia and partly in Alzheimer’s disease, might play an

important role in initiating degeneration of basal forebrain neurons (Nardone et al., 2008; Roman, 2005; Roman and Kalaria, 2006).

1.8 Basal forebrain in aging and other neurodegenerative diseases

The basal forebrain has been shown to undergo slow and progressive age-related degeneration starting from early adulthood (Grothe et al., 2011; Lowes-Hummel et al., 1989; Mann et al., 1984; McGeer et al., 1984). In normal aging, beginning around 65-70 years of age, the rate of basal forebrain degeneration is increased and it has been proposed that by the age of 90 approximately 30% of basal forebrain neurons have died. In Alzheimer's disease, these cellular changes are greatly aggravated and a further 60% of basal forebrain neurons can be lost (Mann et al., 1984). The age-related atrophy appears to occur in all nuclei of the basal forebrain, anterior and posterior, and, equally in both brain hemispheres. However tendencies towards increased cell loss in the nucleus basalis of Meynert (Grothe et al., 2011) and in the left hemisphere (Lowes-Hummel et al., 1989) have been reported.

In healthy aging, the decline of basal forebrain volume over time does not occur in a linear fashion, but is stable over the early years before volume loss starts to show in some subjects from about 50 years of age (Grothe et al., 2011). It has been further suggested that the annual rate of basal forebrain degeneration is greater than that of the hippocampus, or grey matter in general (Grothe et al., 2012). However recently, the presence of significant age-related cell loss in the brain has been challenged, and early histological studies documenting this cell loss have been questioned with respect to technical and methodological issues such as tissue processing and sampling design (Burke et al., 2006). Functional decline in advanced age, such as a decline in cognitive function, is more likely to occur due to axonal and dendritic degeneration of neurons, decrements in gene expression, impairments in intracellular signalling and cytoskeletal transport rather than frank neuronal cell loss (Burke and Barnes, 2006; Morrison and Hof, 1997). In disease, however, particularly in those conditions that are accompanied by a form of dementia or significant decline in cognitive function, loss of basal forebrain neurons is well documented.

Degeneration of the basal forebrain neurons has been reported in conditions including Alzheimer's disease, Down's syndrome, Parkinson's disease (Arendt et al., 1983; Jellinger, 2000; Whitehouse et al., 1983), progressive supranuclear palsy, Creutzfeldt-

Jakob disease (Arendt et al., 1984) and Korsakoff's syndrome (Arendt et al., 1983; Terry and Buccafusco, 2003) as well as being implicated in response to chronic ethanol intake (McKinney et al., 2005), traumatic brain injury (Donat et al., 2010; Salmond et al., 2005) and other conditions. Cholinergic cells of the basal forebrain might show a particular vulnerability to neurodegenerative changes. The reasons for this vulnerability are largely unknown but it has been partly attributed to a possible higher energy demand of the cholinergic neurons, as these cells require acetyl-CoA for both energy production and acetylcholine synthesis (Szutowicz et al., 2006) and are therefore more sensitive to aging-related energy (glucose) deprivation. In line with this, a recent study has shown age-related changes in the metabolic activity of cholinergic basal forebrain neurons, such as strong upregulation of the transcription factor GA-binding protein alpha, which controls expression of nuclear genes encoding mitochondrial proteins (Baskerville et al., 2008). In addition cholinergic neurons express the neurotrophin receptors TrkA and p75NTR which bind NGF, a neurotrophic substance that has been shown to be important for the survival these neurons (Coulson et al., 2009; Mufson, 2003). Imbalances in trophic support can affect the function and plasticity of cholinergic basal forebrain neurons and this mechanism has been suggested to play an important role in both aging and neurodegenerative disease (Mufson et al., 2003).

1.9 Biomarkers of Alzheimer's disease

Accurately diagnosing people with or at risk of developing Alzheimer's disease, and monitoring their progress over time, will be vital to reducing the economic and social burden of this condition by enabling existing treatments and care options to be tailored for each patient, as well as demonstrating the efficacy of experimental drugs. The current method of making a clinical diagnosis of Alzheimer's disease prior to autopsy is by neuropsychological testing. An exciting recent development in this field is the demonstration that positron emission tomography (PET) imaging of live patients, using Pittsburg compound B (PiB), a modified stain that binds to amyloid plaques, can give an indication of plaque load prior to autopsy. This raises the possibility of identifying people at risk of developing Alzheimer's disease (Villemagne et al., 2011). However whether atrophy of the basal forebrain is correlated to amyloid levels measured using PiB imaging has not been investigated. However amyloid load, measured either at post-mortem or *in vivo* with PET, does not correlate well with clinical measures of cognitive impairment (Drachman, 2014). Likewise a recent study found that amyloid deposition and neurodegeneration, such

as hippocampal atrophy, are “biologically independent processes”. On the other hand, a certain amount of underlying amyloid pathology is associated with increased neurodegeneration (Jack et al., 2014). Jack and colleagues recently published a review focused on discussing the use of biomarkers including amyloid-PET and MRI in tracking the pathophysiological processes in Alzheimer’s disease (Jack et al., 2013). However, in this article, the authors identify a clear need for development of new biomarkers and point out a lack of studies in the field of PET and structural MRI.
Unlike amyloid, tau pathology is strongly correlated with cognitive decline and neurodegeneration, with an increase in subcortical tau correlating with loss of cholinergic basal forebrain neurons as well as Alzheimer’s disease neuropathology and cognitive decline (Mufson et al., 2014; Vana et al., 2011). More recently PET tracers capable of measuring tau levels in the brain have been developed and verified to show a profile of tau in the brain of Alzheimer’s disease patients similar to the distribution found at autopsy (Fodero-Tavoletti et al., 2011; Okamura et al., 2014; Villemagne et al., 2014). Whether there is an interaction of structural changes of the basal forebrain with tau levels measured by these PET tracers *in vivo* in humans remains to be determined.

Simultaneous assessment using structural MRI and tau-PET markers of subjects at risk of developing Alzheimer’s disease could be of great use in aiding with diagnosis. On the other hand, by the time atrophy of a structure can be detected as a volumetric reduction with structural MRI, significant cell and tissue loss has already occurred. Furthermore, as the diagnosis of mild cognitive impairment or Alzheimer's disease currently occurs at a stage at which the cholinergic system has been irreversibly damaged, it is not surprising that acetylcholine esterase inhibitors have mild to little effect in prolonging cognitive function (Mancuso et al., 2011). Non-invasive early detection of basal forebrain neurodegeneration prior to overt tissue loss therefore has the potential to improve the window of efficacy of acetylcholine esterase inhibitors for the treatment of Alzheimer's disease.

Diffusion MRI (dMRI) is a technique that can be used to analyse differences in structural integrity and brain connectivity, and has been successfully employed to detect differences between Alzheimer’s patients and healthy control subjects (Kiuchi et al., 2009; Pievani et al., 2010; Teipel et al., 2010). dMRI measures water diffusion within a tissue, and various dMRI parameters can be extracted for individual brain regions as well as for streamlines generated from dMRI data by tractography, a technique that is used to infer the connectivity of the brain, particularly of white-matter tracts (Mori and Zhang, 2006). These

methods show promising sensitivity as diagnostic tools for detecting early pathological changes in humans, although further validation is still required, and whether these methods can be used to assess the integrity of the basal forebrain and its projections is not known.

Levels of amyloid and tau protein (total and phosphorylated tau) can also be determined from cerebrospinal fluid (CSF) samples of patients. These CSF biomarkers can be used to distinguish Alzheimer's disease subjects from mild cognitively impaired subjects and correlate with the progression of Alzheimer's disease. However measuring CSF concentrations of tau and amyloid is not a feasible way to discriminate Alzheimer's disease from other dementias (Sui et al., 2014). Unfortunately, blood biomarkers used to detect tau, phosphorylated tau, amyloid as well as other proteins associated with Alzheimer's disease are also unable to provide valid diagnostic information to date (Snyder et al., 2014). Several issues connected to protocols and methods of blood biomarker sampling and therefore problems with standardization have so far halted their development, but if successful, blood-based biomarkers would certainly provide the most cost-efficient way for diagnosis of Alzheimer's disease.

Alzheimer's disease is a complex condition in which only a combination of multiple factors yields a successful diagnosis, e.g. amyloid pathology alone is not sufficient, and researchers increasingly discern the development of certain Alzheimer's disease hallmarks as independent processes, e.g. rate of amyloid accumulation is independent of neurodegeneration, tau and amyloid deposition are independent processes (Jack et al., 2013), and so on. Therefore a combination of different biomarkers might be required to successfully diagnose and monitor this condition.

1.10 Project proposal

Degeneration of basal forebrain neurons is a pathological hallmark of Alzheimer's disease at autopsy, together with the presence of protein aggregates in the brain composed of extracellular amyloid and intracelluar tau. Patients also suffer from severe cognitive decline in late stage Alzheimer's disease; however whether this cognitive decline relates to basal forebrain atrophy has not been extensively investigated. In addition, how amyloid and tau accumulation in the brain influences degeneration of the basal forebrain neurons *in vivo* is completely unknown.

1.10.1 Aim

The overall aim of this proposal is to generate and validate structural and dMRI methods to quantify basal forebrain neurons and their projections in mouse models and humans. Once developed, the MRI methods will be used to test the hypotheses that quantification of the basal forebrain cholinergic neurons can be used as a method of diagnosing and/or monitoring progression of Alzheimer's disease. Furthermore the methods will be used to investigate the relationship of basal forebrain degeneration and amyloid as well as tau accumulation in live Alzheimer's disease patients. Finally, this work will explore whether the basal forebrain is associated with spatial navigation and working memory and whether the dysfunction of these cognitive processes in Alzheimer's disease are correlated to basal forebrain degeneration.

1.10.2 Hypothesis

The basal forebrain degenerates during the development of Alzheimer's disease and changes will be detectable in amnestic mild cognitively impaired patients. This degeneration will correlate with cognitive decline and will be related to the level of amyloid as well as tau pathology. The basal forebrain will further be associated with navigation performance and its atrophy will be paralleled by a decline in navigational ability.

1.10.3 Specific research questions

1. Does the basal forebrain selectively degenerate in Alzheimer's disease, and its prodromal stage, amnestic mild cognitive impairment?
2. Is basal forebrain degeneration correlated to the cognitive decline observed in Alzheimer's disease?
3. Is basal forebrain atrophy linked to amyloid and tau accumulation during the development of Alzheimer's disease?
4. Can degeneration of cholinergic basal forebrain neurons be measured using diffusion MRI and tractography?
5. Is basal forebrain degeneration involved in spatial navigation impairments observed in Alzheimer's disease patients?

The following chapters describe the results of the hypothesis and are formatted as per

submitted to journals including separate introduction and discussion for further commentary for each study.

Chapter 2: Basal forebrain degeneration is associated with amyloid accumulation in Alzheimer's disease

2.1 Introduction

Two critical events in the aetiology of Alzheimer's disease are accumulation of amyloid-beta and degeneration of basal forebrain neurons. At the time the work reported in the following chapter was performed, nothing was known about the *in vivo* relationship between these two features either in Alzheimer's disease, or its prodromal stage, mild cognitive impairment. However *in vitro* (Coulson, 2006) and *in vivo* (Sotthibundhu et al., 2008) studies performed in the Coulson laboratory were pointing towards a potential mechanism whereby amyloid-beta could induce death of basal forebrain neurons through activating cascades mediated by the p75NTR neuronal death receptor, which is expressed almost exclusively in the adult brain by cholinergic basal forebrain neurons.

Advances in PET imaging had made it possible to use compounds such as PiB to assess amyloid burden in living subjects (Villemagne et al., 2011). PiB-PET imaging in combination with structural MRI scans had been performed in a large number of subjects of the longitudinal Australian Imaging Biomarkers and Lifestyle Flagship Study of Ageing (AIBL) study, which enabled the evaluation of the effects of amyloid on brain structural changes. Therefore we decided to investigate whether basal forebrain volumes were correlated to amyloid burden in subjects of the AIBL study.

One particular finding from amyloid imaging was that a significant portion (~30%) of normal control subjects/healthy elderly people had an amyloid burden comparable with that of Alzheimer's disease subjects. Likewise, many mild cognitively impaired subjects, in particular amnestic mild cognitively impaired subjects, also displayed a considerable amyloid load by this method. Thus it was hypothesized that subjects with high amyloid burden in clinical groups were at higher risk of developing cognitive impairment (normal controls showing high amyloid load), or progression to Alzheimer's disease (mild cognitively impaired subjects with high amyloid load) status. Hence we were particularly interested in investigating the relationship between basal forebrain volume and amyloid load in these amyloid-defined subgroups.

However, in order to perform these correlations it was first imperative to develop masks that could be used for structural MRI measures of the basal forebrain. The masks were developed using data from the AIBL study and then validated in an independent data set

from the Alzheimer's disease Neuroimaging Initiative (ADNI) study. Details about the creation of these maps and illustrations of each map can be seen in the following chapter.

This study has been published in the journal *Neuroimage Clinical*.

2.2 Basal forebrain atrophy correlates with amyloid β burden in Alzheimer's disease

[1]**GM Kerbler**, [2]J Fripp, [3]C Rowe, [3,4]VL Villemagne, [2]O Salvado, [2]S Rose, [1]EJ Coulson, for the Alzheimer's Disease Neuroimaging Initiative. (2014) Basal forebrain atrophy correlates with amyloid β burden in Alzheimer's disease. *Neuroimage Clinical*, DOI: http://dx.doi.org/10.1016/j.nicl.2014.11.015

[1]Queensland Brain Institute, Clem Jones Centre for Ageing Dementia Research, The University of Queensland, Brisbane, 4072 Qld. Australia
[2]Commonwealth Scientific and Industrial Research Organisation, Computational Informatics, Brisbane, 4029 Qld. Australia
[3]Department of Nuclear Medicine and Centre for PET. Austin Health, Melbourne, 3084 Vic. Australia
[4]The Florey Institute of Neuroscience and Mental Health, The University of Melbourne, Melbourne, 3084 Vic. Australia

Abstract

The brains of patients suffering from Alzheimer's disease (AD) have three classical pathological hallmarks: amyloid-beta (Aβ) plaques, tau tangles, and neurodegeneration, including that of cholinergic neurons of the basal forebrain. However the relationship between Aβ burden and basal forebrain degeneration has not been extensively studied. To investigate this association, basal forebrain volumes were determined from magnetic resonance images of controls, subjects with amnestic mild cognitive impairment (aMCI) and AD patients enrolled in the longitudinal Alzheimer's Disease Neuroimaging Initiative (ADNI) and Australian Imaging, Biomarkers and Lifestyle (AIBL) studies. In the AIBL cohort, these volumes were correlated within groups to neocortical gray matter retention of Pittsburgh compound B (PiB) from positron emission tomography images as a measure of Aβ load. The basal forebrain volumes of AD and aMCI subjects were significantly reduced compared to those of control subjects. Anterior basal forebrain volume was significantly correlated to neocortical PiB retention in AD subjects and aMCI subjects with high Aβ burden, whereas posterior basal forebrain volume was significantly correlated to neocortical PiB retention in control subjects with high Aβ burden. Therefore this study provides new evidence for a correlation between neocortical Aβ accumulation and basal forebrain degeneration. In addition, cluster analysis showed that subjects with a whole basal forebrain volume below a determined cut-off value had a 7 times higher risk of having a worse diagnosis within ~18 months.

Keywords

Basal forebrain, amyloid, Alzheimer's disease, magnetic resonance imaging, PET

Abbreviations

3D: 3-dimensional
Aβ: amyloid-beta
AD: Alzheimer's disease
ADNI: Alzheimer's Disease Neuroimaging Initiative
AIBL: Australian Imaging, Biomarkers and Lifestyle Flagship Study of Aging
aMCI: amnestic mild cognitive impairment
CSF: cerebrospinal fluid
GM: gray matter
HC: healthy control
MCI: mild cognitive impairment
MNI: Montreal Neurological Institute
MPM: maximum probability maps
MPRAGE: magnetization prepared rapid gradient echo
MRI: magnetic resonance imaging
OR: odds ratio
PET: positron emission tomography
PiB: Pittsburgh compound B
SPSS: Statistics Software Package for the Social Sciences
SUVR: standard uptake value ratio
SyN: symmetric normalization
T1W: T1-weighted
TG-ROC: two-graph receiver operating characteristic
WM: white matter

1. Introduction

Alzheimer's disease (AD) is a progressive neurodegenerative disorder that results in widespread brain atrophy of both gray and white matter brain regions. Other hallmarks of the disease include the extracellular deposition of amyloid-β (Aβ) and intracellular accumulation of hyper-phosphorylated tau. An emerging method of early diagnosis of AD is to assess brain Aβ burden through Pittsburgh compound B (PiB)-positron emission tomography (PET) imaging. This measure has shown promise in identifying people at risk of developing AD (Villemagne et al., 2011); however, reports of correlations between PiB retention and hippocampal atrophy, the magnetic resonance imaging (MRI) measure most widely used together with traditional cognitive assessment for the diagnosis of AD (Frisoni et al., 2010), have been inconsistent. Therefore it remains unclear what additional factors control the progression to dementia of healthy subjects with high Aβ load.

Cholinergic neurons in the basal forebrain, a gray matter region located in the medial and ventral aspects of the brain, provide the neurotransmitter acetylcholine to a variety of different brain regions. Anterior basal forebrain nuclei, including the medial septum and diagonal band send projections to the hippocampus, olfactory bulb, and piriform and entorhinal cortices. Posterior basal forebrain nuclei, including the nucleus basalis of Meynert project to the amygdala and frontal, cingulate and parietal cortices, as well as to the orbital and peristrate cortices and the temporal lobe (Mesulam et al., 1983; Zaborszky et al., 2008). Regulation of acetylcholine supply to these brain regions is involved in local activation and modulation of plasticity, and cholinergic basal forebrain neurons can therefore influence critical behaviors such as attention, learning and memory (Mufson, 2003; Schliebs and Arendt, 2011). Post-mortem assessment has revealed significant degeneration of these neurons as an early pathological feature of AD patients, and their degeneration, which is likely to underpin aspects of cognitive decline associated with the disease (Contestabile, 2011; Mesulam, 2004; Schliebs and Arendt, 2011), drove the development of the now widely prescribed acetyl cholinesterase inhibitor class of drugs.

Consistent with this, recent studies have demonstrated that AD patients, as well as patients with mild cognitive impairment (MCI), a prodromal stage to AD, show significant basal forebrain volume loss compared to age-matched controls (Grothe et al., 2011; Hall et al., 2008; Muth et al., 2010), with atrophy of discrete regions within the basal forebrain being significantly associated with global cognitive decline as well as delayed recall scores in AD subjects (Grothe et al., 2010). Although the basal forebrain has been shown to

degenerate in normal aging, the rate of atrophy is significantly higher in subjects suffering from dementia (Grothe et al., 2012), and specific areas within the basal forebrain appear to be particularly vulnerable to AD-associated degeneration (Grothe et al., 2011).

An association between basal forebrain atrophy and Aβ burden in AD has recently been reported using MRI and AV45-PET data (Grothe et al., 2014; Teipel et al., 2013) acquired from the Alzheimer's Disease Neuroimaging Initiative (ADNI) cohort. In this study we also found a significant association between basal forebrain atrophy, based on a histological mask restricted to AD-specific degeneration, and Aβ load using PiB-PET, including a correlation between these hallmarks that extends to healthy control subjects of the Australian Imaging, Biomarkers and Lifestyle (AIBL) cohort (Ellis et al., 2009). Furthermore, we determined that degeneration of the basal forebrain is a significant risk factor for further cognitive decline in control and MCI cohorts, irrespective of Aβ burden.

2. Materials and Methods

2.1 Subjects

Data analyzed for this report were obtained from the AIBL study (Ellis et al., 2009) (http://www.aibl.csiro.au/) and the ADNI study (adni.loni.ucla.edu). From the AIBL study, longitudinal PiB and 3T T1-weighted (T1W) MRI images of AD, amnestic MCI (aMCI) and healthy control (HC) subjects at two time-points (Table 1) were used. The HC and aMCI groups were further subdivided into subjects with high (PiB+) and low (PiB-) PiB retention levels, as previously reported (Villain et al., 2012). The methodology for cohort recruitment and evaluation has been reported elsewhere (Ellis et al., 2009). From the ADNI-2/GO study, 3T T1W MRI images of HC, aMCI and AD subjects (Table 2) were examined.

2.2 Imaging protocol

From the ADNI cohort, 3T MR images were acquired using the magnetization prepared rapid gradient echo (MPRAGE) imaging protocol in accordance with ADNI's guidelines for these scans (http://adni.loni.ucla.edu/research/protocols/mri-protocols). For the AIBL cohort, 3T MR structural images were acquired on a Siemens 3T Trio. Participants received a MRI scan using the ADNI 3D MPRAGE sequence, with 1x1mm in-plane resolution and 1.2mm slice thickness, TR/TE/T1=2300/2.98/900, flip angle 9° and field of view 240x256 and 160 slices. In addition, each AIBL subject received ~370MBq PiB intravenously over 1 minute. A 30-minute acquisition in 3-dimensional (3D) mode starting 40 minutes after injection of PiB was performed with a Philips Allegro PET camera. A transmission scan was performed for attenuation correction. PET images were reconstructed using a 3D RAMLA algorithm.

	AIBL study							
	Baseline				Follow up (~18 months)			
	HC PiB-	HC PiB+	aMCI	AD	HC PiB-	HC PiB+	aMCI	AD
Number of subjects	101 (89)	44 (35)	40 (21)	38 (16)	83	39	17	22
Age	71.1 ± 6.7	75.1 ± 6.8	76.5 ± 7.2	72.5 ± 8.5	72.2 ± 6.5	74.9 ± 7.0	77.0 ± 6.8	74.3 ± 7.9
Sex F/M	57/44	23/21	20/20	22/16	49/34	14/25	9/8	11/11
MMSE	28.8 ± 1.2	28.8 ± 1.2	27.3 ± 2.2	20.6 ± 5.2	28.8 ± 1.4	28.5 ± 1.5	27.4 ± 2.0	20 ± 5.7
CDR	0	0	0.5	0.5-3	0	0-0.5	0-0.5	0.5-2

Table 1: Demographics of AIBL cohort at baseline and follow up. Numbers in brackets at baseline indicate the number of subjects used for calculation of longitudinal changes. At baseline, the ages of the HC PiB- and HC PiB+ subjects ($p<0.05$), as well as the HC PiB- and aMCI ($p<0.001$) subjects, were significantly different. There was no gender difference between groups. Mini-mental state examination (MMSE) scores between aMCI/AD and all other groups were significantly different. Years of education were not significantly different between groups. For representation of the healthy population we set clinical dementia rating (CDR)=0 as the criterion for the HC groups at baseline. Age and MMSE scores are expressed as mean ± SD.

	ADNI study		
	HC	aMCI	AD
Number of subjects	69	127	30
Age	73.5 ± 6.7	72.3 ± 8.2	77.1 ± 7.5
Sex F/M	41/28	53/74	13/17
MMSE	28.9 ± 1.2	28.3 ± 1.5	23.4 ± 2.1
CDR	0	0-1	0.5-1

Table 2: Demographics of the ADNI cohort. There was a significant difference for age between the AD and aMCI groups. Subject groups did not differ based on gender or years of education. For representation of the healthy population we set CDR=0 as the criterion for the HC groups at baseline. Age and MMSE scores are expressed as mean ± SD.

2.3 MRI processing

The hippocampus, pons and gray matter (GM), white matter (WM) and cerebrospinal fluid (CSF) were segmented from the MPRAGE images using the method outlined in (Bourgeat et al., 2010). A skull strip mask was generated from the GM, WM and CSF segmentation. All volume calculations reported are normalized by intracranial volume.

Using the AIBL study data, the skull-stripped MPRAGE images of all subjects were normalized to create an average elderly template brain using the open-source deformable registration tool ANTS. ANTS provides functionality for generating optimal templates, given a collection of images, which offers advantages over *a priori* templates for image normalization (for instance in the hippocampus; Avants et al., 2010). The population-specific template was generated by iteratively registering images to the current template estimate. A new shape and intensity average were then computed from the results of the registrations and the current template estimate was set as the average. This template generation procedure was repeated iteratively (I=5). Each registration in this procedure used the greedy symmetric normalization algorithm (SyN, parameters outlined below) and the cross-correlation after subtracting the local mean from the image match metric. A z-score map of the deformation field of the AD subjects with HC subjects from the AIBL cohort was generated.

The registration between each subject's MPRAGE image (AIBL and ADNI) and the population-specific template was performed using the SyN algorithm (GradStep = 0.5, regularization sigma = 2.0). The image match metric was the cross-correlation between the images. Cross-correlation after subtracting the local mean from the image at each voxel was computed using a 5×5×5 voxel window. Registration was performed in a multi-resolution scheme, with a maximum of 30 iterations at 4× subsampling, 90 iterations at 2× subsampling, and 50 iterations at full resolution.

To establish basal forebrain masks encompassing only those areas that undergo atrophy in AD patients (Fig. 1), we compared all control and AD subjects from the AIBL cohort and overlaid the resultant z-score map (set to -0.5 and -1 standard deviations) on a standard Montreal Neurological Institute (MNI) brain (z-score map, Fig. 1A, B). Using published probabilistic basal forebrain maps derived from histological data as a guide for the limits of the structure (Zaborszky et al., 2008), we then manually segmented the regions of atrophy within the standard space corresponding to the basal forebrain area. Using this method we created two types of basal forebrain masks.

First, we used published raw probabilistic maps (Zaborszky et al., 2008) from at least one post-mortem brain as a guide, resulting in a basal forebrain mask covering a large number of basal forebrain voxels (BF raw; size: 3193 voxels; Fig. 1A, B) and a final delineated area of intermediate anatomical specificity. Second, we used maximum probability maps (MPMs; Zaborszky et al., 2008) as guidance, resulting in a basal forebrain mask covering voxels that were identified as lying in the basal forebrain in ten post-mortem brains (BF MPM; size: 1160 voxels; Fig. 1A, B) and a final delineated area of high anatomical specificity. One aim of this study was to assess and compare the sensitivity of both BF raw and MPM masks in detecting volumetric changes as well as identifying associations with global Aβ burden. To study anterior and posterior basal forebrain compartments separately, we further divided the BF MPM map into an anterior BF MPM volume (size: 595 voxels; Fig. 1A), covering Ch1-3 as well as Ch4 anterior cell groups, and a posterior BF MPM volume (size: 565 voxels; Fig. 1B), covering Ch4 intermediate and posterior cell groups (nomenclature according to Mesulam et al., 1983).

The final BF raw and BF MPM masks comprised areas throughout the entire extent of the basal forebrain area (Ch1-4 cell groups) and were validated by overlaying the masks onto newly developed raw probabilistic and MPM basal forebrain post-mortem maps (Eickhoff et al., 2006; Eickhoff et al., 2007; Eickhoff et al., 2005), respectively. This showed an overlap of 50% for the BF raw mask with the raw probabilistic post-mortem map, an overlap of 85% for the BF MPM map with the raw probabilistic post-mortem map and an overlap of 46% for the BF MPM map with the MPM post-mortem map. Neither the BF raw nor the BF MPM map was specific for cholinergic cells of the basal forebrain, but rather represented the general basal forebrain area. Using the aforementioned registration between the subject and atlas, the basal forebrain masks were propagated into the subjects' space and any voxels labeled as CSF (from CSF segmentation) were removed. The resulting mask was then used to extract the GM volume.

Because the basal forebrain masks were created based on atrophy maps derived from comparing AD and control subjects from the AIBL cohort, we tested whether the BF raw mask was able to detect changes in the AIBL cohort as well as in an independent cohort, namely the ADNI cohort (Fig. 2). This analysis revealed similar changes between AD and control subjects as well as AD and aMCI subjects in both cohorts.

2.4 PET image processing

The PET images were processed as described by Bourgeat et al. (2010). In summary, PET and MR images were co-registered. The PiB images were standard uptake value ratio (SUVR) normalized (pons WM) with PiB+ defined as SUVR>0.71 (Villain et al., 2012) and neocortical PiB retention calculated within the GM segmentation.

2.5 Statistical analysis

The Statistics Software Package for the Social Sciences (SPSS, v20.0) was used to determine significant differences and correlations. Group comparisons were performed using ANOVA followed by the Bonferroni post-hoc test. The parameters compared between groups were corrected for age. Partial correlations controlling for age were used to determine significant associations between parameters. There was no significant difference for sex or years of education between groups. Basal forebrain volume, hippocampal volume and neocortical PiB retention values were significantly correlated to age but not sex or years of education.

Hierarchical cluster analysis was used to determine the basal forebrain volumes that distinguished discrete clusters. Two-step cluster analysis automatically identified three existing clusters in the basal forebrain volume data, and both non-hierarchical (K-means) cluster analysis and two-step cluster analysis provided highly similar cluster groups. The two-graph receiver operating characteristic (TG-ROC) was used to determine cut-off values between clusters (Greiner, 1995). The odds ratio (OR) was calculated to determine the probability of subjects being within the in high/medium vs. low-risk basal forebrain volume group at baseline if their diagnosis worsened at follow-up. A chi-square test was used to determine the significance of this ratio.

3. Results

3.1 Differences in basal forebrain volume between HC, aMCI and AD subjects

To measure basal forebrain atrophy in this study, four different masks were used (Fig. 1). These masks were based on raw probabilistic (BF raw) and MPM maps (BF MPM, BF MPM anterior and BF MPM posterior) of post-mortem delineations of the basal forebrain, and further restricted to represent basal forebrain areas found to undergo atrophy in AD subjects versus age-matched controls. The results of group comparisons of BF raw volumes in the AIBL and ADNI cohorts (Fig. 2) and group comparisons of BF MPM volumes in the AIBL cohort (Table 3) are shown. All basal forebrain volumes of the AD group were significantly less than those of HC subjects. In addition AD subjects had significantly smaller basal forebrain volumes than aMCI subjects. The BF raw volumes between the HC and aMCI groups in the ADNI cohort were not significantly different. Furthermore all basal forebrain volumes of aMCI subjects were significantly smaller than those of HC PiB- subjects (control subjects showing low PiB retention values), but only the BF raw volume of aMCI subjects was significantly different from that of HC PiB+ subjects (control subjects showing high PiB retention values). To test whether controls at risk of developing AD, according to PiB retention status, namely HC PiB+ subjects, had smaller basal forebrain volumes than HC PiB- subjects, we compared the two groups. No significant difference in the mean basal forebrain volume between the HC PiB+ and HC PiB- groups was detected.

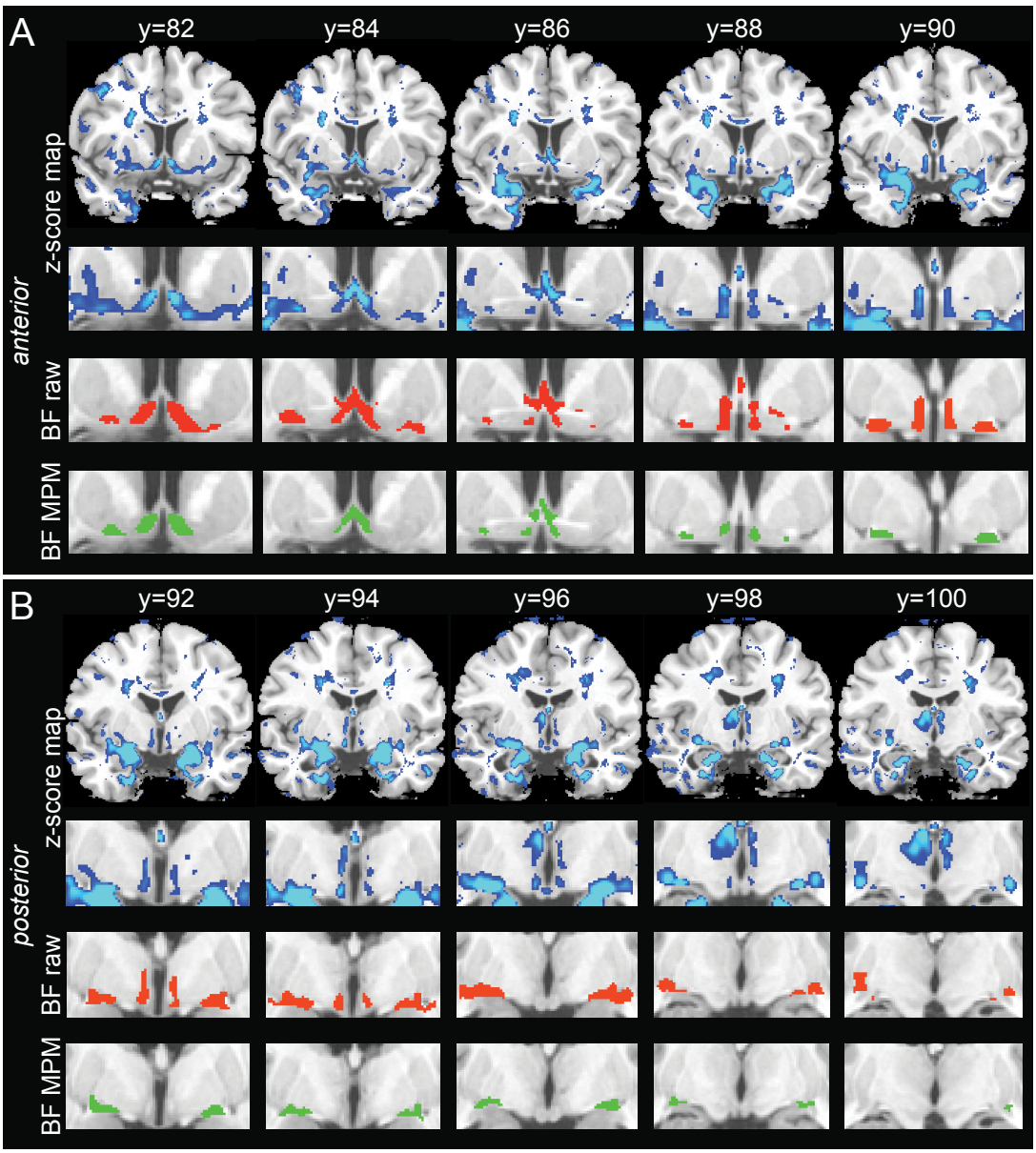

Figure 1: Basal forebrain masks of AD-specific changes in template space. Coronal slices illustrating the z-score map on a whole template brain (blue; top row A, B) calculated by comparing the HC and AD groups in the AIBL study. In the lower rows (A, B), a magnified view of the basal forebrain area is shown to better illustrate the z-score map (blue) as well as individual basal forebrain volumes. The BF raw mask (red; A, B) was used as a combination of the anterior and posterior parts for analysis of the whole basal forebrain area. The BF MPM mask (green; A, B) was used both as a combination of the anterior and posterior regions, and the anterior and posterior regions individually, to analyze the basal forebrain area. The same slices at different levels from rostral to caudal are shown in A and B, on a T1-weighted image. BF = basal forebrain, MPM = maximum probability map.

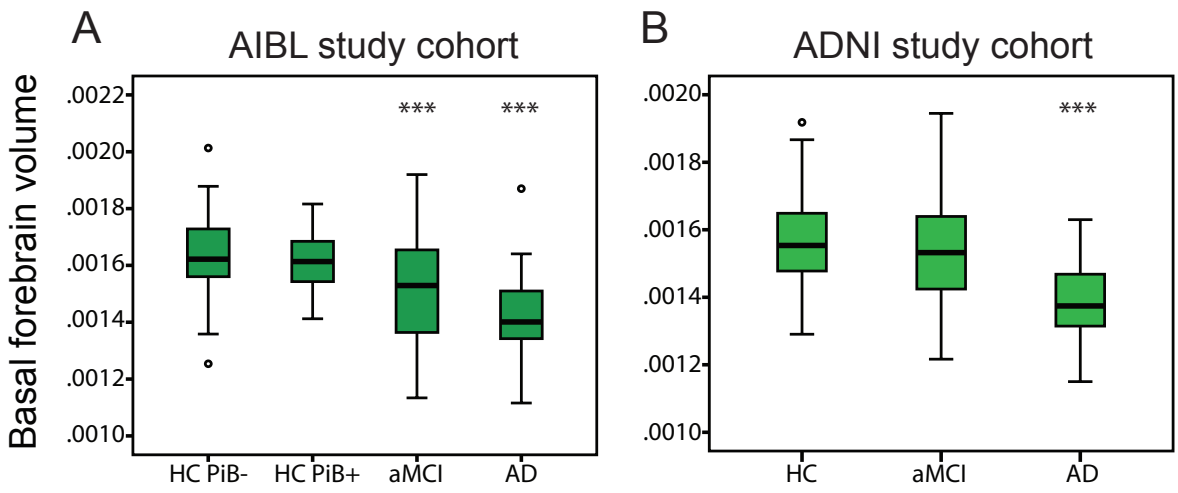

Figure 2: Group comparisons of basal forebrain volume in the AIBL and ADNI study cohorts. In the AIBL (A) study, the basal forebrain volume was significantly decreased in the AD and aMCI groups compared to controls. In the ADNI study (B), the basal forebrain volume of the AD subject group was significantly smaller than that of the HC and aMCI subject groups. Basal forebrain volumes of the aMCI groups display high variability in both study cohorts. *** p<0.001. Whiskers represent min/max values except data points (circles) more than 1.5 interquartile ranges away from the 75th percentile.

Volume	AD vs HC PiB+	AD vs HC PiB-	AD vs aMCI	aMCI vs HC PiB+	aMCI vs HC PiB-	HC PiB+ vs HC PiB-
BF raw	<0.001	<0.001	0.002	0.02	<0.001	1.0
BF MPM	<0.001	<0.001	0.001	0.151	0.002	1.0
BF MPM anterior	<0.001	<0.001	0.026	0.066	0.001	1.0
BF MPM posterior	<0.001	<0.001	0.021	0.393	0.001	0.385

Table 3: P-values of group comparisons of basal forebrain volumes in the AIBL cohort. All volumes were significantly different between the AD and control, AD and aMCI as well as aMCI and HC PiB- groups, whereas only the BF raw volume was significantly different between the aMCI and HC PiB+ subjects. BF = basal forebrain, MPM = maximum probability map.

3.2 Correlation between whole basal forebrain volumes and neocortical amyloid burden

To determine whether the volume of the whole basal forebrain area was correlated to the neocortical amyloid level measured by PiB-PET we performed partial age-controlled correlations between the two measures in the AIBL cohort. Scatter plots of BF raw volume correlations are shown in Fig. 3 and r- and p-values of BF raw as well as BF MPM volumes are listed in Table 4. We found that, on average, subjects with high Aβ burden, regardless of clinical diagnosis, had smaller BF raw and BF MPM volumes, whereas subjects with low Aβ burden had basal forebrain volumes in the normal range. Correlations in individual groups, namely in the HC (PiB+ and PiB-), aMCI (PiB+ and PiB-) and AD groups revealed that the BF raw volume was correlated to the neocortical PiB retention value in the AD ($r=0.39$; $p<0.05$) and HC PiB+ ($r=0.31$; $p<0.05$) groups, but not in the aMCI PiB+ ($r=0.33$; $p=0.12$), aMCI PiB- ($r=0.17$; $p=0.55$) and HC PiB- ($r=0.09$; $p=0.36$) groups. In contrast, neither BF MPM volume, nor hippocampal volume (data not shown), was correlated to the neocortical PiB retention in any of the abovementioned groups.

3.3 Correlation between anterior/posterior basal forebrain volumes and neocortical amyloid burden

Anterior basal forebrain volume (BF MPM anterior), representing the medial septum (Ch1 nucleus) and the vertical (Ch2 nucleus) and horizontal diagonal band of Broca (Ch3 nucleus), as well as anterior parts of the nucleus basalis of Maynert (Ch4 nucleus), was significantly correlated to neocortical PiB retention (Fig. 4, Table 4) when pooling all subjects together ($r=0.43$; $p<0.001$), as well as in the AD ($r=0.42$; $p<0.05$) and aMCI PiB+ ($r=0.43$; $p<0.05$) groups but not the HC PiB+ ($r=0.06$; $p=0.71$) group alone. Notably the posterior basal forebrain volume (BF MPM posterior), corresponding to intermediate and posterior parts of the NbM (Ch4 nucleus), was correlated to neocortical PiB retention (Fig. 4, Table 4) in all subjects ($r=0.44$; $p<0.001$) and HC PiB+ subjects (0.33; $p<0.05$) alone, but not in the aMCI PiB+ ($r=0.29$; $p=0.19$) and AD ($r=0.22$; $p=0.19$) subject groups. There was no correlation of either BF MPM anterior or BF MPM posterior volume to neocortical Aβ burden in the HC PiB- and aMCI PiB- groups.

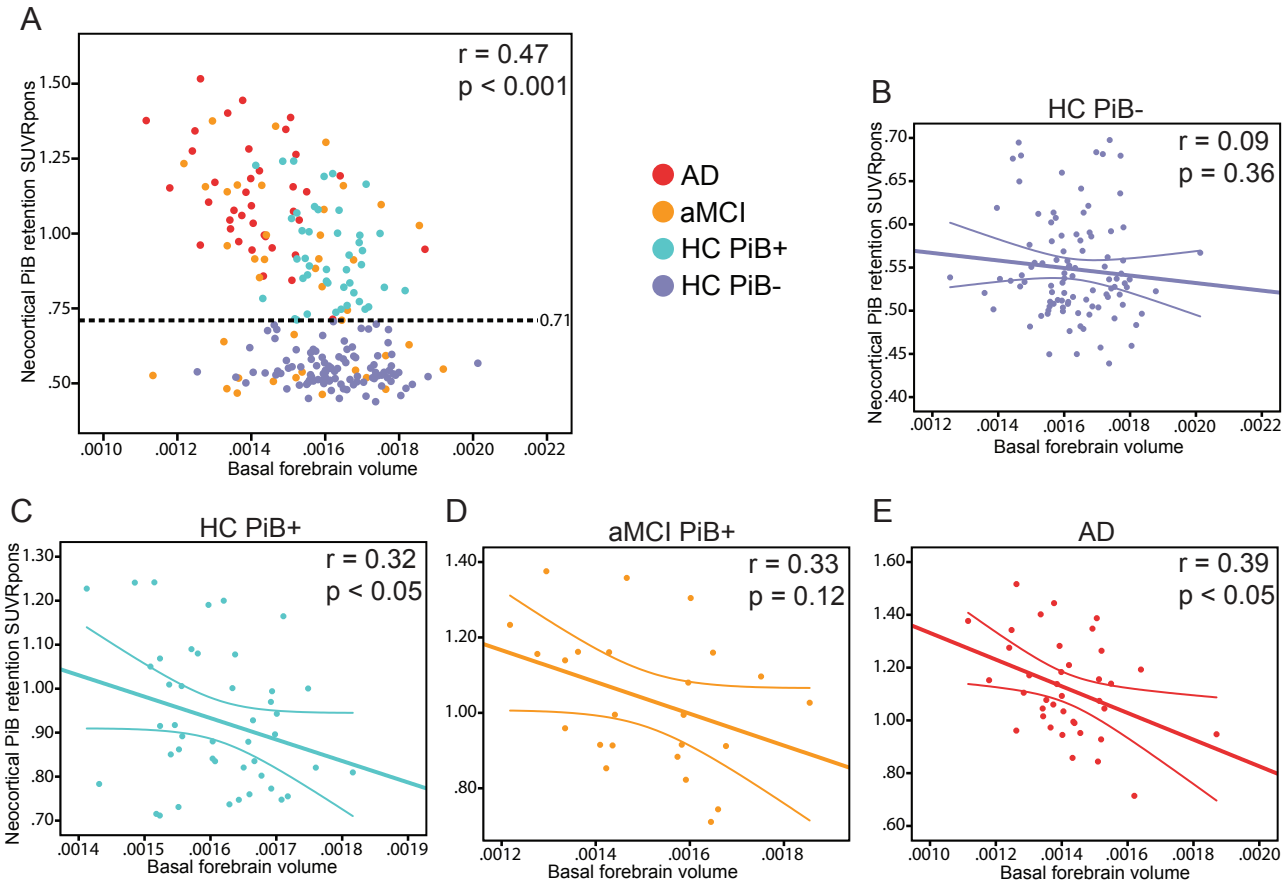

Figure 3: Correlation of BF raw volume (x-axis) to neocortical PiB retention (y-axis) in the AIBL study. The interaction between the two measures is shown for all subjects pooled together (A) as well for individual subject groups (B-E). The cut-off value used to determine high and low PiB status (0.71) at the baseline time point is indicated in (A) by the horizontal dashed line. Significant interactions were observed in the HC PiB+ (C) and AD (D) subject groups. Even though the correlation coefficient was high in the aMCI PiB+ group, the interaction was not significant. A linear fit line with 95% confidence interval is shown.

Volume		All subjects	HC PiB-	HC PiB+	aMCI	aMCI PiB+	AD
BF raw	r	0.47	0.09	0.32	0.18	0.33	0.39
	p-value	<0.001	0.36	<0.05	0.27	0.12	<0.05
BF MPM	r	0.46	0.17	0.24	0.26	0.39	0.32
	p-value	<0.001	0.1	0.12	0.11	0.066	0.053
BF MPM anterior	r	0.43	0.17	0.06	0.23	0.43	0.42
	p-value	<0.001	0.1	0.71	0.16	<0.05	<0.05
BF MPM posterior	r	0.44	0.13	0.33	0.25	0.29	0.22
	p-value	<0.001	0.19	<0.05	0.12	0.19	0.19

Table 4: Correlations of basal forebrain volumes to the neocortical PiB retention values in groups of the AIBL cohort. Significant interactions were found for BF raw and BF MPM posterior volumes in the HC PiB+ group, whereas BF raw and BF MPM anterior volumes showed significant interactions in the AD group. Only the BF MPM anterior volume was significantly correlated to neocortical PiB retention in aMCI PiB+ subjects. BF = basal forebrain, MPM = maximum probability map.

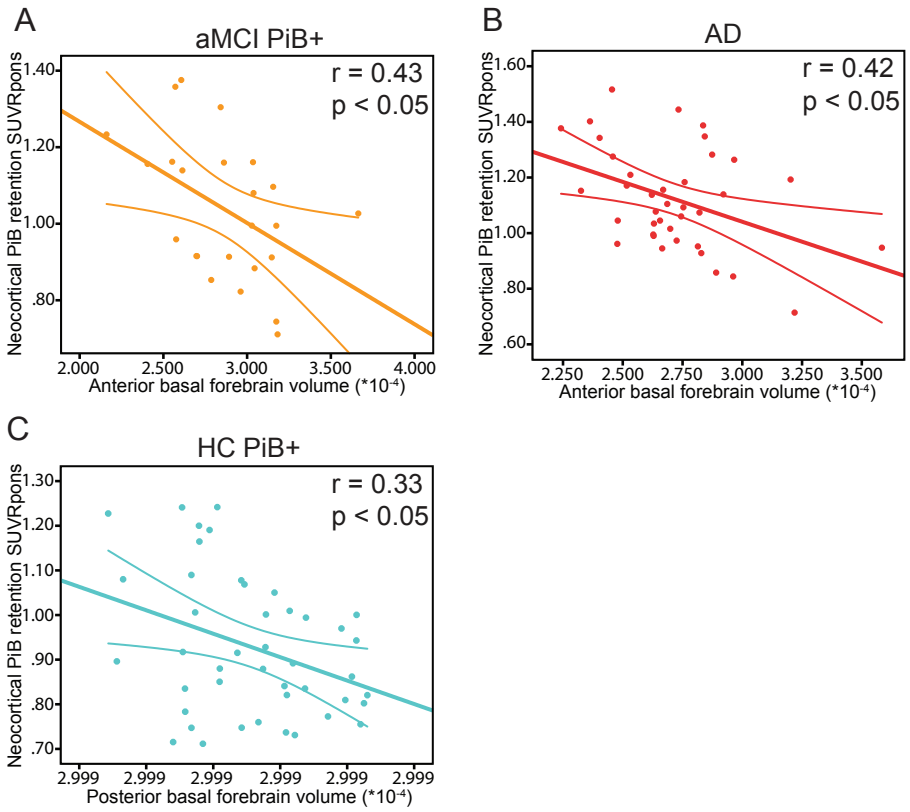

Figure 4: Significant correlations of anterior and posterior BF MPM posterior volumes (x-axis) to neocortical PiB retention (y-axis) in the AIBL study. Whereas BF MPM anterior volume showed significant correlations in aMCI PiB+ (A) and AD (B) subjects, BF MPM posterior volume was significantly correlated to neocortical PiB retention in HC PiB+ (C) subjects. A linear fit line with 95% confidence interval is shown.

3.4 Basal forebrain cluster analysis for diagnosis of converters

To test the diagnostic potential of basal forebrain volume in identifying subjects at risk of converting from either HC to aMCI, or aMCI to AD clinical status, we performed cluster analysis of basal forebrain volume (BF raw) in the AIBL (Figure 5) and ADNI (data not shown) cohorts using all subjects, irrespective of diagnostic status. Three clusters of normal, reduced and low basal forebrain volume were revealed, and similar cut-off values were found to separate the clusters in both study cohorts. The mean basal forebrain volume of the AD and the aMCI groups fell into the low and reduced basal forebrain volume clusters, respectively. In addition, the mean basal forebrain volume of the HC subjects who were PiB+ fell within the reduced basal forebrain cluster. Moreover, in both the AIBL and ADNI cohorts, the basal forebrain volumes of subjects whose diagnosis changed from either HC to aMCI (AIBL, n=3), HC to AD (AIBL, n=1) or aMCI to AD (AIBL, n=5; ADNI, n=3) were found in either the low or reduced basal forebrain volume group (with the exception of one PIB+ aMCI subject). Cluster analysis of hippocampal volume (data not shown) revealed that all but one PiB- subject, whose diagnosis worsened, fell in either the low or reduced hippocampal volume cluster. Finally, we found that the risk of having a worse diagnosis within ~18 months (based on calculations using AIBL data) was significantly greater (OR=7.2; chi-squared=4.53, $p<0.05$) for subjects falling into either the low or reduced basal forebrain volume category, as compared to subjects with a basal forebrain volume in the normal range.

3.5 Neocortical and cerebellar volume group comparisons and correlations with basal forebrain volume

The AD group was found to have a significantly reduced mean neocortical volume as compared to the HC PiB+ group (Table 5). There were no other neocortical volume differences between groups, and cerebellar volumes were not significantly reduced in any of the subject groups (Table 5). To assess whether basal forebrain atrophy was associated with neocortical atrophy or cerebellar volume, correlations of basal forebrain volumes with neocortical and cerebellar volumes were performed. No significant correlation of basal forebrain volume to either neocortical or cerebellar volume was found.

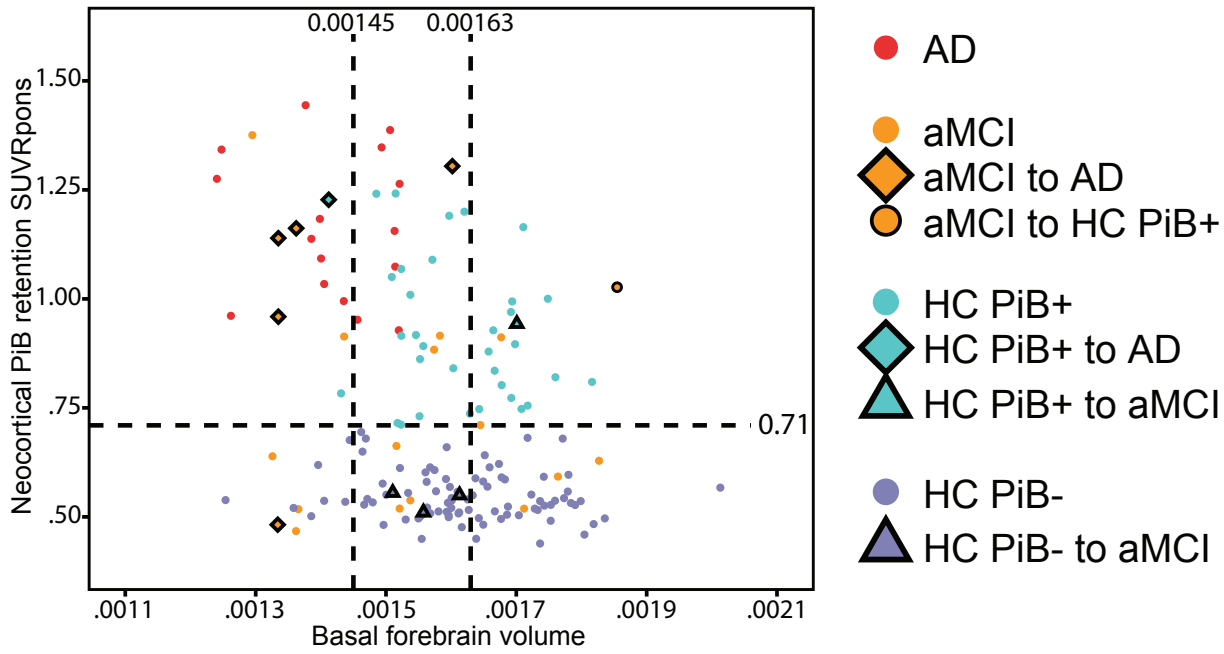

Figure 5: Delineations based on basal forebrain cluster analysis using the BF raw volume, highlighting the subjects in the AIBL study whose diagnosis worsened ('converters'). In the AIBL study. Basal forebrain cut-off values of 0.00145 and 0.00163 were determined by hierarchical cluster analysis to distinguish three clusters (delineated by vertical dashed lines); the PiB cut-off value of 0.71 is indicated by the horizontal dashed line. Subjects are colored according to their group status at baseline. The mean basal forebrain volume for each group is as follows (given in mean ± SD): AD: 0.001414 ± 0.000138; aMCI: 0.001525 ± 0.000184; HC PiB+: 0.001612 ± 0.000089; HC PiB-: 0.001629 ± 0.000123. The converters are indicated by the diamond-shaped (conversion to AD), triangular (conversion to aMCI) and circular (reversion to HC) data points, with the fill showing the group status at baseline. All but one HC PiB+ to aMCI converting subject fall into the high or medium risk clusters. The subject reverting from aMCI to HC PiB+ group status is shown as a circular data point with a black border. aMCI to AD = aMCI diagnosis at baseline, AD diagnosis at follow up; aMCI to HC PiB+ = aMCI diagnosis at baseline, HC PiB+ diagnosis at follow up; HC PiB+ to AD = HC PiB+ diagnosis at baseline, AD diagnosis at follow up; HC (PiB+ or PiB-) to aMCI = HC diagnosis at baseline, aMCI diagnosis at follow up.

	Neocortex				Cerebellum			
Group	Volume	Group comparisons vs	p-value	Correlation (r)	Volume	Group comparisons vs	p-value	Correlation (r)
HC PiB-	0.433 ±0.021	HC PiB+ aMCI AD	0.3 1.0 0.53	0.14	0.011 ±0.001	HC PiB+ aMCI AD	1.0 1.0 1.0	0.08
HC PiB+	0.440 ±0.018	aMCI AD	1.0 0.02 *	0.08	0.011 ±0.001	aMCI AD	1.0 1.0	0.02
aMCI	0.437 ±0.019	AD	0.13	0.14 (0.18)[#]	0.011 ±0.001	AD	1.0	0.28 (0.1)[#]
AD	0.426 ±0.022	HC PiB+/-	0.02 *	0.12	0.010 ±0.001	HC PiB+/-	0.14	0.05

Table 5: Results of neocortical and cerebellar volume analysis in the AIBL cohort. Average volumes, group comparisons and correlation coefficients of each structure to BF raw volumes are shown. There was a significant difference for neocortical volume between the AD and HC PiB+ group (denoted by *), but not between other groups. We did not find differences in the cerebellar volume and no significant correlation of basal forebrain volume to either neocortical or cerebellar volume was found. Volumes are expressed as mean ± SD.

* significant difference at $p<0.05$

[#] correlation value for the aMCI PiB+ group is shown in bracket

4. Discussion

Despite AD being characterized by both accumulation of Aβ and atrophy of the basal forebrain, the relationship between these two pathological features has not been widely investigated within independent patient cohorts. We confirm the findings recently published using data from the ADNI cohort (Grothe et al., 2014; Teipel et al., 2013) and demonstrate here that whole basal forebrain volume significantly correlates with neocortical Aβ burden, measured through PiB retention, in AD and HC PiB+ groups. In the HC PiB+ group, neocortical Aβ burden correlates with posterior basal forebrain volume, whereas in aMCI PiB+ and AD groups, neocortical Aβ burden correlates with anterior basal forebrain volume. Furthermore, subjects who retrospectively converted from a diagnosis of either HC to aMCI or aMCI to AD were found to have reduced basal forebrain volumes prior to conversion. These findings provide validity to emerging human and animal studies demonstrating a link between cholinergic basal forebrain neuron degeneration and Aβ production and/or deposition (Gil-Bea et al., 2012; Grothe et al., 2014; Ramos-Rodriguez et al., 2013; Teipel et al., 2013).

The interaction between basal forebrain volume and neocortical Aβ burden was studied using whole, anterior or posterior basal forebrain masks created by delimiting those areas found to undergo atrophy in AD subjects (versus age-matched controls) within the basal forebrain area. However the final masks showed only partial overlap with not yet publicly available post-mortem maps, developed by Eickhoff (Heinrich-Heine University Düsseldorf) and colleagues, being significantly larger; We acknowledge that this may represent areas of atrophy in anatomically close brain regions in some subjects, but nonetheless, we reasoned that this method of estimating basal forebrain volume may provide increased sensitivity to detect change in AD over the purely post-mortem -based segmentations previously used by others. Indeed, the results of our volumetric analysis using the atrophy-based whole basal forebrain mask are consistent with the findings of previous studies in which subnuclei of the basal forebrain or closely located brain regions were analyzed (Grothe et al., 2012; Grothe et al., 2011; Grothe et al., 2010), with differences in average basal forebrain volume being detected when comparing healthy controls to AD, very mild AD, and MCI groups. The analysis of the ADNI cohort shown here (Fig. 2) further supports data presented previously (George et al., 2011).

Interestingly, there was a significant difference between aMCI and HC PiB+ groups for BF raw but not BF MPM volumes in the AIBL cohort. This might be explained by the fact that

the BF raw volume is almost three times the size of the BF MPM volume and may therefore be more sensitive to overall changes. The absence of a significant correlation between basal forebrain volume and either neocortical volume or cerebellar volume (Table 5) further strengthens the specificity of basal forebrain degeneration assessed by our measurements as a feature of AD pathology.

In order to investigate whether the correlations between whole basal forebrain volume with neocortical PiB retention observed in this study were driven by interactions with sub-areas of the basal forebrain, we performed correlations of the anterior (Ch1, Ch2, Ch3 and Ch4 anterior nuclei) and posterior (Ch4 intermediate and posterior nuclei) basal forebrain volumes with neocortical PiB retention. In the earliest stages of AD the posterior and intermediate parts of the Ch4 cell group, which are represented by the BF MPM posterior volume in this paper, are the regions predominantly affected by pathological changes (Grothe et al., 2011). The posterior basal forebrain nuclei send projections to the temporal lobe, amygdala and peristrate and orbital cortices, as well as to brain regions subject to heavy Aβ deposition, such as the frontal, cingulate and parietal cortices (Klunk et al., 2004). Furthermore, loss of cholinergic innervation to the aforementioned regions was recently found *in vivo* in MCI patients (Haense et al., 2012). Thus it is significant that we found a correlation between posterior basal forebrain volume and neocortical PiB retention in the HC PiB+ group, a cohort which represents a control subgroup that might be at high risk of developing AD.

We also observed significant correlations of neocortical PiB retention with BF MPM anterior volume in the aMCI PiB+ and AD groups. In this study, even though the BF raw mask was more sensitive than the BF MPM maps in identifying volumetric differences between groups, BF MPM volumes showed higher correlation coefficients and identified additional significant interactions with neocortical PiB retention as compared to the associations with BF raw volume. In addition, raw probabilistic maps have been shown to be at risk of misclassifying voxels, whereas MPM maps should not suffer from this limitation despite showing similar sensitivity (Eickhoff et al., 2006). Therefore we recommend the use of BF MPM maps, particularly subregional anterior/posterior volumes, for the future study of associations between global Aβ burden and basal forebrain volumes.

The associations between basal forebrain volumes and amyloid burden presented in this work are consistent with previous reports of a correlation between AV45 retention and basal forebrain volume (Grothe et al., 2014), and the finding that, as subjects progress to

aMCI and AD clinical status, changes in anterior basal forebrain areas, containing nuclei that project to the hippocampus, olfactory bulb and piriform and entorhinal cortices, become much more pronounced (Grothe et al., 2011). In line with this are also recent studies demonstrating cholinergic neuronal dysfunction in the cerebral cortex in MCI and AD based on the use of PET to assess the activity of the key cholinergic enzyme acetylcholine esterase. Acetylcholine esterase is primarily membrane-bound and located on presynaptic cholinergic neurons, and its activity is known to reflect the integrity of the ascending cholinergic system (Garibotto et al., 2013). Degeneration of the cortical cholinergic projection system arising from posterior basal forebrain nuclei, represented by the posterior mask in this paper, was found to occur at early stages of dementia (Haense et al., 2012; Herholz et al., 2008). This is consistent with early dysfunction of posterior nucleus basalis of Meynert neurons, and acetylcholine esterase activity in temporal lobe regions has also been correlated to memory impairment in MCI and AD patients (Haense et al., 2012; Marcone et al., 2012).

While the correlations between basal forebrain volume and neocortical PiB retention reported here may merely reflect the progressive nature of basal forebrain atrophy occurring independently of increasing Aβ load, we hypothesize that this is not the case. Firstly, Aβ burden does not correlate with atrophy of other brain areas, including the hippocampus. Previous work using data from the AIBL study has reported a correlation between hippocampal volume and temporal neocortical PiB retention in the HC PiB+ group (Bourgeat et al., 2010) and subjective cognitively impaired subjects (Chetelat et al., 2010). However, no correlations were found for the AD or the MCI groups, and atrophy of the hippocampus did not correlate with hippocampal PiB retention in another AIBL study (Rowe et al., 2010). Furthermore, similar analyses of AIBL subjects, performed in the present study, failed to reveal any correlation between hippocampal volume and neocortical PiB retention in any subject group (data not shown). Moreover, the correlation in the AD group between BF raw volume and PiB retention increased from $r = 0.39$ to $r = 0.42$ when controlling for hippocampal volume. This indicates that the relationship between basal forebrain volume and Aβ deposition is not driven purely by reduced hippocampal volume, even though these volumes are strongly correlated (data not shown).

Furthermore, in agreement with our findings, a recent study suggested that basal forebrain atrophy can predict cortical amyloid burden, and is more closely associated with cortical amyloid burden than hippocampal atrophy (Teipel et al., 2013). Secondly, a causal relationship is supported by emerging studies in animal models of AD in which cholinergic

basal forebrain neuron shrinkage, synaptic loss and axonal degeneration partly caused by, or causing, Aβ deposition in the brain, have been reported (Gil-Bea et al., 2012; Knowles et al., 2009; Ramos-Rodriguez et al., 2013; Sotthibundhu et al., 2008). Although our basal forebrain measurments encompasse a structure which is heterogenous in nature, the cholinergic neurons of the basal forebrain are preferentially lost in AD (Mufson, 2003) and their degeneration could, at least partly, account for the observed reduction in basal forebrain volume. It also remains to be determined what other factors might correlate with or drive basal forebrain volume loss and/or Aβ burden. Of particular relevance is the development of tau pathology that occurs in basal forebrain neurons (Braak et al., 2006; Braak and Del Tredici, 2004, 2011). Tau pathology is more strongly associated with cognitive decline (Braak and Braak, 1991) and is likely to have pronounced effects on basal forebrain volumetric measures.

Regardless of the cause of the observed basal forebrain volume loss, in support of the assertion that early basal forebrain atrophy is a key disease hallmark, cluster analysis of raw BF volume, including analysis of subjects whose diagnosis converted to more cognitively impaired, revealed that most subjects converting from HC to aMCI or from aMCI to AD had a low basal forebrain volume prior to conversion. All converters in both the AIBL and ADNI studies (with the exception of one aMCI PiB+ subject) fell into the low or reduced basal forebrain volume clusters prior to conversion, which could be considered to be the high/medium risk categories. In the AIBL study the mean basal forebrain volumes of AD subjects fell into the low volume cluster whereas mean basal forebrain volumes of the aMCI, HC PiB+ and HC PiB+ groups fell into the reduced volume cluster. Subjects in the latter groups were found in all three volume clusters indicating that the range of basal forebrain volumes is large even in non-demented elderly subjects, which is a limitation of using only basal forebrain volumetric measures for diagnostic purposes.

Nevertheless we found that subjects belonging to the high/medium risk categories in the AIBL study were 7.2 times more likely to convert to more cognitively impaired than subjects in the low risk category. Interestingly, 3 of the normal controls in the medium risk category who were cognitively impaired at follow up were PiB- at the time of baseline diagnosis, again indicating that basal forebrain atrophy might be a preclinical marker of dementia, albeit that these people may not progress to AD. Although the sample size used to assess basal forebrain volumes for risk of conversion was small, and additional longitudinal data are required to verify our findings, the significant cumulative evidence for basal forebrain atrophy being observed in life in AD clinical cohorts provides increasing

impetus for including basal forebrain volume in the general “atrophy signature” for the diagnosis of patients at risk of, or with, AD. Furthermore, basal forebrain measures used in conjunction with other disease markers, such as Aβ load (Kim et al., 2012; Villemagne et al., 2011), may further delineate subjects at risk of progressing to AD or those for whom other interventions, including anti-Aβ treatments, may be of most benefit.

Acknowledgements

GMK was funded by an ANZ Trustees PhD scholarship for medical research and a University of Queensland International Scholarship. EJC was supported by a National Health and Medical Research Council of Australia Career Development Fellowship (569601). This project was funded by a Mason Foundation grant and Queensland State Government National and International Research Alliance Project grant. The study was partially supported by the Commonwealth Scientific Industrial Research Organisation Preventative Health Flagship Program through the Australian Imaging, Biomarkers, and Lifestyle flagship study of aging, the Austin Hospital Medical Research Foundation, Neurosciences Victoria, and the University of Melbourne. The funding sources had no input into the design of this study, the analysis of data, or writing of the manuscript.
Data collection and sharing for this project was funded by the Alzheimer's Disease Neuroimaging Initiative (ADNI) (National Institutes of Health Grant U01 AG024904). ADNI is funded by the National Institute on Aging, the National Institute of Biomedical Imaging and Bioengineering, and through generous contributions from the following: Alzheimer's Association; Alzheimer's Drug Discovery Foundation; BioClinica, Inc.; Biogen Idec Inc.; Bristol-Myers Squibb Company; Eisai Inc.; Elan Pharmaceuticals, Inc.; Eli Lilly and Company; F. Hoffmann-La Roche Ltd and its affiliated company Genentech, Inc.; GE Healthcare; Innogenetics, N.V.; IXICO Ltd.; Janssen Alzheimer Immunotherapy Research & Development, LLC.; Johnson & Johnson Pharmaceutical Research & Development LLC.; Medpace, Inc.; Merck & Co., Inc.; Meso Scale Diagnostics, LLC.; NeuroRx Research; Novartis Pharmaceuticals Corporation; Pfizer Inc.; Piramal Imaging; Servier; Synarc Inc.; and Takeda Pharmaceutical Company. The Canadian Institutes of Health Research are providing funds to support ADNI clinical sites in Canada. Private sector contributions are facilitated by the Foundation for the National Institutes of Health (www.fnih.org). The grantee organization is the Northern California Institute for Research and Education, and the study is coordinated by the Alzheimer's Disease Cooperative Study at the University of California, San Diego. ADNI data are disseminated by the Laboratory for Neuro Imaging at the University of California, Los Angeles. This research was also supported by NIH grants P30 AG010129 and K01 AG030514.
We would like to thank Pierrick Bourgeat for helpful discussions and Chris Bell for technical assistance.

References

Avants, B.B., Yushkevich, P., Pluta, J., Minkoff, D., Korczykowski, M., Detre, J., Gee, J.C., 2010. The optimal template effect in hippocampus studies of diseased populations. NeuroImage 49, 2457-2466.

Bourgeat, P., Chetelat, G., Villemagne, V.L., Fripp, J., Raniga, P., Pike, K., Acosta, O., Szoeke, C., Ourselin, S., Ames, D., Ellis, K.A., Martins, R.N., Masters, C.L., Rowe, C.C., Salvado, O., 2010. Beta-amyloid burden in the temporal neocortex is related to hippocampal atrophy in elderly subjects without dementia. Neurology 74, 121-127.

Braak, H., Alafuzoff, I., Arzberger, T., Kretzschmar, H., Del Tredici, K., 2006. Staging of Alzheimer disease-associated neurofibrillary pathology using paraffin sections and immunocytochemistry. Acta Neuropathologica 112, 389-404.

Braak, H., Braak, E., 1991. Neuropathological stageing of Alzheimer-related changes. Acta Neuropathologica 82, 239-259.

Braak, H., Del Tredici, K., 2004. Alzheimer's disease: intraneuronal alterations precede insoluble amyloid-beta formation. Neurobiology of Aging 25, 713-718; discussion 743-716.

Braak, H., Del Tredici, K., 2011. The pathological process underlying Alzheimer's disease in individuals under thirty. Acta Neuropathologica 121, 171-181.

Chetelat, G., Villemagne, V.L., Bourgeat, P., Pike, K.E., Jones, G., Ames, D., Ellis, K.A., Szoeke, C., Martins, R.N., O'Keefe, G.J., Salvado, O., Masters, C.L., Rowe, C.C., 2010. Relationship between atrophy and beta-amyloid deposition in Alzheimer disease. Annals of Neurology 67, 317-324.

Contestabile, A., 2011. The history of the cholinergic hypothesis. Behavioural Brain Research 221, 334-340.

Eickhoff, S.B., Heim, S., Zilles, K., Amunts, K., 2006. Testing anatomically specified hypotheses in functional imaging using cytoarchitectonic maps. NeuroImage 32, 570-582.

Eickhoff, S.B., Paus, T., Caspers, S., Grosbras, M.H., Evans, A.C., Zilles, K., Amunts, K., 2007. Assignment of functional activations to probabilistic cytoarchitectonic areas revisited. NeuroImage 36, 511-521.

Eickhoff, S.B., Stephan, K.E., Mohlberg, H., Grefkes, C., Fink, G.R., Amunts, K., Zilles, K., 2005. A new SPM toolbox for combining probabilistic cytoarchitectonic maps and functional imaging data. NeuroImage 25, 1325-1335.

Ellis, K.A., Bush, A.I., Darby, D., De Fazio, D., Foster, J., Hudson, P., Lautenschlager, N.T., Lenzo, N., Martins, R.N., Maruff, P., Masters, C., Milner, A., Pike, K., Rowe, C., Savage, G., Szoeke, C., Taddei, K., Villemagne, V., Woodward, M., Ames, D., 2009. The

Australian Imaging, Biomarkers and Lifestyle (AIBL) study of aging: methodology and baseline characteristics of 1112 individuals recruited for a longitudinal study of Alzheimer's disease. International Psychogeriatrics 21, 672-687.
Frisoni, G.B., Fox, N.C., Jack, C.R., Jr., Scheltens, P., Thompson, P.M., 2010. The clinical use of structural MRI in Alzheimer disease. Nature Reviews Neurology 6, 67-77.
Garibotto, V., Tettamanti, M., Marcone, A., Florea, I., Panzacchi, A., Moresco, R., Virta, J.R., Rinne, J., Cappa, S.F., Perani, D., 2013. Cholinergic activity correlates with reserve proxies in Alzheimer's disease. Neurobiology of Aging 34, 2694 e2613-2698.
George, S., Mufson, E.J., Leurgans, S., Shah, R.C., Ferrari, C., deToledo-Morrell, L., 2011. MRI-based volumetric measurement of the substantia innominata in amnestic MCI and mild AD. Neurobiology of Aging 32, 1756-1764.
Gil-Bea, F.J., Gerenu, G., Aisa, B., Kirazov, L.P., Schliebs, R., Ramirez, M.J., 2012. Cholinergic denervation exacerbates amyloid pathology and induces hippocampal atrophy in Tg2576 mice. Neurobiology of Disease 48, 439-446.
Greiner, M., 1995. Two-graph receiver operating characteristic (TG-ROC): a Microsoft-EXCEL template for the selection of cut-off values in diagnostic tests. Journal of Immunological Methods 185, 145-146.
Grothe, M., Heinsen, H., Teipel, S., 2012. Longitudinal measures of cholinergic forebrain atrophy in the transition from healthy aging to Alzheimer's disease. Neurobiology of Aging 34, 1210-1220.
Grothe, M., Heinsen, H., Teipel, S.J., 2011. Atrophy of the cholinergic basal forebrain over the adult age range and in early stages of Alzheimer's disease. Biological Psychiatry 71, 805-813.
Grothe, M., Zaborszky, L., Atienza, M., Gil-Neciga, E., Rodriguez-Romero, R., Teipel, S.J., Amunts, K., Suarez-Gonzalez, A., Cantero, J.L., 2010. Reduction of basal forebrain cholinergic system parallels cognitive impairment in patients at high risk of developing Alzheimer's disease. Cerebral Cortex 20, 1685-1695.
Grothe, M.J., Ewers, M., Krause, B., Heinsen, H., Teipel, S.J., 2014. Basal forebrain atrophy and cortical amyloid deposition in nondemented elderly subjects. Alzheimer's & Dementia, doi: 10.1016/j.jalz.2013.09.011.
Haense, C., Kalbe, E., Herholz, K., Hohmann, C., Neumaier, B., Krais, R., Heiss, W.D., 2012. Cholinergic system function and cognition in mild cognitive impairment. Neurobiology of Aging 33, 867-877.
Hall, A.M., Moore, R.Y., Lopez, O.L., Kuller, L., Becker, J.T., 2008. Basal forebrain atrophy is a presymptomatic marker for Alzheimer's disease. Alzheimer's & Dementia 4, 271-279.

Herholz, K., Weisenbach, S., Kalbe, E., 2008. Deficits of the cholinergic system in early AD. Neuropsychologia 46, 1642-1647.
Kim, M.J., Lee, K.M., Son, Y.D., Jeon, H.A., Kim, Y.B., Cho, Z.H., 2012. Increased basal forebrain metabolism in mild cognitive impairment: an evidence for brain reserve in incipient dementia. Journal of Alzheimer's disease 32, 927-938.
Klunk, W.E., Engler, H., Nordberg, A., Wang, Y., Blomqvist, G., Holt, D.P., Bergstrom, M., Savitcheva, I., Huang, G.F., Estrada, S., Ausen, B., Debnath, M.L., Barletta, J., Price, J.C., Sandell, J., Lopresti, B.J., Wall, A., Koivisto, P., Antoni, G., Mathis, C.A., Langstrom, B., 2004. Imaging brain amyloid in Alzheimer's disease with Pittsburgh Compound-B. Annals of Neurology 55, 306-319.
Knowles, J.K., Rajadas, J., Nguyen, T.V., Yang, T., LeMieux, M.C., Vander Griend, L., Ishikawa, C., Massa, S.M., Wyss-Coray, T., Longo, F.M., 2009. The p75 neurotrophin receptor promotes amyloid-beta(1-42)-induced neuritic dystrophy in vitro and in vivo. The Journal of Neuroscience 29, 10627-10637.
Marcone, A., Garibotto, V., Moresco, R.M., Florea, I., Panzacchi, A., Carpinelli, A., Virta, J.R., Tettamanti, M., Borroni, B., Padovani, A., Bertoldo, A., Herholz, K., Rinne, J.O., Cappa, S.F., Perani, D., 2012. [11C]-MP4A PET cholinergic measurements in amnestic mild cognitive impairment, probable Alzheimer's disease, and dementia with Lewy bodies: a Bayesian method and voxel-based analysis. Journal of Alzheimer's disease 31, 387-399.
Mesulam, M., 2004. The cholinergic lesion of Alzheimer's disease: pivotal factor or side show? Learning & Memory 11, 43-49.
Mesulam, M.M., Mufson, E., Levey, A.I., Wainer, B.H., 1983. Cholinergic innervation of cortex by the basal forebrain: cytochemistry and cortical connectinos of the septal area, diagonal band nuclei, nucleus basalis (substantia innominata), and hypothalamus in the rhesus monkey. Journal of Comparative Neurology 214, 170-197.
Mufson, E., 2003. Human cholinergic basal forebrain: chemoanatomy and neurologic dysfunction. Journal of Chemical Neuroanatomy 26, 233-242.
Muth, K., Schonmeyer, R., Matura, S., Haenschel, C., Schroder, J., Pantel, J., 2010. Mild cognitive impairment in the elderly is associated with volume loss of the cholinergic basal forebrain region. Biological Psychiatry 67, 588-591.
Ramos-Rodriguez, J.J., Pacheco-Herrero, M., Thyssen, D., Murillo-Carretero, M.I., Berrocoso, E., Spires-Jones, T.L., Bacskai, B.J., Garcia-Alloza, M., 2013. Rapid beta-amyloid deposition and cognitive impairment after cholinergic denervation in APP/PS1 mice. Journal of Neuropathology and Experimental Neurology 72, 272-285.

Rowe, C.C., Ellis, K.A., Rimajova, M., Bourgeat, P., Pike, K.E., Jones, G., Fripp, J., Tochon-Danguy, H., Morandeau, L., O'Keefe, G., Price, R., Raniga, P., Robins, P., Acosta, O., Lenzo, N., Szoeke, C., Salvado, O., Head, R., Martins, R., Masters, C.L., Ames, D., Villemagne, V.L., 2010. Amyloid imaging results from the Australian Imaging, Biomarkers and Lifestyle (AIBL) study of aging. Neurobiology of Aging 31, 1275-1283.

Schliebs, R., Arendt, T., 2011. The cholinergic system in aging and neuronal degeneration. Behavioural Brain Research 221, 555-563.

Sotthibundhu, A., Sykes, A.M., Fox, B., Underwood, C.K., Thangnipon, W., Coulson, E.J., 2008. Beta-amyloid(1-42) induces neuronal death through the p75 neurotrophin receptor. The Journal of neuroscience : the official journal of the Society for Neuroscience 28, 3941-3946.

Teipel, S., Heinsen, H., Amaro, E., Jr., Grinberg, L.T., Krause, B., Grothe, M., 2013. Cholinergic basal forebrain atrophy predicts amyloid burden in Alzheimer's disease. Neurobiology of Aging, doi: 10.1016/j.neurobiolaging.2013.09.029.

Villain, N., Chetelat, G., Grassiot, B., Bourgeat, P., Jones, G., Ellis, K.A., Ames, D., Martins, R.N., Eustache, F., Salvado, O., Masters, C.L., Rowe, C.C., Villemagne, V.L., 2012. Regional dynamics of amyloid-beta deposition in healthy elderly, mild cognitive impairment and Alzheimer's disease: a voxelwise PiB-PET longitudinal study. Brain 135, 2126-2139.

Villemagne, V.L., Pike, K.E., Chetelat, G., Ellis, K.A., Mulligan, R.S., Bourgeat, P., Ackermann, U., Jones, G., Szoeke, C., Salvado, O., Martins, R., O'Keefe, G., Mathis, C.A., Klunk, W.E., Ames, D., Masters, C.L., Rowe, C.C., 2011. Longitudinal assessment of Abeta and cognition in aging and Alzheimer disease. Annals of Neurology 69, 181-192.

Zaborszky, L., Hoemke, L., Mohlberg, H., Schleicher, A., Amunts, K., Zilles, K., 2008. Stereotaxic probabilistic maps of the magnocellular cell groups in human basal forebrain. NeuroImage 42, 1127-1141.

2.3 Discussion and implication of findings

Overall, the work presented in this chapter demonstrated for the first time that global amyloid load in all evaluated groups, namely Alzheimer's disease and mild cognitively impaired subjects as well as healthy controls, is correlated to basal forebrain volume. In addition subjects with a basal forebrain volume below a certain cut-off value at the baseline time point of the study were at increased risk to show cognitive deterioration at the follow-up time point.

Through showing that the basal forebrain volume is significantly reduced in Alzheimer's disease and amnestic mild cognitive impairment we demonstrate that basal forebrain volumetrics might have significant diagnostic utility in the future. Furthermore, associations of basal forebrain volume with Aβ load and the potential predictive power of conversion of subjects strengthen this argument. Therefore the methods developed in this chapter represent the ground-work for future imaging studies aimed at examining basal forebrain degeneration in humans. Our findings of an amyloid-basal forebrain interaction were also recently confirmed by others in the field (Grothe et al., 2014).

Having observed a significant correlation between amyloid beta and basal forebrain degeneration the next question is whether this is due to a direct interaction and whether one phenomenon drives the other. Additional mechanistic investigations aiming to characterise an interaction between amyloid accumulation and basal forebrain neuronal degeneration in more detail will be required to answer this question. In particular, one model that could be tested based on the results of this study is that the neurons located in the nucleus basalis of Meynert, which were associated with amyloid in the healthy control group, could be particularly vulnerable to degeneration early on in the disease process.

Later in disease, atrophy of anterior basal forebrain areas, at least partly driven by amyloid accumulation, might become more pronounced. Another question is whether other features of Alzheimer's disease, such as the accumulation of tau, might have an additional effect on basal forebrain neuronal integrity, and this is the focus of the next chapter.
In summary, we developed new ways of imaging basal forebrain degeneration and demonstrated that these methods can be used to separate clinical groups. By showing that basal forebrain degeneration correlates with amyloid accumulation we have also further established basal forebrain degeneration as a hallmark of early Alzheimer's disease aetiology, and revealed that this process might commence in subjects with no apparent signs of cognitive impairment.

Chapter 3: Basal forebrain degeneration is associated with tau accumulation in Alzheimer's disease

3.1 Introduction

In addition to amyloid accumulation, aggregation of tau neurofibrillary tangles in Alzheimer's disease represents a key pathological hallmark of this condition. Unlike amyloid, tau has been shown to be associated with measures of cognitive decline such as MMSE and CDR in this condition (Okamura et al., 2014; Villemagne et al., 2014). It has been known for a while that the basal forebrain is one of the first places where tau accumulates in the brain. Subsequently temporal lobe areas and then other cortical areas are affected which are also brain regions receiving basal forebrain neuronal connections (Braak et al., 2006). However, like the interaction with amyloid accumulation, the relationship of tau aggregation with basal forebrain degeneration *in vivo* in humans remained unknown until the study in the following chapter was conducted.

Unlike amyloid imaging, a technology which has been available for ten years (Klunk et al., 2004), *in vivo* imaging of tau using PET compounds in humans was not possible until very recently. In collaboration with researchers from the AIBL study and the Tohuku University, who pioneered the initial development and first application of PET compounds capable of imaging tau NFTs in the human and animal brain (Fodero-Tavoletti et al., 2011; Okamura et al., 2014; Villemagne et al., 2014), we were able to investigate the relationship of basal forebrain volume with tau burden in two cohorts of normal controls and Alzheimer's disease patients using two different tracers to measure tau burden.

As imaging of both amyloid beta and tau was performed in the same subjects, another aim of the study was to compare the interaction of basal forebrain volume with tau aggregation, and amyloid aggregation.

This work is in preparation for submission to the journal *Nature Neuroscience* as a brief communication.

3.2 Cortical tau pathology is linked to basal forebrain degeneration in Alzheimer's disease

[1]**GM Kerbler**, [2]J Fripp, [2]S Rose, [5,6]M Fodero-Tavoletti, [7]S Furumoto, [3]C Rowe, [7]N Okamura, [3,4]VL Villemagne# and [1]EJ Coulson#. (2014) Cortical tau pathology is linked to basal forebrain degeneration in Alzheimer's disease. *In preparation for submission* to *Nature Neuroscience*

[1]Queensland Brain Institute, Clem Jones Centre for Ageing Dementia Research, The University of Queensland, Brisbane, 4072 Qld. Australia
[2]Commonwealth Scientific and Industrial Research Organisation, Computational Informatics, Brisbane, 4029 Qld. Australia
[3]Department of Nuclear Medicine and Centre for PET, Austin Health, Melbourne, 3084 Vic. Australia
[4]The Florey Institute of Neuroscience and Mental Health, The University of Melbourne, Melbourne, 3084 Vic. Australia
[5]Department of Pathology, The University of Melbourne, Melbourne, 3084 Vic. Australia
6Bio21 Molecular and Biotechnology Institute, The University of Melbourne, Melbourne, 3084 Vic. Australia
[7]Department of Pharmacology, Graduate School of Medicine, Tohoku University, Sendai, 980-8575, Japan
Joint senior authors

Abstract

Due to advances in clinical imaging, the preclinical relationships between the key pathological Alzheimer's disease (AD) hallmarks of amyloid-beta (Aβ) plaques, tau neurofibrillary tangles (NFTs) and neurodegeneration, can now be investigated. Here we show that basal forebrain atrophy correlates with cognitive performance, amyloid burden and tau aggregate levels in two independent cohorts of AD patients and controls, suggesting a close etiological relationship between these disease features.

Main text

The formation of Aβ plaques and NFTs are key hallmarks of AD that underpin synaptic and neuronal dysfunction and ultimately lead to gray matter atrophy and cognitive decline. Whereas Aβ is mostly deposited in allocortical structures such as the frontal, cingulate and parietal cortices [1], tau deposits are initially found in the locus coeruleus, basal forebrain (BF) and temporal lobe [2], before spreading to neocortical areas [3]. Another hallmark of the disease, loss of BF cholinergic neurons [4], may play a role in the cognitive dysfunction observed in AD patients [5] and these neurons are the target of the widely prescribed choline esterase inhibitors [6]. In particular the intermediate and posterior part of the nucleus basalis of Meynert of the BF, that projects to regions including the neocortex and the temporal lobe, is one of the areas that undergoes atrophy early in AD, whereas the anterior medial septal and diagonal band BF areas, which project to the orbitofrontal cortex and hippocampus, are affected later in the course of the disease [7].

Atrophy of the BF as measured by MRI has been shown to correlate with neocortical Aβ level in elderly cohorts [8, 9] However, Aβ load does not correlate well with clinical measures of cognitive impairment [10]. In contrast, at autopsy the level of subcortical tau correlates with loss of cholinergic BF neurons as well as AD neuropathology and preclinical cognitive decline [11, 12]. However a link between BF degeneration and tau pathology has not been established *in vivo*.

Recently PET tracers have been developed to image NFTs in living subjects [13, 14]. ^{18}F-THK523 and the second generation tracer ^{18}F-THK5105 bind to recombinant tau and NFTs in transgenic mice and human post-mortem tissue, but not to Aβ [13, 14]. Moreover, although the diagnostic use of tau tracers is still in the developmental phase, *in vivo* cortical retention of these tracers in AD patients reflects the histopathological distribution of

tau, and correlates with hippocampal atrophy and cognitive impairment [15, 16].
To determine the relationship between tau burden and BF volume *in vivo*, we assessed two cohorts of AD patients and controls (Supplementary Tables 1 and 2). Subjects in the first cohort underwent ^{18}F-THK523 and PiB PET scans (Figure 1) as well as a structural 3D T1-weighted MRI scan to allow BF volumes, restricted to areas of AD-specific degeneration, to be extracted for each patient (Supplementary Figure 1; see *MRI processing*). The volumes for Ch4 intermediate and posterior areas, and the anterior volume covering the Ch1-3 and Ch4 anterior cell groups, were analysed separately. The second cohort of subjects underwent ^{18}F-THK5105 and PiB PET scans as well as a structural 3D T1-weighted MRI scan.

As previously been reported [17], we found that the combined AD subject group (n=18) had a significantly reduced average BF volume in comparison to that of the combined HC subjects (n=17; BF anterior, p=0.045; BF posterior, p=0.001). Furthermore, correlational analysis revealed that both the anterior and posterior BF volumes correlated with measures of cognitive function (Supplementary Table 3).

Correlations were then performed in cohort 1 between anterior/posterior BF volumes and ^{18}F-THK523 standardized uptake value ratios (SUVRs) for regions anatomically connected to either anterior or posterior basal forebrain areas [18]. When the HC and AD subject groups were combined, we found significant negative correlations were found between the anterior BF volume and the hippocampal, orbitofrontal and gyrus rectus ^{18}F-THK523 SUVR (Table 1). In addition, the posterior BF volume was significantly correlated to the parietal, inferior temporal and neocortical ^{18}F-THK523 SUVR (Table 1, Figure 2). When the AD group was considered alone, significant correlations were found between the anterior BF volume and hippocampal and orbitofrontal ^{18}F-THK523 SUVR, as well as between the posterior BF volume and the inferior temporal ^{18}F-THK523 SUVR. No significant correlations were identified when the HC group was analyzed separately.

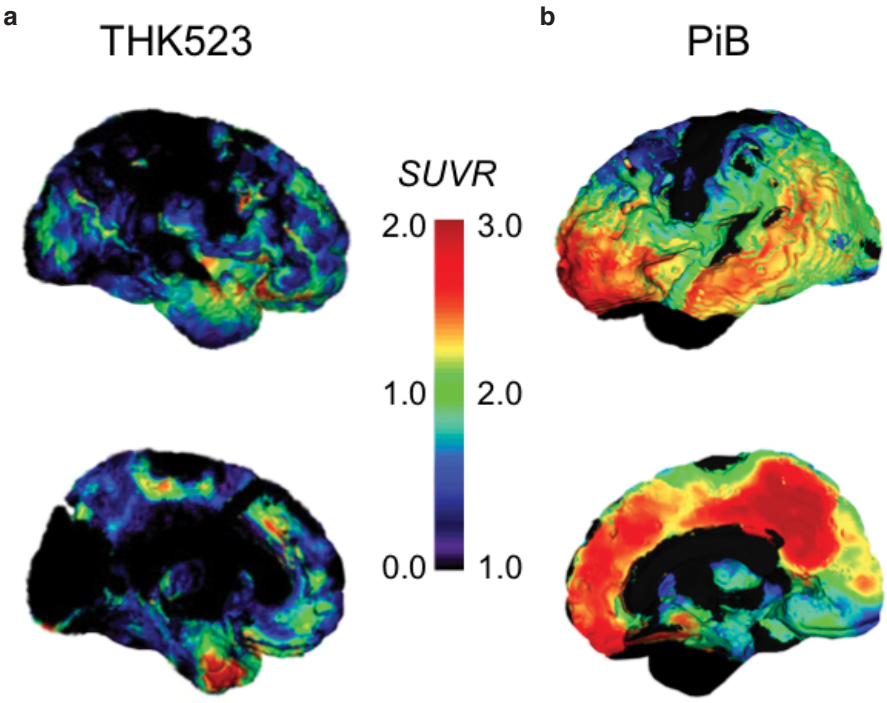

Figure 1: Representative surface projection maps for (**a**) aggregated tau (^{18}F-THK523) and (**b**) amyloid plaques (^{11}C-PiB) in an AD patient (82 yo male, MMSE 11) showing the different brain regional distribution of each pathology. For comparison purposes, the scale is set at the maximal (100%) SUVR for each tracer, but ^{11}C-PiB SUVR was three times higher than that of ^{18}F-THK523.

To validate these findings, correlations between BF volume and regional tau SUVR found to be significant in cohort 1 were tested in the second cohort. The posterior BF volume was again significantly correlated to parietal and neocortical, but not inferior temporal, ^{18}F-THK5105 SUVR (Table 2, Figure 2). Anterior BF volume did not correlate with either hippocampal or orbitofrontal ^{18}F-THK5105 SUVR (Table 2). However, as the most clinically accurate tau tracer is yet to be confirmed, we suggest that these findings should not yet be dismissed as irrelevant.

In assessing Aβ burden, when all subjects were analyzed together, we found a significant correlation between retention of neocortical PiB with the combined BF volume (r^2_{adj}=0.11; p=0.031). However, when we undertook correlations between PiB and individual BF regions or the independent cohorts no significant interactions were found. This suggests that a weaker correlation exists between BF atrophy and Aβ load.

Our results indicate that a strong correlation exists between BF atrophy, particularly of the posterior BF, and tau burden in brain regions that are typically affected by NFT pathology and which are also anatomically connected to the posterior BF, namely the parietal lobe and neocortex. Tau and basal forebrain atrophy are associated with degree of cognitive decline [11,12] whereas Aβ burden is not [10]. Our findings therefore support the idea that Aβ accumulation is a necessary but insufficient cause for progression to AD, with secondary, downstream or parallel events being required to trigger tau aggregation and BF degeneration, which then directly underpin cognitive decline.

	HC/AD		AD	
	(n= 19)		(n=10)	
	r^2_{adj}	p	r^2_{adj}	p
BF anterior				
Hippocampus	0.34	0.005 *#	0.44	0.021 *
Orbitofrontal	0.27	0.014 *#	0.33	0.047 *
Gyrus rectus	0.17	0.047 *	-0.10	0.675
Posterior cingulate	-0.06	0.825	0.25	0.079
Parietal	-0.01	0.380	-0.07	0.557
Amygdala	-0.06	0.970	-0.12	0.917
BF posterior				
Ventrolateral prefrontal	-0.06	0.848	-0.05	0.470
Parietal	0.17	0.047 *	-0.06	0.514
Superior temporal	-0.01	0.360	-0.10	0.682
Inferior temporal	0.51	< 0.001 * #	0.35	0.041 *
Neocortical	0.17	0.046 *	-0.12	0.937

Table 1: Linear regression analysis between basal forebrain (BF) volumes and THK523 retention in the whole sample, healthy control (HC)/Alzheimer's disease (AD), and the AD group alone. (* Significant correlation, # Significant correlation after correction for multiple comparisons.)

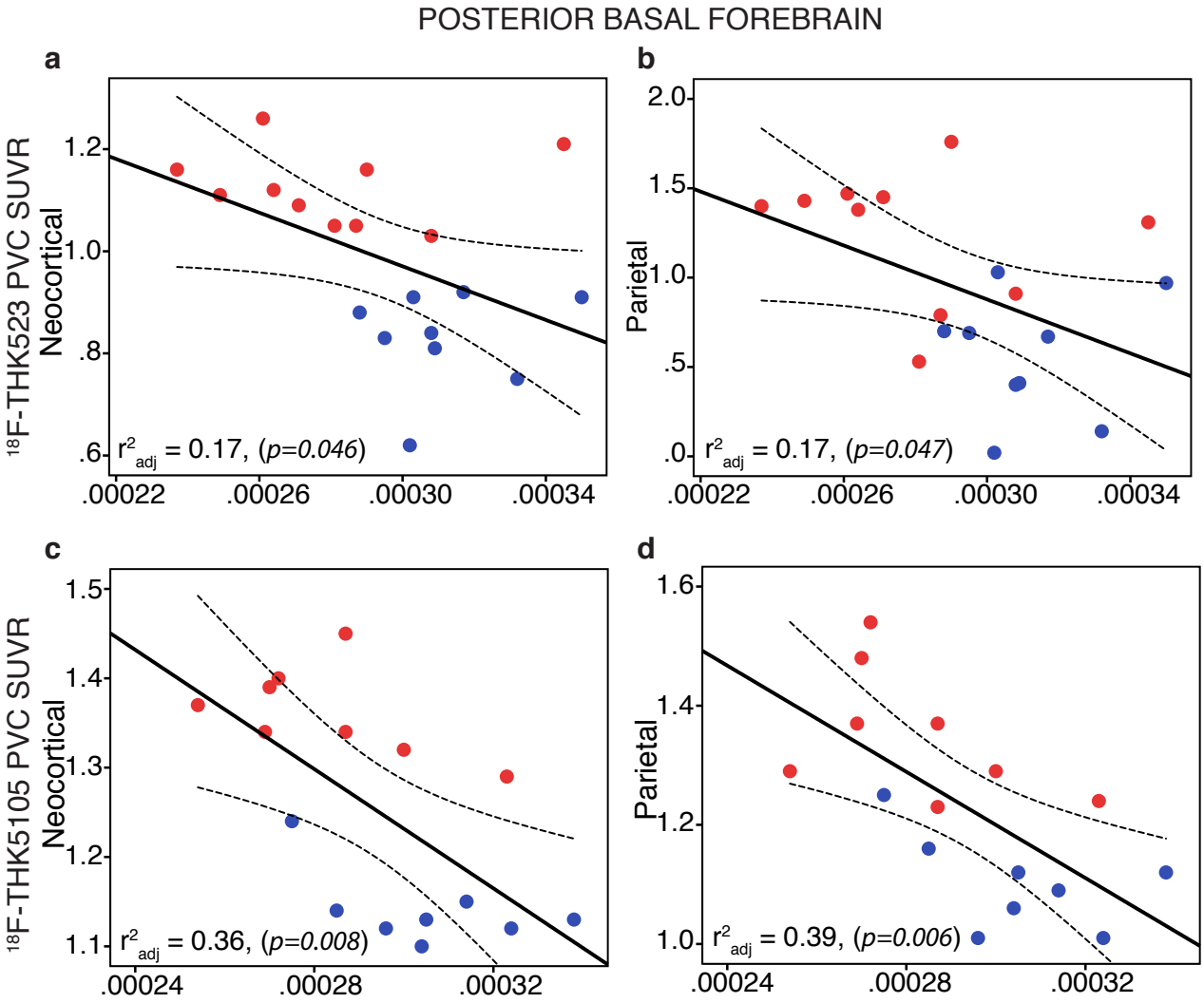

Figure 2: Tau burden correlates with posterior basal forebrain atrophy. Regression analysis between age-corrected posterior BF volumes (x-axes) and (**a,b**) ^{18}F-THK523 or (**c,d**) ^{18}F-THK5105 retention (y-axes) in neocortex (**a,c**) and parietal lobe (**b,d**).

	HC/AD	
	(n=16)	
	r^2_{adj}	P
BF anterior		
Hippocampus	-0.06	0.688
Orbitofrontal	-0.06	0.666
Gyrus rectus	0.04	0.222
BF posterior		
Parietal	0.39	0.006 * #
Inferior temporal	0.05	0.211
Neocortical	0.36	0.008 * #

Table 2: Linear regression analysis between basal forebrain (BF) volumes and THK5105 retention in the whole sample, healthy control (HC)/Alzheimer's disease (AD). (* Significant correlation, # Significant correlation after correction for multiple comparisons.)

Methods

Subjects.

Written informed consent was obtained from all participants. Approval for the study was obtained from the Austin Health Human Research Ethics Committee. The methodology for cohort recruitment and evaluation has been reported elsewhere [15]. Briefly, healthy elderly controls (HC) were recruited by advertisement in the community and dementia patients were recruited from tertiary Memory Disorders Clinics or from physicians who specialize in dementia care. All participants were classified on the basis of their clinical and neuropsychological performance by consensus of a neurologist and a neuropsychologist. Individuals classified as HC performed within normal limits on cognitive tests. AD patients met NINCDS-ADRDA criteria for probable AD [19]. None of the AD patients had a family history of dementia. Subject details are provides in Supplementary Tables 1 and 2.

MRI processing.

The pons and gray matter (GM), white matter (WM) and cerebrospinal fluid (CSF) were segmented from the MPRAGE images using the method outlined in [20]. A skull strip mask was generated from the GM, WM and CSF segmentation. All volume calculations reported are normalized by intracranial volume.

The skull stripped MPRAGE images of 80 healthy elderly subjects from the Australian Imaging Biomarkers and Lifestyle study (AIBL; http://www.aibl.csiro.au/) were normalized to create an average elderly template brain using the open-source deformable registration tool ANTS. The population-specific template was generated by iteratively registering images to the current template estimate. A new shape and intensity average were then computed from the results of the registrations and the current template estimate was set as the average. This template generation procedure was repeated iteratively (I=5). Each registration in this procedure used the greedy Symmetric Normalization algorithm (SyN, parameters outlined below) and the cross-correlation after subtracting the local mean from the image match metric.

The registration between each subject's MPRAGE image and the population-specific template was performed using the SyN algorithm (GradStep = 0.5, regularization sigma = 2.0). The image match metric was the cross-correlation between the images. Cross-correlation after subtracting the local mean from the image at each voxel was computed using a 5×5×5 voxel window. Registration was performed in a multi-resolution scheme, with a maximum of 30 iterations at 4× subsampling, 90 iterations at 2× subsampling, and

50 iterations at full resolution.

To establish BF masks encompassing only those areas that undergo atrophy in AD patients, we previously compared control (n=80) and AD (n=38) subjects from the AIBL cohort 9 and overlaid the resultant z-score map (set to -0.5 and -1 standard deviations) on a standard Montreal Neurological Institute (MNI) brain. Using published probabilistic BF maps derived from histological data as a guide for the limits of the structure [18], regions of atrophy within the standard space corresponding to the BF area were then segmented. We used maximum probability maps [18] as guidance, resulting in a BF mask covering voxels that were identified as lying in the BF in ten post-mortem brains and a final delineated area of high anatomical specificity. To study anterior and posterior BF compartments separately, we further divided the BF map into an anterior volume (size: 595 voxels; top row, Supplementary Figure 1), covering Ch1-3 as well as Ch4 anterior cell groups, and a posterior volume (size: 565 voxels; bottom row, Supplementary Figure 1), covering Ch4 intermediate and posterior cell groups (nomenclature according to [18]). Note that BF MRI maps used by us and other researchers are not specific for cholinergic cells of the BF, but rather represent the general BF area. The BF masks were propagated to the subjects' space to extract the BF volume, and GM and WM masks were used to remove any falsely included CSF voxels.

Positron emission tomography.

Productions of ^{11}C-PIB, ^{18}F-THK523 and ^{18}F-THK5105 were performed in the Centre for PET, Austin Hospital. ^{11}C-PIB was synthesized using the one step ^{11}C-methyl triflate approach as previously described [21]. The decay corrected average radiochemical yield for ^{11}C-PIB was 30% with a radiochemical purity of > 98% and a specific activity of 30 ± 7. 5 GBq/μmol. ^{18}F-THK523 and ^{18}F-THK5105 were synthesized by nucleophilic substitution of their respective tosylate precursors as previously described [15, 16]. Briefly, the decay-corrected average radiochemical yield of the production of ^{18}F-THK523 was 22.5%, with a radiochemical purity of >95% and a specific activity of 225.6±134.8 GBq/μmol (6.2±3.3 Ci/μmol). The decay-corrected average radiochemical yield of the production of ^{18}F-THK5105 was 45%, with a radiochemical purity of >95% and a specific activity of 229.6 GBq/μmol (6.2±3.3 Ci/μmol).

A 30-min acquisition (6 x 5-min frames) on an Allegro™ PET camera started 40 min after intravenous injection of 300 MBq ^{11}C-PiB. A 90-min and a 120-min list-mode emission acquisition was performed in 3D mode after injection of 200 MBq ^{18}F-THK523 and ^{18}F-THK5105, respectively. List-mode raw data were sorted off-line into 6 x 30 sec, 7 x 1-min,

4 x 2.5-min, 2 x 5-min and 6 x 10-min frames. The sorted sinograms were reconstructed using a 3D RAMLA algorithm. The interval between the ^{18}F-THK523 and PiB PET studies was 0.3±3.8 months. The interval between the ^{18}F-THK5105 and PiB PET studies was 0.9±2.4 months.

PET images were processed using a semi-automatic region of interest (ROI) method as previously described [22]. Briefly, PET images were co-registered to each individual's MRI using SPM8 (Wellcome Trust Centre for Neuroimaging, London, UK), and the same ROI template was applied. SUVR for PiB and THK523 were generated using the cerebellar cortex as reference region [21]. Neocortical tau and Aβ burden were expressed as the average SUVR for the following ROIs: frontal (dorsolateral prefrontal, ventrolateral prefrontal and orbitofrontal regions), superior parietal, lateral temporal, lateral occipital and anterior and posterior cingulate regions.

Partial volume correction, accounting for both gray matter atrophy and white matter spill-over was performed applying a 3-compartment approach using PMOD 3.1 (PMOD Technologies Ltd.).

Statistical analysis.

Normality of distribution was tested using the Shapiro-Wilk test and visual inspection of variable histograms. Linear regression analyses were conducted between imaging and clinical variables. One-way analysis of variance was used for group comparisons of variables. Data are presented as mean ± standard deviation unless otherwise stated. Tau values were not adjusted for age as we observed no significant interaction between age and global ^{18}F-THK523 ($p = 0.726$) and ^{18}F-THK5105 ($p = 0.078$) SUVR. Before conducting statistical analyses of BF volumes the effect of age was removed, as significant interactions between age and BF volume have been reported. Correction for multiple comparisons was performed using false discovery rate. The p-values given are uncorrected values.

Acknowledgements

G.M.K. was funded by an ANZ Trustees PhD scholarship for medical research and a University of Queensland International Scholarship. E.J.C. was supported by a National Health and Medical Research Council of Australia Career Development Fellowship (569601). V.L.V. was supported by a National Health and Medical Research Council of Australia Research Fellowship (1046471). The study was partially supported by an Alzheimer Drug Discovery Foundation Research Grant (20101208 AFTD) and by a National Health and Medical Research Council of Australia Project Grant 1044361.

Contributions

G.M.K. and V.L.V designed the study. J.F., M.F.-T., S.F. and N.O. conducted the experiments. J.F., M.F.-T., S.F., N.O., V.L.V. and G.M.K. analyzed the data. G.M.K and E.J.C. wrote the manuscript with input from all authors. The study was managed by S.R., C.C.R. and V.L.V.

Competing financial interests

The authors declare no competing financial interests.

References

1. Klunk, W.E., *et al.* Imaging brain amyloid in Alzheimer's disease with Pittsburgh Compound-B. *Ann Neurol* **55**, 306-319 (2004).
2. Braak, H. & Del Tredici, K. The pathological process underlying Alzheimer's disease in individuals under thirty. *Acta Neuropathol* **121**, 171-181 (2011).
3. Braak, H., Alafuzoff, I., Arzberger, T., Kretzschmar, H. & Del Tredici, K. Staging of Alzheimer disease-associated neurofibrillary pathology using paraffin sections and immunocytochemistry. *Acta Neuropathol* **112**, 389-404 (2006).
4. Mufson, E.J., *et al.* Loss of basal forebrain $p75^{NTR}$ immunoreactivity in subjects with mild cognitive impairment and Alzheimer's disease. *J Comp Neurol* **443**, 136-153 (2002).
5. Schliebs, R. & Arendt, T. The significance of the cholinergic system in the brain during aging and in Alzheimer's disease. *J Neural Transm* **113**, 1625-1644 (2006).
6. Schneider, L.S., *et al.* Clinical trials and late-stage drug development for Alzheimer's disease: an appraisal from 1984 to 2014. *J Intern Med* **275**, 251-283 (2014).
7. Grothe, M., Heinsen, H. & Teipel, S.J. Atrophy of the cholinergic basal forebrain over the adult age range and in early stages of Alzheimer's disease. *Biol Psychiatry* **71**, 805-813 (2011).
8. Teipel, S., *et al.* Cholinergic basal forebrain atrophy predicts amyloid burden in Alzheimer's disease. *Neurobiol Aging* **35**, 482-491 (2013).
9. Kerbler, G.M., *et al.* Basal forebrain atrophy correlates with amyoid β burden in Alzheimer's disease. *Neuroimage Clin* (2014).
10. Drachman, D.A. The amyloid hypothesis, time to move on: Amyloid is the downstream result, not cause, of Alzheimer's disease. *Alzheimers Dement* (2014).
11. Mufson, E.J., Ward, S. & Binder, L. Prefibrillar tau oligomers in mild cognitive impairment and Alzheimer's disease. *Neurodegener Dis* **13**, 151-153 (2014).
12. Vana, L., *et al.* Progression of tau pathology in cholinergic Basal forebrain neurons in mild cognitive impairment and Alzheimer's disease. *Am J Pathol* **179**, 2533-2550 (2011).
13. Fodero-Tavoletti, M.T., *et al.* 18F-THK523: a novel in vivo tau imaging ligand for Alzheimer's disease. *Brain* **134**, 1089-1100 (2011).
14. Okamura, N., *et al.* Novel 18F-labeled arylquinoline derivatives for noninvasive imaging of tau pathology in Alzheimer disease. *J Nucl Med* **54**, 1420-1427 (2013).
15. Villemagne, V.L., *et al.* In vivo evaluation of a novel tau imaging tracer for Alzheimer's disease. *Eur J Nucl Med Mol Imaging* (2014).
16. Okamura, N., *et al.* Non-invasive assessment of Alzheimer's disease neurofibrillary

pathology using 18F-THK5105 PET. *Brain* **137**, 1762-1771 (2014).

17. George, S.*, et al.* MRI-based volumetric measurement of the substantia innominata in amnestic MCI and mild AD. *Neurobiol Aging* **32**, 1756-1764 (2011).

18. Zaborszky, L.*, et al.* Stereotaxic probabilistic maps of the magnocellular cell groups in human basal forebrain. *Neuroimage* **42**, 1127-1141 (2008).

19. McKhann, G.*, et al.* Clinical diagnosis of Alzheimer's disease: report of the NINCDS-ADRDA Work Group under the auspices of Department of Health and Human Services Task Force on Alzheimer's Disease. *Neurology* **34**, 939-944 (1984).

20. Bourgeat, P.*, et al.* b-amyloid burden in the temporal neocortex is related to hippocampal atrophy in elderly subjects without dementia. *Neurology* **74**, 121-127 (2010).

21. Rowe, C.C.*, et al.* Imaging b-amyloid burden in aging and dementia. *Neurology* **68**, 1718-1725 (2007).

22. Villemagne, V.L.*, et al.* Longitudinal assessment of Ab and cognition in aging and Alzheimer disease. *Ann Neurol* **69**, 181-192 (2011).

3.3 Supplementary data

Supplementary Table 1: Demographics of healthy control (HC) and Alzheimer's disease (AD) patients of the THK523 sample.

	HC	**AD**
	(n=9)	(n=10)
Age	76.3 ± 10.0	75.6 ± 9.5
Gender (M/F)	2/7	4/6
MMSE	29.4 ± 1.0	16.7 ± 6.6*
CDR	0.0	1.3 ± 0.6*
CDR SOB	0.1 ± 0.2	7.3 ± 4.5*
Years of education	15.0 ± 2.7	11.5 ± 3.6*
Episodic memory scores	-0.4 ± 0.6	-3.8 ± 0.5*
Non-memory scores	-0.1 ± 0.4	-3.4 ± 1.6*
Aβ burden (PiB SUVR)	1.45 ± 0.6	2.87 ± 0.5*

* Significantly different from HC ($p < 0{\cdot}05$) Abbreviations: MMSE: Mini mental state examination; CDR: Clinical dementia rating; CDR-SOB: Clinical dementia rating sum of boxes; PiB: Pittsburgh compound B; SUVR: Standardized uptake value ratio.

Supplementary Table 2: Demographics of healthy control (HC) and Alzheimer's disease (AD) patients of the THK5105 sample.

	HC	**AD**
	(n=8)	(n=8)
Age	70.5 ± 4.4	74.1± 6.9
Gender (M/F)	3/5	3/5
MMSE	28.8 ± 1.5	17.3 ± 6.6*
CDR	0.0	0.9 ± 0.5*
CDR SOB	0.0	6.1 ± 4.9*
Years of education	15.4 ± 2.4	11.3 ± 3.2*
Episodic memory scores	-0.06 ± 0.8	-3.8 ± 0.3*
Non-memory scores	-0.06 ± 0.5	-3.0 ± 1.9*
Aβ burden (PiB SUVR)	1.2 ± 0.1	2.0 ± 0.2*

* Significantly different from HC ($p < 0{\cdot}05$) Abbreviations: MMSE: Mini mental state examination; CDR: Clinical dementia rating; CDR-SOB: Clinical dementia rating sum of boxes; PiB: Pittsburgh compound B; SUVR: Standardized uptake value ratio.

Supplementary Table 3: Linear regression analysis between basal forebrain (BF) volumes and cognitive scores in the whole sample.

	BF anterior		**BF posterior**	
	r^2_{adj}	p	r^2_{adj}	p
MMSE	0.246	0.001 * #	0.282	< 0.001 * #
CDR	0.233	0.002 * #	0.288	< 0.001 * #
CDR-SOB	0.250	0.001 * #	0.253	0.001 * #
Episodic memory	0.147	0.013 * #	0.347	< 0.001 * #
Episodic non-memory	0.160	0.010 * #	0.271	< 0.001 * #

* Significant correlation, # Significant correlation after correction for multiple comparisons (n = 35). Abbreviations: MMSE: Mini mental state examination; CDR: Clinical dementia rating; CDR-SOB: Clinical dementia rating sum of boxes; PiB: Pittsburgh compound B; SUVR: Standardized uptake value ratio.

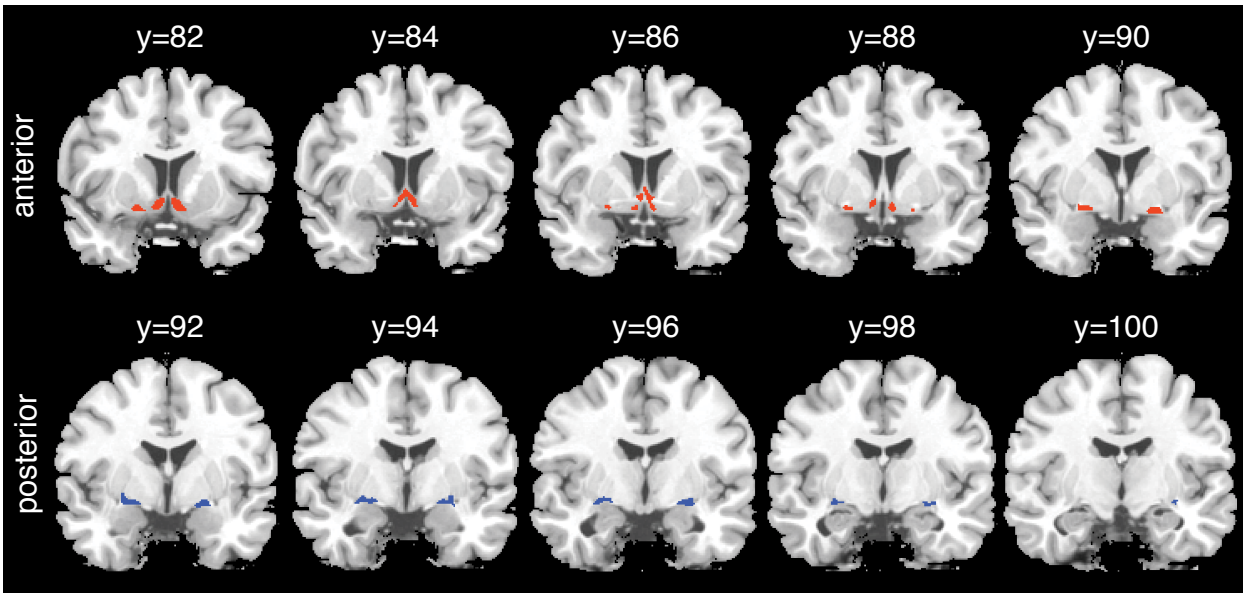

Supplementary Figure 1: BF masks of the anterior and posterior areas in template space. Coronal slices from rostral (left) to caudal (right) showing (top row, red) the anterior and (bottom row, blue) the posterior BF mask used to calculate volumes for each patient. Both masks were restricted to encompass only those areas within the boundaries of the BF that undergo atrophy in AD patients in order to investigate the interaction of these areas with NFT burden in an AD cohort. Coronal slices at different levels from rostral to caudal are shown on a T1-weighted image.

3.4 Discussion and implication of findings

Strikingly, the results of this chapter show for the first time that there is a strong correlation of basal forebrain volume with tau burden *in vivo* in a human Alzheimer's disease cohort. The fact that the interaction with amyloid accumulation was found to be not as strong in this study possibly indicates that tau aggregation is more closely related to basal forebrain degeneration.

Here we demonstrated a potential mechanistic link between basal forebrain integrity and NFT burden in regions closely associated with basal forebrain neurons through their projections. Taken together with the previous finding that basal forebrain degeneration correlates with amyloid burden, which was also replicated in the current study, we have now demonstrated that basal forebrain degeneration in Alzheimer's disease also correlates with other features of disease progression in humans *in vivo*. This further shows the potential of basal forebrain measures as biomarkers of Alzheimer's disease. However, we are also starting to discern potential differences in the interaction of basal forebrain degeneration with amyloid and tau accumulation. Future studies aimed at investigating the potential underlying biological mechanisms will be required to understand the causal relationship between these features.

The fact that we were able to show similar interactions between basal forebrain atrophy and tau burden employing two different PET tracers in two independent subject cohorts particularly strengthens the findings of this study. It was recently demonstrated, that THK5105 has higher binding affinity to synthetic tau fibrils, human Alzheimer's disease post-mortem brain homogenates as well as human post-mortem brain sections, as compared to THK523. Therefore, THK5105 might be a more promising candidate as PET tracer for the future.

Here, we also replicated our previous results (section 2.2) of significant basal forebrain volumetric differences between Alzheimer's and control subjects. In addition the correlations of basal forebrain volume with cognitive scores were confirmed in this new study.

Interestingly, tau also seems to be a significantly better predictor and correlate of cognitive status in human subjects (Fodero-Tavoletti et al., 2011) when compared to amyloid burden. Given basal forebrain volume is also associated with cognition, this warrants further investigation into the specific involvement of the basal forebrain in general cognitive status, as well as more explicit cognitive functions such as navigation, which has been

shown to be impaired in Alzheimer's subjects (Hort et al., 2014) and this will be the focus of the next chapter.

Chapter 4: Basal forebrain degeneration is associated with spatial navigation deficits in Alzheimer's disease

4.1 Introduction

As demonstrated in the previous chapter and by others in the field, basal forebrain volume is correlated with memory scores such as episodic memory (chapter 3) and MMSE (e.g. Grothe et al., 2011), especially in Alzheimer's disease subjects; however not many studies in humans have explored the involvement of the basal forebrain in more specific cognitive functions. Work carried out in mice by members of the Coulson laboratory has revealed an effect of cholinergic basal forebrain degeneration on spatial navigation performance (Hamlin et al., 2013). In this study, loss of cholinergic neurons was shown to impair idiothetic navigation of mice, whereas the animals did not display any changes in cued navigation or generalized learning or memory, fear-related tasks and sleep-wake cycle characteristics.

This animal study prompted us to investigate whether the basal forebrain plays a similar role in humans, such that Alzheimer's disease subjects with basal forebrain atrophy display impaired uncued navigation. With the structural MRI methods developed in this thesis, we were able to study the association of basal forebrain volume with performance of normal controls, amnestic mild cognitively impaired subjects and Alzheimer's disease patients, on spatial navigation tasks. Furthermore different subtypes of tasks allowed us to specifically look into the association of basal forebrain volume with either egocentric (uncued) or allocentric (cued) navigation. This work was conducted in collaboration with researchers from the Charles University in Prague, who collected MRI data as well as performing cognitive testing on site.

This work has been submitted to the journal *Brain Structure and Function*.

4.2 The basal forebrain contributes to cue-based spatial navigation performance in Alzheimer's disease

[1]**GM Kerbler**, [2,3]Z Nedelska, [4]J Fripp, [2,3]J Laczo, [2,3]M Vyhnalek, [5]J Lisy, [6]AS Hamlin, [4]S Rose, [2,3]J Hort and [1]EJ Coulson. (2014) The basal forebrain contributes to cue-based spatial navigation performance in Alzheimer's disease. *Under submission* in *Brain Structure and Function*

[1]Queensland Brain Institute, Clem Jones Centre for Ageing Dementia Research, The University of Queensland, Brisbane, 4072 Qld. Australia
[2]Memory Clinic, Department of Neurology, Charles University in Prague, 2nd Faculty of Medicine and University Hospital Motol, 150 06 Prague 5, Czech Republic
[3]International Clinical Research Center, St. Anne's University Hospital Brno, 656 91 Brno, Czech Republic
[4]Commonwealth Scientific and Industrial Research Organisation, Computational Informatics, Brisbane, 4029 Qld. Australia
[5]Department of Radiology, Charles University in Prague, 2nd Faculty of Medicine and University Hospital Motol, 150 06 Prague 5, Czech Republic
[6]School of Biomedical Sciences, Charles Sturt University, Wagga Wagga, 2678 Nsw. Australia

Abstract

The basal forebrain degenerates in Alzheimer's disease (AD) and this process is believed to contribute to the cognitive decline observed in AD patients. Impairment in spatial navigation is an early feature of the disease but whether basal forebrain dysfunction is responsible for the impaired navigation skills of AD patients is not known. Our objective was to investigate the relationship between the basal forebrain volume and performance in real space as well as computer-based navigation paradigms in an elderly cohort comprising cognitively normal controls, subjects with amnestic mild cognitive impairment and those with AD. We also tested whether basal forebrain volume could predict the participants' ability to perform allocentric- vs. egocentric-based navigation tasks. The basal forebrain volume was calculated from 1.5 T MRI scans and navigation skills were assessed using the human analog of the Morris water maze employing allocentric, egocentric and mixed allo/egocentric real space as well as computerized tests. We found that basal forebrain volume was correlated with spatial accuracy in allocentric (cued) and mixed allo/egocentric navigation tasks but not the egocentric (uncued) task in the entire sample, demonstrating an important role of the basal forebrain in mediating cue-based spatial navigation capacity. Regression analysis revealed that although hippocampal volume reflected navigation performance across the entire sample, basal forebrain volume contributed to mixed allo/egocentric navigation in the AD group, whereas hippocampal volume did not. This suggests that atrophy of the basal forebrain contributes to aspects of navigation impairment in AD that are independent of hippocampal changes.

Keywords

Basal forebrain, navigation, Alzheimer's disease, cholinergic dysfunction, cognitive impairment

Introduction

The basal forebrain, encompassing the septum, vertical and horizontal diagonal bands of Broca and the nucleus basalis of Meynert, degenerates in Alzheimer's disease (AD) and this process plays a role in the general cognitive decline observed in AD patients (Mufson, 2003; Schliebs and Arendt, 2006). Using magnetic resonance imaging (MRI), smaller basal forebrain volumes have been shown to be associated with poorer performance in a multitude of cognitive tests used to measure memory dysfunction in AD, such as the clinical dementia rating (George et al., 2011; Grothe et al., 2012) and the California verbal learning test (Butler et al., 2012), as well as the mini mental state examination (MMSE; Grothe et al., 2011).

Moreover, basal forebrain neurons (e.g. cholinergic neurons), which project to the hippocampus, amygdala and almost the entire neocortex, have been shown to play a role in attention in humans (Hasselmo and McGaughy, 2004; Sarter et al., 2006).
Lesion studies in rodents have also demonstrated that selective loss of basal forebrain cholinergic neurons causes impairment in both egocentric (uncued) and allocentric (cued) spatial navigation (Berger-Sweeney et al., 2001; Hamlin et al., 2013). The basal forebrain cholinergic system has also been shown to be involved in feature binding – the ability to process different features of objects and combine these into a complete picture (Botly and De Rosa, 2009) – and visuospatial attention (Botly and De Rosa, 2012), which together are crucial for correct allocentric navigation. More specifically, acetylcholine is released from basal forebrain neurons when spatial cues are detected, but not when cues are missed (Parikh et al., 2007).

Likewise, the administration of donepezil, an acetylcholine esterase inhibitor that is used to treat cognitive dysfunction in patients diagnosed with mild AD, by prolonging synaptic acetylcholine availability, has been shown to improve the allocentric navigation performance of patients in a human analog of the Morris water maze (hMWM; Hort et al., 2014), a commonly used spatial working memory task. Taken together, these studies suggest a role for basal forebrain function in allocentric navigation; however the role of the basal forebrain in allocentric versus egocentric spatial navigation has never been studied *in vivo* in humans.

Here we investigated the relationship between basal forebrain volume (measured by MRI) and performance in cued (allocentric), uncued (egocentric) and mixed allo/egocentric spatial navigation in the real space and computerized versions of the hMWM task. We also

assessed differences in basal forebrain volume between groups and determined whether impaired performance in hMWM tasks in amnestic mild cognitive impaired (aMCI) and AD patients was associated with basal forebrain volume.

Subjects and Methods

Subjects

Between October 2010 and October 2012, eligible subjects (Supplementary Table 1) with probable AD (n=22) or aMCI (n=27) were consecutively recruited and followed up at the Memory Disorders Clinic, Department of Neurology, Charles University and Motol University Hospital in Prague, the Czech Republic (a longitudinal memory clinic-based cohort). Cognitively normal elderly subjects, who we refer to as normal controls (NC; n=17), were recruited from the University of the Third Age, Charles University in Prague, or patients' family members. Eligibility was defined as 1) absence of primary neurological disease other than aMCI and AD that could interfere with cognitive functioning, and 2) sufficient brain scan quality free of structural abnormalities such as tumors, cortical infarcts, subdural hematoma or hydrocephalus, although lacunar infarcts and white matter hyperintensities were not excluded. The study was approved by the institutional review board, and informed consent was obtained from subjects or their proxies.

Clinical evaluations and diagnosis

Subjects received annual clinical, neurological and laboratory evaluations, neuropsychology tests, brain MRI, and spatial navigation testing using the hMWM. Based on a panel consensus conference of 3 neurologists, and 3 neuropsychologists, subjects were diagnosed as probable AD (McKhann et al., 1984) or aMCI (Petersen, 2004). Memory impairment was established when the patient scored more than 1.5 SD below the mean of age- and education-adjusted norms on any memory test (Laczo et al., 2011). Details of neuropsychological testing are described elsewhere (Vyhnalek et al., 2014).

Spatial navigation testing using the human analogue of the Morris water maze

Spatial navigation was tested using in-house developed real space and computerized versions of the hMWM (Hort et al., 2014) based in the Laboratory of Spatial Cognition, a joint workplace of the Department of Neurology, 2nd Faculty of Medicine, Charles University in Prague, Czech Republic and Institute of Physiology, Academy of Sciences of the Czech Republic v.v.i., Prague, Czech Republic. The hMWM has been designed to examine separately the two basic types of navigation: 1) allocentric (cued) which is

hippocampus-driven, self-position independent, and uses salient distal cues to find the goal (Astur et al., 2002, and 2) egocentric (uncued), which is predominantly parietal cortex- and caudate nucleus-driven, and is self and start position dependent (Weniger et al., 2009). The real space and computer-based versions are described in detail elsewhere (Hort et al., 2007; Laczo et al., 2011).

Briefly, the real space task was conducted within a fully enclosed arena surrounded by a dark blue velvet curtain and operated by a computer program. The computer-based 2D task was conducted using the map-view of the velvet arena represented by a circle on a computer touch screen. The purpose of the tasks regardless of the version used was to locate the invisible goal on the arena floor or within the circle on the computer screen using either the start position (uncued, egocentric), two distal orientation cues (cued, allocentric), or both the start position and distal cues (mixed allo/egocentric). The (invisible) goal was initially shown to subjects for approximately 10-15 seconds immediately prior to the first trial. In the computer-based version, subjects were asked to use a mouse and screen to draw the way from the start to the goal. In the real space version, they were asked to walk directly from the start, and to indicate where they thought the goal was by pointing a long stick with a light-emitting diode to the floor once they walked into goal's presumed position.

Navigation performance was recorded automatically based on the position of either the point drawn by patient on the computer screen or the diode on the stick location. The navigation accuracy was measured as the distance error (in pixels in the computerized version and in centimetres in the real space version) between the goal position determined by the subject, and the correct goal position. Each of allocentric, egocenric or mixed tasks consisted of eight trials in both versions. Each computerized task preceded the respective real space task. The order of the tasks was as follows: 1) mixed allo/egocentric, 2) egocentric and 3) allocentric. Trials had no time limit, mainly to reduce bias caused by differences in cognitive, sensory, and physical functioning. Examiners were blinded to the diagnosis and supervised the task without interference beyond standard instructions.

MRI acquisition

Images were acquired at 1.5T (Siemens AG, Erlangen, Germany) using T1-weighted 3-dimensional high resolution magnetization-prepared rapid acquisition with a gradient echo (MPRAGE) sequence with the following parameters: TR/TE/TI = 2000/3.08/1100 ms, flip

angle 15°, 192 continuous partitions, slice thickness 1.0 mm, and in-plane resolution 1 mm. Scans were visually examined by a single neuroradiologist (J.Li.), blinded to the diagnosis, for appropriate quality and structural findings contradicting eligibility.

MRI processing

The hippocampus, pons and gray matter (GM), white matter (WM) and cerebrospinal fluid (CSF) were segmented from the MPRAGE images using the method outlined in Bourgeat et al. (2010). A skull strip mask was generated from the GM, WM and CSF segmentation. All volume calculations reported are normalized by intracranial volume.

The skull stripped MPRAGE images of 80 healthy elderly subjects from the Australian Imaging Biomarkers and Lifestyle study (AIBL; http://www.aibl.csiro.au/) were normalized to create an average elderly template brain using the open-source deformable registration tool ANTS (Avants et al., 2010). The population-specific template was generated by iteratively registering images to the current template estimate. A new shape and intensity average were then computed from the results of the registrations and the current template estimate was set as the average. This template generation procedure was repeated iteratively (I=5). Each registration in this procedure used the greedy symmetric normalization algorithm (SyN, parameters outlined below; Avants et al., 2008) and the cross-correlation after subtracting the local mean from the image match metric.
The registration between each subject's MPRAGE image and the population-specific template was performed using the SyN algorithm (GradStep = 0.5, regularization sigma = 2.0). The image match metric was the cross-correlation between the images. Cross-correlation after subtracting the local mean from the image at each voxel was computed using a 5×5×5 voxel window. Registration was performed in a multi-resolution scheme, with a maximum of 30 iterations at 4× subsampling, 90 iterations at 2× subsampling, and 50 iterations at full resolution.

We have previously established a mask of the entire basal forebrain, encompassing only those areas that undergo atrophy in AD patients, by comparing control (n=80) and AD (n=38) subjects from the AIBL cohort (Kerbler et al., *submitted*) and overlaid the resultant z-score map (set to -0.5 and -1 standard deviations) on a standard Montreal Neurological Institute (MNI) brain. Using published probabilistic basal forebrain maps derived from histological data as a guide for the limits of the structure (Zaborszky et al., 2008), regions of atrophy within the standard space corresponding to the basal forebrain were then

segmented.

We used maximum probability maps (MPMs; Zaborszky et al., 2008) as guidance, resulting in a mask covering voxels that were identified as lying in the basal forebrain in ten post-mortem brains and a final delineated area of high anatomical specificity. To study anterior and posterior basal forebrain compartments separately, we further divided the basal forebrain map into an anterior volume (size: 595 voxels), covering the medial septum and diagonal bands of Broca (Ch1-3) as well as anterior regions of the nucleus basalis of Meynert (Ch4), and a posterior volume (size: 565 voxels), covering the intermediate and posterior nucleus basalis of Meynert (nomenclature according to Zaborszky et al., 2008). Note, that basal forebrain MRI maps used by us and other researchers are not specific for cholinergic cells of the basal forebrain, as basal forebrain nuclei also contain other neuronal subtypes (e.g GABAergic projection neurons). The masks were propagated to the subjects' space to extract the basal forebrain volume, and GM and WM masks were used to remove any falsely included CSF voxels.

Statistics

Basal forebrain and hippocampal volumes as well as navigation scores were corrected for age, education and gender. Analysis of variance (ANOVA) in conjunction with Bonferroni post-hoc testing was used to calculate group differences. A two-tailed Pearson's product moment correlation between age-, education- and gender-corrected variables was used. Multiple linear regressions were performed to assess the relationships between modalities in predicting distance error in navigation tests.

Results

Basal forebrain volumes are significantly reduced in AD

In order to compare the basal forebrain integrity between clinical groups, we first calculated the basal forebrain volume of the whole structure, as well as its anterior and the posterior regions. These volumes were then corrected for age, education and gender and subsequently compared between the NC, aMCI and AD groups as well as correlated to hippocampal volumes. Group comparisons revealed that the mean whole (Supplementary Fig. 1A; $p=0.032$), as well as the anterior (Supplementary Fig. 1B; $p=0.044$), but not the posterior (Supplementary Fig. 1C) basal forebrain volumes, were significantly reduced in aMCI subjects compared to NC subjects. No other significant differences in mean basal forebrain volume were found between diagnostic groups, perhaps due to the small group sizes. Furthermore, whole ($p<0.001$), anterior ($p<0.001$) and posterior ($p<0.001$) basal forebrain volumes were all highly correlated to hippocampal volume.

Basal forebrain correlates with navigation scores in the whole cohort

To investigate the relationship between allocentric, egocentric as well as mixed allo/egocentric spatial navigation performance and the basal forebrain we correlated the navigation scores of both the real space and computer-based versions of the navigation tasks with the basal forebrain volumes of NC, aMCI and AD subjects. In the whole cohort (Fig. 1), the distance error in the allocentric real space task was correlated to the anterior (Fig. 1A; $R=0.32$, $p=0.041$), posterior (Fig. 1B; $R=0.34$, $p=0.028$) and whole ($R=0.35$, $p=0.022$) basal forebrain volume. Furthermore, the distance error in the mixed allo/egocentric real space test was significantly associated with the anterior (Fig. 1C; $R=0.38$, $p=0.009$) and whole ($R=0.34$, $p=0.019$) but not the posterior basal forebrain volume. Associations between computer-based navigation test scores with basal forebrain volumes revealed that only the mixed allo/egocentric computer-based navigation task was significantly correlated to the posterior (Fig. 1D; $R=0.31$, $p=0.027$) and whole basal forebrain ($R=0.29$, $p=0.037$) volumes. This was in spite of the performances of subjects in the real space and computer-based versions of the navigation tasks being significantly correlated: allocentric, $R=0.78$, $p<0.001$; egocentric, $R=0.79$, $p<0.001$; allo/egocentric, $R=0.84$, $p<0.001$.

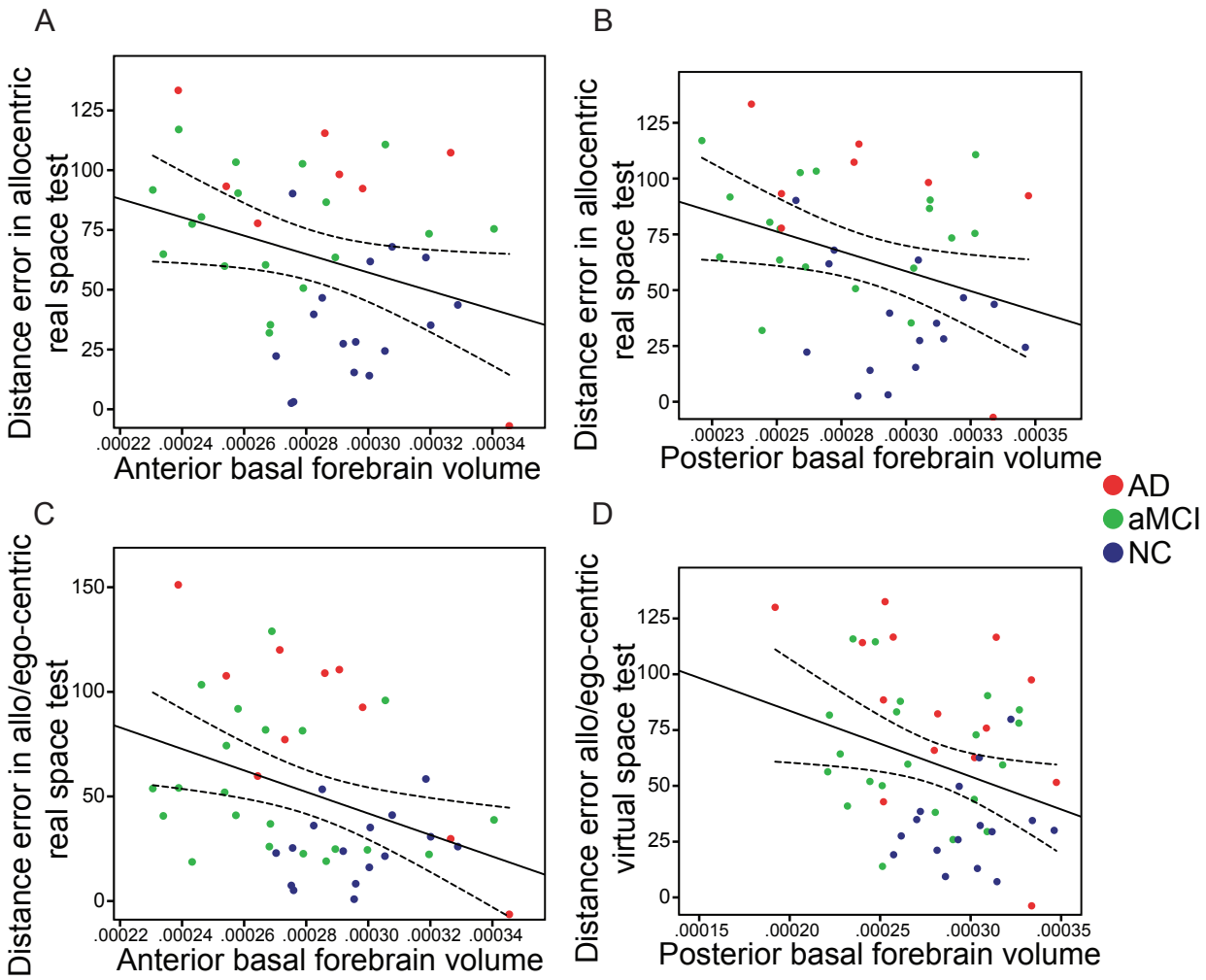

Figure 1: Significant correlations of anterior and posterior basal forebrain volumes (x-axis) to distance error (y-axis) in allocentric (A, B) and mixed allo/egocentric (C, D) real space tests. Both anterior (A) and posterior (B) basal forebrain volumes were significantly correlated to distance error in the allocentric real space test. Furthermore distance error in the mixed allo/egocentric real space test was also correlated to anterior (C) and posterior (D) basal forebrain volume. Data points are colored according to clinical diagnosis. A linear fit line with 95% confidence interval is shown.

Basal forebrain volume correlates with navigation scores in AD patients

To test whether basal forebrain volumes were correlated to navigation dysfunction in clinical groups, we performed correlations of basal forebrain volumes and navigation task scores in individual groups. This analysis revealed no significant interactions of any basal forebrain volumetric measure with distance error in any of the real space or computer-based navigation tasks in the aMCI and NC groups. However in the AD group, the anterior (Fig. 2; R=0.82, p=0.003) and whole (R=0.68, p=0.029) basal forebrain volumes were significantly correlated to distance error in the allo/egocentric real space task.

Regression analysis in the whole cohort and in the AD group

Basal forebrain measures (anterior and posterior) which showed significant correlations with real space navigation scores were entered into regression models with and without hippocampal volume to determine their relative contributions in predicting performance in the allocentric and mixed allo/egocentric navigation tasks for the whole cohort, and mixed allo/egocentric navigation performance for AD patients.

When mixed allo/egocentric navigation performance for the whole cohort was considered as the dependent variable and each modality (anterior basal forebrain volume and hippocampal volume) was entered separately into the model, the relationship was significant for each modality (Table 1, Model 1). Both modalities were then entered together into the model to determine whether each modality independently contributed to mixed allo/egocentric navigation deficits when taking into account the effect of another modality (Table 1, Model 2). This model was still found to be predictive of mixed allo/egocentric navigation scores; however only hippocampal volume remained significantly associated with navigation performance.

When allocentric navigation performance in the whole cohort was considered as the dependant variable and each modality (anterior, posterior basal forebrain volume and hippocampal volume) was entered separately into the model, relationships were significant for all modalities (Table 2, Model 1). However when entering combinations of two modalities into the model (Table 2, Model 2), only those combinations including hippocampal volume showed significant association with allocentric test scores. When entering hippocampal volume and basal forebrain volume together into the model, only

hippocampal volume remained significantly associated with allocentric navigation performance.

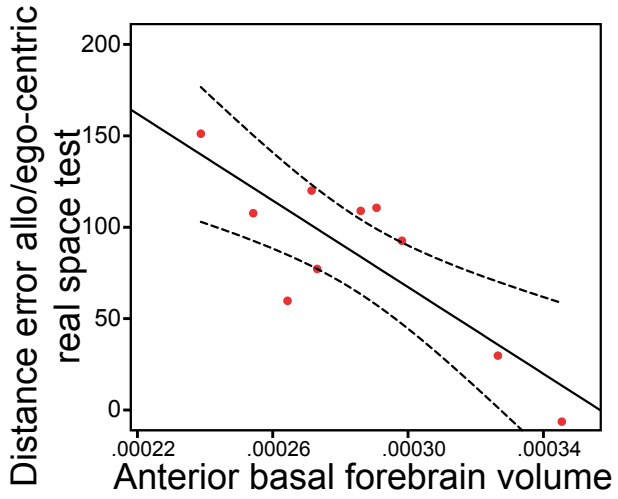

Figure 2: Anterior basal forebrain volume is significantly correlated to distance error in the mixed allo/egocentric real space test. A linear fit line with 95% confidence interval is shown.

By contrast, when mixed allo/egocentric navigation performance in the AD group was considered as the dependent variable and each modality (anterior basal forebrain volume and hippocampal volume) was entered separately into the model, the relationship was only significant for anterior basal forebrain volume (Table 3, Model 1). Therefore, when entering both modalities together into the model, only anterior basal forebrain volume, and not hippocampal volume, remained significantly associated with mixed allo/egocentric navigation performance in the AD group.

Table 1: Results of the regression models with distance error in the allo/egocentric real space test as the dependent variable and anterior basal forebrain volume and hippocampal volume separately (Model 1) or simultaneously (Model 2) entered as predictive variables, while controlling for age, gender and years of education, within the whole cohort. BF: basal forebrain

Model	Volume	R^2	Beta	t-value	P-value
1					
	BF Anterior	0.14**	-0.378	-2.738	0.009
	Hippocampus	0.17**	-0.414	-3.047	0.004
2					
	BF Anterior	0.20**	-0.210	-1.272	0.21
	+ Hippocampus		-0.293	-1.780	0.082

R^2 = R^2 value of the overall model significant at ** $p<0.01$. Beta = standardized regression coefficient. P-value = association of each modality with the dependent variable.

Table 2: Results of the regression models with distance error in the allocentric real space test as the dependent variable and anterior basal forebrain volume, posterior basal forebrain volume and hippocampal volume separately (Model 1) or simultaneously (Model 2 and Model 3) entered as predictive variables, while controlling for age, gender and years of education, within the whole cohort. BF: basal forebrain

Model	Volume	R^2	Beta	t-value	P-value
1					
	BF Anterior	0.10*	-0.316	-2.107	0.041
	BF Posterior	0.12*	-0.339	-2.279	0.028
	Hippocampus	0.26**	-0.512	-3.772	0.001
2					
	BF Anterior	0.13	-0.232	-1.056	0.297
	+ BF Posterior		-0.147	-0.668	0.508
	BF Anterior	0.26**	0.011	0.060	0.952
	+ Hippocampus		-0.519	-2.931	0.006
	BF Posterior	0.27**	-0.064	-0.383	0.704
	+ Hippocampus		-0.475	-2.823	0.007
3					
	BF Anterior	0.27**	0.075	0.342	0.734
	+ BF Posterior		-0.106	-0.507	0.615
	+ Hippocampus		-0.498	-2.718	0.01

R^2 = R^2 value of the overall model significant at * $p<0.05$, ** $p<0.01$. Beta = standardized regression coefficient. P-value = association of each modality with the dependent variable.

Table 3: Results of the regression models with distance error in the allo/egocentric real space test as the dependent variable and anterior basal forebrain volume and hippocampal volume separately (Model 1) or simultaneously (Model 2) entered as predictive variables, while controlling for age, gender and years of education, within the AD group. BF: basal forebrain

Model	Volume	R^2	Beta	t-value	P-value
1					
	BF Anterior	0.68**	-0.824	-4.107	0.003
	Hippocampus	0.18	-0.428	-1.339	0.217
2					
	BF Anterior	0.68*	-0.829	-3.284	0.013
	+ Hippocampus		0.010	0.041	0.969

R^2 = R^2 value of the overall model significant at * $p<0.05$, ** $p<0.01$. Beta = standardized regression coefficient. P-value = association of each modality with the dependent variable.

Discussion

Here we show, that the basal forebrain, particularly the anterior area, undergoes significant atrophy in AD. In all groups, basal forebrain volumes were significantly correlated to real space allocentric, as well as to mixed allo/egocentric navigation in real space and computer-based tasks, whereas no interactions with purely egocentric-based navigation performances were found. Furthermore, individual group correlations revealed a significant association of mixed allo/egocentric navigation performance with anterior basal forebrain volume in the AD group, an association that was independent of hippocampal change. This suggests that anterior basal forebrain degeneration is most closely associated with the navigation impairment observed in AD subjects. As we consistently found that significant interactions of navigation scores with whole basal forebrain could be explained by an interaction of navigation scores with a specific sub-region (anterior or posterior) of the basal forebrain, only results for anterior and posterior basal forebrain volumes are discussed below.

In particular, we demonstrated that the interaction between anterior basal forebrain volume and performance in the allocentric and mixed allo/egocentric navigation task of AD patients was strong. By contrast, we did not find significant associations of basal forebrain volume with purely egocentric-type navigation. In the AD group, the significant correlations observed herein suggest that anterior basal forebrain degeneration contributes to the observed functional decline in allocentric navigation performance in AD subjects. Regression analysis further revealed that the association of anterior basal forebrain volume with the AD-related decline in mixed allo/egocentric navigation ability was independent of hippocampal volume, as the regression model including both anterior basal forebrain volume and hippocampal volume as predictors did not show an improvement of fit (or increase in R^2) over using only anterior basal forebrain as a modality. However, our findings are consistent with those of previous studies in rodents that have demonstrated that basal forebrain-derived acetylcholine is important for tasks involving cues and cue detection, including feature binding (Botly and De Rosa, 2009; Parikh et al., 2007), as well as a report that enhancement of cholinergic neuromodulation using physostigmine, an acetylcholine esterase inhibitor, increases the selectivity of neural responses during visual working memory tasks in humans (Furey et al., 2000).

Furthermore, supply of acetylcholine to the hippocampus via the anterior Ch1-2 basal forebrain neurons is important for the plasticity of hippocampal place cells (Ikonen et al.,

2002), and we have shown that the acetyl cholinesterase inhibitor donepezil improves navigation performance in the allocentric but not egocentric hMWM tasks (Hort et al., 2014). Therefore, our work provides additional evidence for the role of basal forebrain-supplied acetylcholine, particularly from the anterior nuceli, in allocentric spatial memory performance in humans.

Although basal forebrain volume and navigation performance were correlated in the AD group, and significant interactions were identified in the entire sample between basal forebrain volumes and allocentric as well as mixed allo/egocentric test scores, no significant interactions were found between basal forebrain and navigation test scores in the other subgroups (NC, aMCI) when considered independently. A similar interaction has been reported for hippocampal volume (Nedelska et al., 2012). When considering the effect of hippocampal as well as basal forebrain volume in the navigation performance of the entire cohort, the relationship of basal forebrain subregion (anterior, posterior) with navigation in either task (allocentric, mixed allo/egocentric) became non-significant, suggesting that atrophy of the basal forebrain in cognitively normal and mildly impaired subjects might be a secondary effect to that of hippocampal dysfunction. In addition cholinergic activity has been shown to be increased in the hippocampus of MCI subjects (DeKosky et al., 2002), suggesting a compensatory increased activity of basal forebrain neurons. Indeed, a deterioration of the entorhinal-hippocampal pathway, which eventuates in MCI (DeKosky et al., 2002; Ikonomovic et al., 2003) might cause increased sprouting of the basal forebrain-hippocampal connection (Stanfield and Cowan, 1982), which in turn could lead to a temporary increase in acetylcholine in the hippocampus (Contestabile, 2011).

By contrast, anterior basal forebrain volume predicted performance independently of hippocampal volume in the AD group. One possibility is that allocentric and mixed allo/egocentric navigation impairment manifests only when both hippocampal and basal forebrain function are compromised, with anterior basal forebrain degeneration occurring predominantly in the transition between mild AD and late-stage AD (Grothe et al., 2011). Therefore in the regression analysis, anterior basal forebrain degeneration would be the most predictive element of early cognitive dysfunction, measured herein as allocentric navigation performance. However given many aMCI subjects respond to cholinergic treatments and already have cholinergic dysfunction that may not fully be reflected by measures of basal forebrain volume loss, functional assessment of basal forebrain activity (e.g. cholinergic activity; Petrou et al., 2014; Kim et al., 2012) may provide increased

sensitivity as a predictor of navigation performance of normal and aMCI subjects, compared to mere volumetric assessment.

Surprisingly, the basal forebrain volume was more strongly associated with real space navigation than navigation performance in the computerized task. Even though real space and computer-based navigation scores were highly correlated for each test (allocentric, egocentric, mixed allo/egocentric) for the whole cohort, only posterior basal forebrain volume was correlated to the computer-based mixed allo/egocentric navigation performance. In rats, the posterior basal forebrain – the nucleus basalis of Meynert, which projects cortically – is implicated in visual search (Botly and De Rosa, 2012), whereas cholinergic cells located in the anterior medial septum release acetylcholine in the hippocampus after stimulation of the vestibular (motion detection) system (Tai and Leung, 2012). Therefore our finding that performance in the mixed allo/egocentric computer-based navigation task was significantly correlated to posterior basal forebrain atrophy would be consistent with the idea that a purely visual task, such as the computer-based version of the hMWM is more dependent on the function of the nucleus basalis of Meynert, whereas the real space hMWM, which involves integration of vestibular as well as visual information, requires functional septal and nucleus basalis basal forebrain neurons.

In conclusion, this study establishes that the basal forebrain is involved in regulating mixed allo/egocentric and allocentric, but not pure egocentric navigation in humans. In addition, atrophy of the basal forebrain contributes to allocentric navigation impairments in subjects with severe dementia, and this is independent of hippocampal changes. Our work also provides added justification for the use of the hMWM as a diagnostic tool for AD and/or aMCI subjects who may be of particular benefit from drugs targeting the cholinergic system.

Acknowledgements

G.M.K. was funded by an ANZ Trustees PhD scholarship for medical research and a University of Queensland International Scholarship. E.J.C. was supported by a National Health and Medical Research Council of Australia Career Development Fellowship (569601). This project was funded by a Mason Foundation grant.

Dr. Laczó has consulted for Pfizer and was a shareholder of Polyhymnia-TS between June 2012 and May 2014. He declares that he has no other competing interests. Dr. Hort has consulted for Pfizer, Janssen, Merck, Novartis, Elan, Zentiva, and Ipsen and was a shareholder of Polyhymnia-TS between June 2012 and May 2014. Other coauthors declare that they have no commercial or financial relationships to resulting in a conflict of interest. Dr. Nedelska, Dr. Laczo and Dr. Hort receive grant support from European Regional Development Fund–Project FNUSA-ICRC (CZ.1.05/1.1.00/02.0123) and project ICRC-ERA-HumanBridge (no. 316345); European Social Fund and the State Budget of the Czech Republic; European Social Fund within the project Young Talent Incubator II (reg. CZ.1.07/2.3.00/20.0117); Grant Agency of Charles University in Prague, grants 624012 and 546113; Ministry of Health, Czech Republic - conceptual development of research organization, University Hospital Motol, Prague, Czech Republic 00064203; Institutional Support of Laboratory Research Grant No. 2/2012 (699002); research projects AV0Z50110509 and RVO:67985823. Dr. Zuzana Nedelska is currently appointed as a research fellow with the Departments of Neurology and Radiology Alzheimer's Disease Imaging Research Laboratory, Mayo Clinic Rochester, MN and is further supported by CTSA Grant Number UL1 TR000135 from the National Center for Advancing Translational Sciences (NCATS), a component of the National Institutes of Health (NIH). Its contents are solely the responsibility of the authors and do not necessarily represent the official view of NIH.

We would like to acknowledge our colleague Kamil Vlcek from the Institute of Physiology, Academy of Sciences of the Czech Republic v.v.i., Prague, and undergraduate students working with us: Jiri Cerman, Ondrej Lerch, Karolina Buresova, Andrea Burianova, Petr Kala, Martina Parizkova, Drahomir Kolencik.

References

Astur, R.S., Taylor, L.B., Mamelak, A.N., Philpott, L., Sutherland, R.J., 2002. Humans with hippocampus damage display severe spatial memory impairments in a virtual Morris water task. Behavioural Brain Research 132, 77-84.

Avants, B.B., Epstein, C.L., Grossman, M., Gee, J.C., 2008. Symmetric diffeomorphic image registration with cross-correlation: evaluating automated labeling of elderly and neurodegenerative brain. Medical Image Analysis 12, 26-41.

Avants, B.B., Yushkevich, P., Pluta, J., Minkoff, D., Korczykowski, M., Detre, J., Gee, J.C., 2010. The optimal template effect in hippocampus studies of diseased populations. NeuroImage 49, 2457-2466.

Berger-Sweeney, J., Stearns, N.A., Murg, S., Floerke-Nashner, L.R., Lappi, D.A., Baxter, M.G., 2001. Selective immunolesions of cholinergic neurons in mice: effects on neuranatomy, neurochemistry, and behavior. Journal of Neuroscience 21, 8164-8173.

Botly, L.C., De Rosa, E., 2009. Cholinergic deafferentation of the neocortex using 192 IgG-saporin impairs feature binding in rats. Journal of Neuroscience 29, 4120-4130.

Botly, L.C., De Rosa, E., 2012. Impaired visual search in rats reveals cholinergic contributions to feature binding in visuospatial attention. Cerebral Cortex 22, 2441-2453.

Bourgeat, P., Chetelat, G., Villemagne, V.L., Fripp, J., Raniga, P., Pike, K., Acosta, O., Szoeke, C., Ourselin, S., Ames, D., Ellis, K.A., Martins, R.N., Masters, C.L., Rowe, C.C., Salvado, O., 2010. Beta-amyloid burden in the temporal neocortex is related to hippocampal atrophy in elderly subjects without dementia. Neurology 74, 121-127.

Butler, T., Blackmon, K., Zaborszky, L., Wang, X., DuBois, J., Carlson, C., Barr, W.B., French, J., Devinsky, O., Kuzniecky, R., Halgren, E., Thesen, T., 2012. Volume of the human septal forebrain region is a predictor of source memory accuracy. Journal of the International Neuropsychological Society 18, 157-161.

Contestabile, A., 2011. The history of the cholinergic hypothesis. Behavioural Brain Research 221, 334-340.

DeKosky, S.T., Ikonomovic, M.D., Styren, S.D., Beckett, L., Wisniewski, S., Bennett, D.A., Cochran, E.J., Kordower, J.H., Mufson, E.J., 2002. Upregulation of choline acetyltransferase activity in hippocampus and frontal cortex of elderly subjects with mild cognitive impairment. Annals of Neurology 51, 145-155.

Furey, M.L., Pietrini, P., Haxby, J.V., 2000. Cholinergic enhancement and increased selectivity of perceptual processing during working memory. Science 290, 2315-2319.

George, S., Mufson, E.J., Leurgans, S., Shah, R.C., Ferrari, C., deToledo-Morrell, L., 2011. MRI-based volumetric measurement of the substantia innominata in amnestic MCI and mild AD. Neurobiology of Aging 32, 1756-1764.
Grothe, M., Heinsen, H., Teipel, S., 2012. Longitudinal measures of cholinergic forebrain atrophy in the transition from healthy aging to Alzheimer's disease. Neurobiology of Aging 34, 1210-1220.
Grothe, M., Heinsen, H., Teipel, S.J., 2011. Atrophy of the cholinergic basal forebrain over the adult age range and in early stages of Alzheimer's disease. Biological Psychiatry 71, 805-813.
Hamlin, A.S., Windels, F., Boskovic, Z., Sah, P., Coulson, E.J., 2013. Lesions of the basal forebrain cholinergic system in mice disrupt idiothetic navigation. PloS One 8, e53472.
Hasselmo, M.E., McGaughy, J., 2004. High acetylcholine levels set circuit dynamics for attention and encoding and low acetylcholine levels set dynamics for consolidation. Progress in Brain Research 145, 207-231.
Hort, J., Andel, R., Mokrisova, I., Gazova, I., Amlerova, J., Valis, M., Coulson, E.J., Harrison, J., Windisch, M., Laczo, J., 2014. Effect of donepezil in Alzheimer disease can be measured by a computerized human analog of the morris water maze. Neuro-degenerative Diseases 13, 192-196.
Hort, J., Laczo, J., Vyhnalek, M., Bojar, M., Bures, J., Vlcek, K., 2007. Spatial navigation deficit in amnestic mild cognitive impairment. Proceedings of the National Academy of Sciences of the United States of America 104, 4042-4047.
Ikonen, S., McMahan, R., Gallagher, M., Eichenbaum, H., Tanila, H., 2002. Cholinergic system regulation of spatial representation by the hippocampus. Hippocampus 12, 386-397.
Ikonomovic, M.D., Mufson, E.J., Wuu, J., Cochran, E.J., Bennett, D.A., DeKosky, S.T., 2003. Cholinergic plasticity in hippocampus of individuals with mild cognitive impairment: correlation with Alzheimer's neuropathology. Journal of Alzheimer's disease 5, 39-48.
Kim, M.J., Lee, K.M., Son, Y.D., Jeon, H.A., Kim, Y.B., Cho, Z.H., 2012. Increased basal forebrain metabolism in mild cognitive impairment: an evidence for brain reserve in incipient dementia. Journal of Alzheimer's Disease 32, 927-938.
Laczo, J., Andel, R., Vlcek, K., Macoska, V., Vyhnalek, M., Tolar, M., Bojar, M., Hort, J., 2011. Spatial navigation and APOE in amnestic mild cognitive impairment. Neuro-degenerative Diseases 8, 169-177.
McKhann, G., Drachman, D., Folstein, M., Katzman, R., Price, D., Stadlan, E.M., 1984. Clinical diagnosis of Alzheimer's disease: report of the NINCDS-ADRDA Work Group

under the auspices of Department of Health and Human Services Task Force on Alzheimer's Disease. Neurology 34, 939-944.
Mufson, E., 2003. Human cholinergic basal forebrain: chemoanatomy and neurologic dysfunction. Journal of Chemical Neuroanatomy 26, 233-242.
Nedelska, Z., Andel, R., Laczo, J., Vlcek, K., Horinek, D., Lisy, J., Sheardova, K., Bures, J., Hort, J., 2012. Spatial navigation impairment is proportional to right hippocampal volume. Proceedings of the National Academy of Sciences of the United States of America 109, 2590-2594.
Parikh, V., Kozak, R., Martinez, V., Sarter, M., 2007. Prefrontal acetylcholine release controls cue detection on multiple timescales. Neuron 56, 141-154.
Petersen, R.C., 2004. Mild cognitive impairment as a diagnostic entity. Journal of Internal Medicine 256, 183-194.
Petrou, M., Frey, K.A., Kilbourn, M.R., Scott, P.J., Raffel, D.M., Bohnen, N.I., Muller, M.L., Albin, R.L., Koeppe, R.A., 2014. In vivo imaging of human cholinergic nerve terminals with (-)-5-(18)F-fluoroethoxybenzovesamicol: biodistribution, dosimetry, and tracer kinetic analyses. Journal of Nuclear Medicine 55, 396-404.
Sarter, M., Gehring, W.J., Kozak, R., 2006. More attention must be paid: the neurobiology of attentional effort. Brain Research Reviews 51, 145-160.
Schliebs, R., Arendt, T., 2006. The significance of the cholinergic system in the brain during aging and in Alzheimer's disease. Journal of Neural Transmission 113, 1625-1644.
Stanfield, B.B., Cowan, W.M., 1982. The sprouting of septal afferents to the dentate gyrus after lesions of the entorhinal cortex in adult rats. Brain Research 232, 162-170.
Tai, S.K., Leung, L.S., 2012. Vestibular stimulation enhances hippocampal long-term potentiation via activation of cholinergic septohippocampal cells. Behavioural Brain Research 232, 174-182.
Vyhnalek, M., Nikolai, T., Andel, R., Nedelska, Z., Rubinova, E., Markova, H., Laczo, J., Bezdicek, O., Sheardova, K., Hort, J., 2014. Neuropsychological correlates of hippocampal atrophy in memory testing in nondemented older adults. Journal of Alzheimer's Disease, doi:10.3233/JAD-132642.
Weniger, G., Ruhleder, M., Wolf, S., Lange, C., Irle, E., 2009. Egocentric memory impaired and allocentric memory intact as assessed by virtual reality in subjects with unilateral parietal cortex lesions. Neuropsychologia 47, 59-69.
Zaborszky, L., Hoemke, L., Mohlberg, H., Schleicher, A., Amunts, K., Zilles, K., 2008. Stereotaxic probabilistic maps of the magnocellular cell groups in human basal forebrain. NeuroImage 42, 1127-1141.

4.3 Supplementary data

Supplementary Table 1: Demographics of NC, aMCI and AD groups. Age and years of education are expressed as mean ± standard deviation.

	NC	aMCI	AD
	(n=17)	(n=27)	(n=22)
Age	70.1 ± 4.8	71.4 ± 8.1	74.7 ± 8.1
Gender M/F	7/10	17/10	10/12
Years of education	15.6 ± 2.3	15.1 ± 3.2	12.1 ± 2.3
MMSE	28.5 ± 1.7	25.3 ± 3.8	19.5 ± 2.9

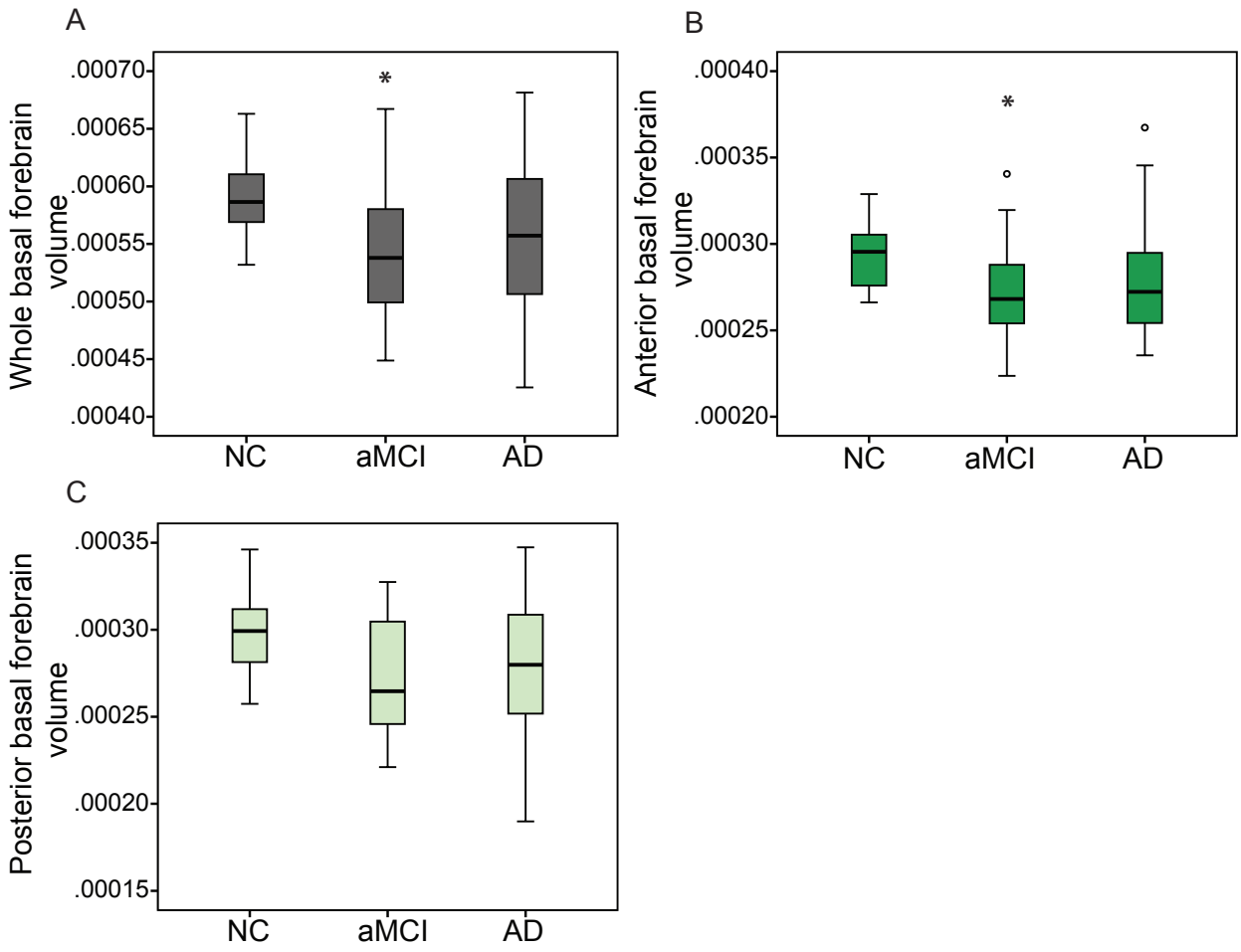

Supplementary Figure 1: Group comparisons of whole, anterior and posterior basal forebrain volumes between NC, aMCI and AD groups. There was a significant reduction in whole (A) and anterior (B) but not posterior (C) basal forebrain volume between the NC and aMCI groups. The AD group was not significantly different from either the NC or aMCI group for any of the basal forebrain volumes. * $p<0.05$. Whiskers represent min/max values except data points (circles) more than 1.5 interquartile ranges away from the 75th percentile.

4.4 Discussion and implication of findings

Two main findings of this study were that (1) basal forebrain volume is indirectly associated with navigation performance in healthy/mild cognitively impaired subjects, possibly through modulation of activity of hippocampal and cortical areas and (2) degeneration of the anterior basal forebrain volume is a strong correlate of navigation impairment in Alzheimer's disease subjects, independent of hippocampal volume. This is the first study to our knowledge that demonstrates involvement of the basal forebrain with a specific type of navigation in a dementia cohort.

Contrary to the hypothesis based on the results of the animal study conducted in the Coulson laboratory, which demonstrated an effect of basal forebrain degeneration on egocentric navigation (Hamlin et al., 2013), we found correlations of basal forebrain volume with allocentric or mixed allo/egocentric navigation, but no interaction with purely egocentric navigation. However, this finding is consistent with a human study showing that an acetylcholine esterase inhibitor aimed at improving basal forebrain neuronal function also improved allocentric but not egocentric navigation (Hort et al., 2014). It must also be remembered that a selective and mild lesion of cholinergic neurons in mice is also not necessarily comparable to severely cognitively impaired human subjects displaying the full spectrum of Alzheimer's dementia symptoms. Indeed the lesion of cholinergic neurons in these mice did not result in basal forebrain atrophy (see next chapter), which has been demonstrated to be a consistent feature of Alzheimer's disease patients (chapters 3, 4). Therefore a more sensitive measure of basal forebrain dysfunction may reveal interactions with other features of Alzheimer's disease (behavioural or pathological) earlier in the disease aetiology.

Indeed MRI imaging methods are also capable of measuring integrity of brain connections, which might have additional diagnostic value, as network disconnection possibly occurs before actual volume change of a brain area, such as the basal forebrain, in Alzheimer's disease. This is the focus of the next chapter.

Chapter 5: Imaging degeneration of basal forebrain cholinergic neuronal connections in a mouse model

5.1 Introduction

The cholinergic lesion mouse model used in the Coulson laboratory displays loss of cholinergic neurons as well as denervation of basal forebrain efferents to the hippocampus, as demonstrated in this chapter. This robust phenotype of degeneration of basal forebrain neuronal connections in a mouse model enabled a proof-of-principle study to test if it was possible to detect corresponding changes through imaging measures and correlate these changes back to histological measures of the lesion. In humans, tractography has previously been used to assess white matter integrity in Alzheimer's disease patients and amnestic mild cognitively impaired subjects compared to controls (e.g. Agosta et al., 2011); however it was not possible to attribute the observed changes to an underlying biological mechanism.

Here, we asked whether dMRI could be used to assess changes in local diffusion in the basal forebrain area as well as changes in diffusion parameters of the basal forebrain-hippocampal pathway as a measure of early basal forebrain degeneration prior to atrophy, using a technique called tractography (Mori and Zhang, 2006).

This study has been published in the journal *Neuroimage*.

5.2 Diffusion-weighted magnetic resonance imaging detection of basal forebrain cholinergic degeneration in a mouse model

[1]**GM Kerbler**, [1]AS Hamlin, [2,3]K Pannek, [3]ND Kurniawan, [3]MD Keller, [2,3]SE Rose, [1]EJ Coulson. (2013) Diffusion-weighted magnetic resonance imaging detection of basal forebrain cholinergic degeneration in a mouse model. *Neuroimage*, 66C: 133-141

[1]Queensland Brain Institute,
[2]Centre for Clinical Research,
[3]Centre for Advanced Imaging,
The University of Queensland, Brisbane, 4072 Qld. Australia

NeuroImage 66 (2013) 133–141

Contents lists available at SciVerse ScienceDirect

NeuroImage

journal homepage: www.elsevier.com/locate/ynimg

Diffusion-weighted magnetic resonance imaging detection of basal forebrain cholinergic degeneration in a mouse model

Georg M. Kerbler [a], Adam S. Hamlin [a], Kerstin Pannek [b,c], Nyoman D. Kurniawan [c], Marianne D. Keller [c], Stephen E. Rose [b,c], Elizabeth J. Coulson [a,*]

[a] Queensland Brain Institute, The University of Queensland, Brisbane, 4072 Qld., Australia
[b] Centre for Clinical Research, The University of Queensland, Brisbane, 4072 Qld., Australia
[c] Centre for Advanced Imaging, The University of Queensland, Brisbane, 4072 Qld., Australia

ARTICLE INFO

Article history:
Accepted 26 October 2012
Available online 2 November 2012

Keywords:
Alzheimer's disease
Cholinergic basal forebrain
Tractography
MRI
Diffusion tensor imaging
Neurodegeneration

ABSTRACT

Loss of basal forebrain cholinergic neurons is an early and key feature of Alzheimer's disease, and magnetic resonance imaging (MRI) volumetric measurement of the basal forebrain has recently gained attention as a potential diagnostic tool for this condition. The aim of this study was to determine whether loss of basal forebrain cholinergic neurons underpins changes which can be detected through diffusion MRI using diffusion tensor imaging (DTI) and probabilistic tractography in a mouse model. To cause selective basal forebrain cholinergic degeneration, the toxin saporin conjugated to a p75 neurotrophin receptor antibody (mu-p75-SAP) was used. This resulted in ~25% loss of the basal forebrain cholinergic neurons and significant loss of terminal cholinergic projections in the hippocampus, as determined by histology. To test whether lesion of cholinergic neurons caused basal forebrain, hippocampal, or whole brain atrophy, we performed manual segmentation analysis, which revealed no significant atrophy in lesioned animals compared to controls (Rb-IgG-SAP). However, analysis by DTI of the basal forebrain area revealed a significant increase in fractional anisotropy (FA; +7.7%), mean diffusivity (MD; +6.1%), axial diffusivity (AD; +8.5%) and radial diffusivity (RD; +4.0%) in lesioned mice compared to control animals. These parameters strongly inversely correlated with the number of choline acetyl transferase-positive neurons, with FA showing the greatest association ($r^2 = 0.72$), followed by MD ($r^2 = 0.64$), AD ($r^2 = 0.64$) and RD ($r^2 = 0.61$). Moreover, probabilistic tractography analysis of the septo-hippocampal tracts originating from the basal forebrain revealed an increase in streamline MD (+5.1%) and RD (+4.3%) in lesioned mice. This study illustrates that moderate loss of basal forebrain cholinergic neurons (representing only a minor proportion of all septo-hippocampal axons) can be detected by measuring either DTI parameters of the basal forebrain nuclei or tractography parameters of the basal forebrain tracts. These findings provide increased support for using DTI and probabilistic tractography as non-invasive tools for diagnosing and/or monitoring the progression of conditions affecting the integrity of the basal forebrain cholinergic system in humans, including Alzheimer's disease.

Introduction

The cholinergic basal forebrain is a key modulator of neurotransmission, function and plasticity of the hippocampus and amygdala, as well as the entire cortical mantle (Mesulam et al., 1983), and is strongly implicated in regulating attention, learning and memory (Mufson, 2003). Pathologically, loss of basal forebrain cholinergic neurons is a pathological hallmark of Alzheimer's disease at autopsy (Mufson et al., 2002; Whitehouse et al., 1982). Furthermore, numerous studies have shown that degeneration of the basal forebrain is linked, albeit indirectly, to early signs of cognitive decline in Alzheimer's disease patients, including deficits in spatial navigation and memory (George et al., 2009; Grothe et al., 2010, 2011; Muth et al., 2010). In these studies, magnetic resonance imaging (MRI) methods were used to detect structural changes associated with atrophy of the basal forebrain (Grothe et al., 2011), which has been correlated with cognitive decline in cohorts of patients diagnosed with Alzheimer's disease or its prodromal stage, mild cognitive impairment (MCI) (Grothe et al., 2011). In some cases, basal forebrain atrophy was observed as early as 4.5 years before the onset of overt clinical symptoms (Hall et al., 2008).

By the time atrophy of a structure can be detected as a volumetric reduction with structural MRI, significant cell and tissue loss has

Abbreviations: AD, axial diffusivity; ChAT, Choline acetyl transferase; DePeX, Distrene-80/Plasticizer/Xylene; dMRI, diffusion MRI; DTI, diffusion tensor imaging; FA, fractional anisotropy; i.p., intraperitoneal; MD, mean diffusivity; MCI, mild cognitive impairment; MRI, magnetic resonance imaging; NHS, normal horse serum; $p75^{NTR}$, p75 neurotrophin receptor; PB, phosphate buffer; PBS, phosphate buffered saline; PBT-X, PB containing 0.2% Triton X-100; RD, radial diffusivity; ROI, region of interest; SAP, saporin; s.c., subcutaneously; TBSS, Tract-based spatial statistics.

* Corresponding author. Fax: +61 7 33466301.
E-mail address: e.coulson@uq.edu.au (E.J. Coulson).

1053-8119/$ – see front matter.
http://dx.doi.org/10.1016/j.neuroimage.2012.10.075

already occurred. The drugs currently prescribed for the treatment of Alzheimer's disease, inhibitors of acetyl cholinesterase, enhance basal forebrain cholinergic function by inhibiting the degradation of acetylcholine produced by the surviving neurons. However, as the diagnosis of MCI or Alzheimer's disease currently occurs at a stage at which the cholinergic system has been irreversibly damaged, it is not surprising that these drugs have mild to little effect in prolonging cognitive function (Mancuso et al., 2011). Non-invasive early detection of basal forebrain neurodegeneration prior to overt tissue loss therefore has the potential to improve the window of therapeutic efficacy.

Diffusion MRI (dMRI), a technique used to analyze structural integrity and brain connectivity, has been successfully employed to detect differences between Alzheimer's patients and healthy control subjects (Kiuchi et al., 2009; Pievani et al., 2010; Teipel et al., 2010). In particular, tractography analysis of axonal regions known to degenerate in Alzheimer's disease, such as the fornix and the cingulum, have shown significant changes in diffusion parameters in humans with the condition (Oishi et al., 2011; Pievani et al., 2010). However the pathophysiological reason for these changes is not known. The aim of the current study was to determine, using a mouse model, whether mild to moderate loss of basal forebrain cholinergic nuclei and axons could underpin changes to dMRI measures and tractography prior to the point at which changes correlate with overt atrophy. The most commonly used transgenic mouse models of Alzheimer's disease show only certain pathological features of the human condition (Kokjohn and Roher, 2009), failing to reproduce the loss of basal forebrain cholinergic neurons characteristic of Alzheimer's disease. Consequently, both diffusion and structural imaging studies of transgenic Alzheimer's disease mice have focused on brain regions other than the basal forebrain (Harms et al., 2006; Lau et al., 2008; Maheswaran et al., 2009; Mueggler et al., 2004; Sun et al., 2005; Thiessen et al., 2010). However, one study of a transgenic mouse model using structural MRI has reported a significant interaction between age and genotype in a variety of brain regions including the medial septum, a sub-nucleus of the basal forebrain (Badea et al., 2010). In the current study, we investigated a robust model of selective basal forebrain cholinergic neuron loss, which results in a similar spatial navigation and memory deficit in mice (Berger-Sweeney et al., 2001; Moreau et al., 2008; Perry et al., 2001) to that seen in Alzheimer's disease patients (Hort et al., 2007). In this model, the toxin saporin, conjugated to an antibody to a receptor almost exclusively expressed by basal forebrain cholinergic neurons (p75 neurotrophin receptor; $p75^{NTR}$) is injected into the ventricles (Berger-Sweeney et al., 2001). Therefore, unlike in transgenic mouse models of Alzheimer's disease, the changes in dMRI induced by cholinergic degeneration can be studied with little influence from other pathological features.

Materials and methods

Animals

Experimentally naive male C57Bl/6 J mice were housed in groups of four and maintained on a 12 h light/dark cycle, with food and water provided *ad libitum*. All procedures were approved by the University of Queensland Animal Ethics Committee.

Surgery

Twelve 8- to 10-week-old male C57Bl/6J mice (22–24 g) were anesthetized by intraperitoneal (i.p.) injection with a mixture of ketamine (130 mg/kg) and the muscle relaxant xylazine (6 mg/kg). Each mouse was then placed in a stereotaxic frame (with the incisor bar maintained at −3.3 mm below horizontal to achieve a flat skull position). Bilateral infusions of mu-p75-saporin (Advanced Targeting Systems, San Diego, CA; 5 mice) or control rabbit-IgG-saporin (Advanced Targeting Systems; 7 mice) dissolved in phosphate buffered saline (PBS; 0.2 μg/ventricle) were performed using a 30 G needle attached to a 5 μl Hamilton syringe. The needle was lowered into the lateral ventricle using the following co-ordinates: A–P, −0.3 mm; M-L, ± 1.0 mm; D-V, −2.0 mm from Bregma (Franklin and Paxinos, 2007). Infusions were conducted over 5 min, after which the needle was left in place for 10 min to allow for diffusion. Immediately after surgery, mice were injected subcutaneously (s.c.) with the analgesic torbogesic (1.3 mg/kg), and the antibiotic Baytril® (0.43 mg/kg).

Fourteen days post-surgery mice were deeply anesthetized with sodium pentobarbital (100 mg/kg i.p.) and perfused transcardially with 20 ml of 0.9% saline, containing 1% sodium nitrite and heparin (5000 I.U./ml), followed by 100 ml of 4% paraformaldehyde in 0.1 M phosphate buffer (PB), pH 7.4. Brains were removed from the skulls and post-fixed overnight in the same fixative, followed by repeated washing in PBS (pH 7.4) for 4 days prior to MRI acquisition.

After close examination of whole brain MR scans and histological sections in each animal, two mice (one control and one lesioned animal) were excluded from the study prior to analysis due to injuries to the fimbria/fornix caused by the injections.

MRI acquisition

Mouse brains were immersed in Fomblin oil (Y06/6 grade, Solvay, NY) and diffusion weighted magnetic resonance images were acquired according to the protocol of Moldrich et al. (2010). Briefly, a small animal MRI system (16.4 T vertical bore; Bruker Biospin, Rheinstetten, Germany; ParaVision v5.0) with a 15 mm linear SAW coil (M2MImaging, Brisbane, Australia) was used. A 3D diffusion-weighted spin-echo sequence was acquired with TR/TE = 400 ms/22.3 ms, signal average of 1, and 1.4 phase encoding accelerations using partial Fourier acquisition. High angular resolution diffusion images were acquired with two minimally diffusion-weighted ($b = 0$ s/mm^2), and 30 high diffusion-weighted images ($\delta/\Delta = 2.5/14$ ms, $b = 5000$ s/mm^2) with the encoding gradient vectors uniformly distributed using the electrostatic approach (Jones et al., 1999). The image data resolution was 100 μm isotropic (uninterpolated) and total acquisition time was 16 h.

Segmentation and DTI analysis

DTI reconstruction of the diffusion data was performed using MRtrix (v0.2.9, www.nitrc.org/projects/mrtrix). The basal forebrain was drawn manually on 12 consecutive coronal slices using color-coded fractional anisotropy (FA) maps and using the mouse brain atlas of Franklin and Paxinos (2007) as a guide. Volumes of the basal forebrain were created, starting at approximately 1.34 mm anterior to Bregma and finishing at approximately 0.26 mm anterior to Bregma, thereby assuring that the mask predominately encompassed the medial septum and the vertical and horizontal diagonal bands of Broca. The anterior-posterior distance covered was 1200 μm (12 slices of 100 μm). However, given the lack of specific anatomical boundaries observable by MRI contrast, the masks were also likely to contain minor parts of the lateral diagonal band of Broca (also called the magnocellular preoptic nucleus), as well as the basal part of the substantia innominata in the posterior section of the mask (ventral part of the mask in Fig. 2E).

The hippocampal volume, starting at approximately −0.88 mm posterior to Bregma and finishing at approximately −4.04 mm posterior to Bregma, and the whole brain volume, were manually segmented on gray-scale FA maps. The basal forebrain volume and hippocampal volume were normalized to the whole brain volume. The whole brain, hippocampal and basal forebrain volumes were measured by a researcher blind to group status. The basal forebrain mask was used to extract FA, mean diffusivity, axial diffusivity and radial diffusivity values.

Tractography

MRtrix (v0.2.9, www.nitrc.org/projects/mrtrix) was used to perform constrained spherical deconvolution and to generate the fiber orientation distribution. Probabilistic tractography was performed with MRtrix (Tournier et al., 2012), creating whole brain tractograms by seeding every voxel five times and using tracking parameters optimized for the mouse brain (step size = 0.01 mm, radius of curvature = 0.07 mm; see Moldrich et al., 2010).

Basal forebrain streamlines were then extracted by applying the basal forebrain volume as a waypoint mask to the whole brain tractograms. To extract streamlines that project from the basal forebrain through the fimbria/fornix to the hippocampus, but not including cortical areas, a hippocampal waypoint region of interest (ROI) was created at approximately −2.60 mm posterior to Bregma. This hippocampal waypoint ROI, together with additional exclusion ROIs used in conjunction with the basal forebrain mask, eliminated false positive streamlines such as the stria terminalis and the optic tract.

To test whether the streamline changes were selective for the basal forebrain tracts, we performed tractography on a control tract, namely the inferior cerebellar peduncle. Bilateral ROIs were drawn on color-coded FA maps on three consecutive slices from approximately −6.00 to −6.24 mm posterior to Bregma, using the mouse brain atlas of Franklin and Paxinos (2007) as guidance. Inferior cerebellar peduncle streamlines were obtained by applying the ROI to whole brain tractograms.

Streamline number was normalized to the voxel number of the corresponding ROI. For every tract, the number of streamlines traversing each voxel was counted, and a threshold of 15 streamlines per voxel (determined empirically) was used to measure track volume. In addition, FA, mean diffusivity, axial diffusivity and radial diffusivity were extracted using the individual tracks for sampling.

MRI data analysis

An unpaired two-tailed Mann–Whitney test (CI = 95%) was used to determine significant differences between groups of the basal forebrain, hippocampus and whole brain volumes, as well as the basal forebrain DTI parametric and tractography measures. Spearman's rho was used to assess correlations between DTI parametric and cholinergic neuron number. A false discovery rate ($\alpha = 0.1$) was used to correct for multiple comparisons.

Immunohistochemistry

Immediately following scanning (see Surgery section) brains were placed in 20% sucrose solution overnight. Brains were blocked using a matrix (Stoelting Co., Wood Dale, IL), aligned to the atlas of Franklin and Paxinos (2007), and 40 μm coronal sections were cut in three serially adjacent sets through the basal forebrain and hippocampus using a sliding microtome (SM2000r, Leica, Sydney, Australia). Sections were stored in 0.1% sodium azide in 0.1 M PBS.

One series of sections was used to reveal choline acetyltransferase (ChAT) using peroxidase immunohistochemistry. Free-floating sections were washed repeatedly in 0.1 M PB, followed by two 30 min washes in 50% ethanol, the second of which contained 3% H_2O_2. Sections were then incubated in 5% normal horse serum (NHS) in PB for 30 min, followed by incubation with goat anti-ChAT antibody (1:3000; Millipore, Billerica, MA), diluted in 0.1 M PB containing 0.1% sodium azide, 2% NHS and 0.2% Triton X-100 (PBT-X), for 48 h at 4 °C with gentle agitation. After washing, sections were incubated overnight at room temperature in biotinylated donkey anti-goat IgG (1:1000; Jackson Immunoresearch Laboratories, West Grove, PA) diluted in 2% NHS PBT-X. Sections were then incubated for 2 h at room temperature in ABC reagent (Vector Elite kit: 6 μl/ml avidin and 6 μl/ml biotin; Vector Laboratories, Burlingame, CA). Black immunoreactive cytoplasm labeled for ChAT was revealed by a nickel-intensified diaminobenzidine reaction, with peroxide being generated by glucose oxidase. First, sections were washed in PB, followed by 0.1 M acetate buffer, and then incubated for 15 min in 0.1 M acetate buffer (pH 6.0) containing 2% nickel sulfate, 0.025% 3,3-diaminobenzidine, 0.04% ammonium chloride, and 0.02% D-glucose. The peroxidase reaction was started by adding glucose oxidase (0.2 μl/ml) and stopped using acetate buffer (pH 6.0). Brain sections were then washed in PB. Sections were mounted onto chrome-alum/gelatin-treated slides, dehydrated, cleared in histolene, and coverslipped with DePeX (Distrene-80/plasticizer/xylene; Crown Scientific, Sydney, Australia).

A second series of sections through the basal forebrain of lesioned and control mice was used to immunohistochemically label parvalbumin. Free-floating sections were washed repeatedly in PBS, followed by a 2 h incubation in PBS containing 10% NHS and 0.5% Triton X-100. Mouse anti-parvalbumin (1:1000; Millipore), diluted in 0.1 M PBS containing 0.1% sodium azide, 2% NHS and 0.2% Triton X-100, was then added to the sections, which were incubated for 48 h at room temperature, with gentle agitation. After washing, sections were incubated for 4 h at room temperature in donkey anti-mouse FITC (1:200; Jackson Immunoresearch Laboratories), diluted in 2% NHS PBT-X. After washing, sections were mounted onto chrome alum/gelatin-treated slides and coverslipped with buffered glycerol (pH 8.6).

Neuronal counting

Bilateral counts of neurons immunoreactive for ChAT were conducted through the rostro-caudal extent of the basal forebrain from 1.32 mm anterior to Bregma to 0.24 mm anterior to Bregma (Franklin and Paxinos, 2007) on sections that were 120 μm apart, to exactly match the basal forebrain mask created by MRI. Images of the sections were taken a Zeiss Axio Imager Z1 and were counted using Imaris software (v7.5, Bitplane) by a researcher blind to the experimental conditions.

Counts of parvalbumin-positive ($p75^{NTR}$-negative) neurons were analyzed as above using images of sections of mu-p75-saporin and Rb-IgG-saporin injected brains. Eight-bit monochrome images were taken of the basal forebrain sections from 1.32 mm anterior to Bregma to 0.98 mm anterior to Bregma. Images were captured using a Zeiss Axio Imager Z1 and AxioVision v4.8 software, before being exported into ImageJ software (NIH) where bilateral counts of parvalbumin-positive nuclei were conducted by a researcher blind to the conditions.

Differences in the mean number of ChAT-immunoreactive and parvalbumin-immunoreactive cells counted for each region of the basal forebrain per animal per group were analyzed using ANOVA.

Results

Mu-p75-SAP induced specific lesion of the cholinergic basal forebrain

To selectively ablate basal forebrain cholinergic neurons, mice were injected with saporin conjugated to either a $p75^{NTR}$ antibody (mu-p75-SAP) or to a rabbit IgG (Rb-IgG-SAP) as a control. Following MRI scans, the extent and specificity of the lesion was determined by immunohistological analysis of the medial septum and the vertical and horizontal diagonal bands of Broca (Fig. 1). These regions contain approximately equal numbers of cholinergic neurons, which express $p75^{NTR}$ (Mufson et al., 1989), and GABAergic neurons, which do not express $p75^{NTR}$ (Wainer et al., 1985). Both neuronal populations provide input to the hippocampus through the fimbria/fornix.

A significant loss of approximately 25% of ChAT-positive (cholinergic) cells in the medial septum, and the vertical and horizontal diagonal bands of Broca was observed in the lesioned animals compared to the controls (Figs. 1A, C). We also observed a clear reduction in ChAT-positive terminal labeling in the hippocampus of the

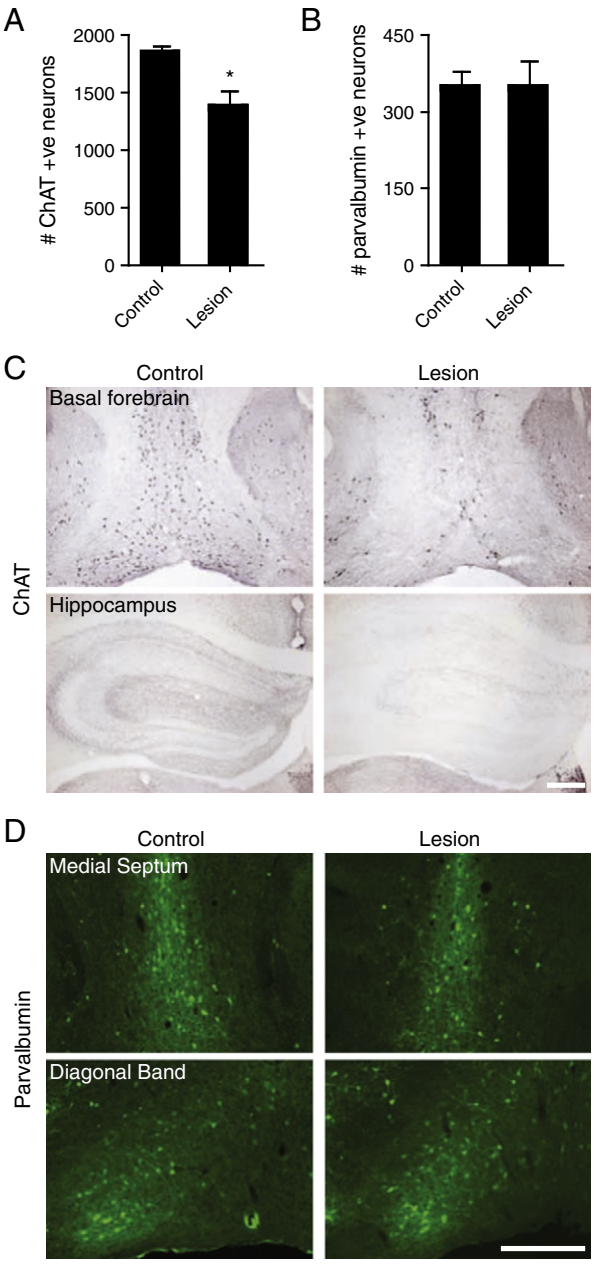

Fig. 1. Intracerebroventricular application of mu-p75-saporin produced a specific lesion of basal forebrain cholinergic neurons. A. Mean (± SEM) total number of ChAT-positive neurons in the basal forebrain following application of mu-p75-SAP (Lesion, $n=4$) or Rb-IgG-SAP (Control, $n=6$). A significant decrease in the number of ChAT-positive neurons was found following application of mu-p75-SAP. B. Mean (± SEM) number of parvalbumin-positive neurons in the basal forebrain following application of mu-p75-SAP ($n=4$) or Rb-IgG-SAP ($n=3$). Application of mu-p75-SAP had no effect on the number of parvalbumin-positive neurons. C. Photomicrographs of ChAT-immunopositive neuronal cell bodies in the basal forebrain and ChAT-immunoreactive terminal fields in the hippocampus following application of Rb-IgG-SAP (left) and mu-p75-SAP (right). D. Photomicrographs of parvalbumin-immunopositive neuronal cell bodies in the medial septum and vertical diagonal band of Broca following application of Rb-IgG-SAP (left) and mu-p75-SAP (right). Scale bar = 400 μm. *$p<0.05$.

lesioned mice compared to control mice (Fig. 1C), indicating that the septo-hippocampal cholinergic system was functionally impaired in these animals.

To determine if the treatment caused a specific loss of the cholinergic cells in the basal forebrain we also quantified the number of GABAergic neurons, visualized by parvalbumin staining, in the medial septum and the vertical diagonal band of Broca (Figs. 1B, D). This analysis revealed no significant effect of mu-p75-SAP injections compared to Rb-IgG-SAP treatment on parvalbumin-positive neuron number (Figs. 1B, D), demonstrating that we had achieved a specific lesion of basal forebrain cholinergic neurons. Furthermore, no overt atrophy of the basal forebrain was appreciable on parvalbumin-immunolabeled histological sections (Fig. 1D).

Manual segmentation analysis showed no volumetric differences between control and lesioned groups

To test if the observed loss of basal forebrain cholinergic neurons induced atrophy of the basal forebrain, the hippocampus or the whole brain, we conducted manual segmentation analysis (see Segmentation and DTI analysis section). Firstly, individual whole brain, hippocampal and basal forebrain masks were created. The latter encompassed the medial septum and the vertical and horizontal diagonal bands of Broca (Fig. 2). We then compared the volumes of these masks between groups. There was no significant reduction in the average whole brain volume of the lesioned group compared to the control group (Table 1), and no significant difference in normalized basal forebrain or hippocampal volume between lesioned and control groups.

Increased diffusion in the basal forebrain was inversely correlated to cholinergic neurodegeneration

To determine whether the lesion could be detected by diffusion MRI measures, the basal forebrain DTI parameters for each of the brains were analyzed. The mean FA (Fig. 2D), mean diffusivity (Fig. 2F), axial diffusivity (Fig. 2G) and radial diffusivity (Fig. 2H) within the basal forebrain volume were then extracted for each mouse and compared between groups. Representative images of the various DTI maps used for the analysis within the basal forebrain area can be seen in Figs. 2D, F–H. Interestingly, this analysis revealed that all diffusion metrics were significantly increased for the basal forebrain area in the lesioned group compared to the control group. Specifically, the mean values for FA (Fig. 3A), mean diffusivity (Fig. 3B), axial diffusivity (Fig. 3C) and radial diffusivity (Fig. 3D) were all significantly higher in the lesioned animals.

To determine the correlation between histological measures and DTI-associated changes in response to basal forebrain cholinergic neuron loss, we performed nonparametric bivariate correlation analysis of the ChAT-positive neuron numbers and DTI parameters. This revealed that all DTI measures except for radial diffusivity were significantly inversely correlated to ChAT-positive neuron number (Figs. 3E–H). This indicates that DTI parameters such as FA, mean diffusivity and axial diffusivity are sensitive measures of neuronal lesions and can reflect the degree of neurodegeneration in this model.

Tractography streamlines showed decreased integrity

We next investigated whether a significant reduction in septo-hippocampal connectivity could be detected in the lesioned group of animals. In order to analyze the streamlines connecting the basal forebrain and hippocampus, whole brain tractograms of mice were created using MRtrix. The basal forebrain mask was used together with a hippocampal waypoint ROI (Fig. 4A; see Tractography section), and applied to the tractograms to delineate the streamlines between these two structures via the fimbria/fornix. The resulting streamlines (Figs. 4A–C) were anatomically verified (Fig. 4D) as innervating the alveus and the oriens layer of the hippocampus and, to a lesser degree, other regions of the hippocampus such as the CA3 region and the dentate gyrus, replicating the innervation of cholinergic axons measured eletrophysiologically (Cole and Nicoll, 1984).

Having established a septo-hippocampal connection, we analyzed the septo-hippocampal streamlines (Fig. 4) in each mouse by comparing FA, mean diffusivity, axial diffusivity, and radial diffusivity, as well as tract volume, streamline length and streamline number

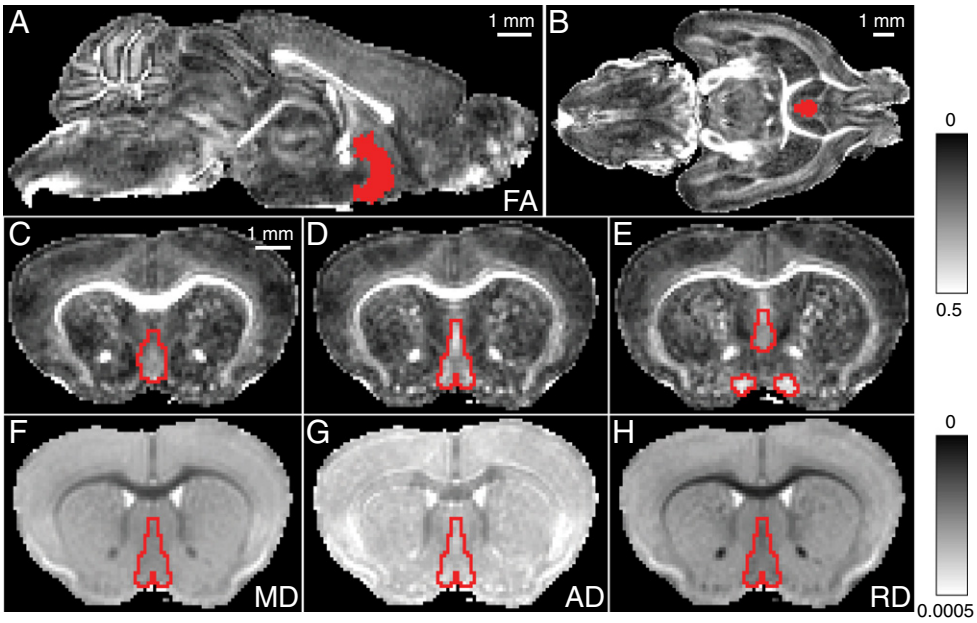

Fig. 2. Basal forebrain mask encompassing the medial septum, and the vertical and horizontal diagonal bands of Broca overlaid on A–E. FA, F. mean diffusivity (MD), G. axial diffusivity (AD) and H. radial diffusivity (RD) maps. The position of the basal forebrain mask (red) in MRI space is shown in three planes: A. sagittal (midline), B. horizontal (level of anterior commissure crossing the midline), and C-H. coronal sections through the extent of the basal forebrain depicting the mask at approximately 1.10 mm (C), 0.86 mm (D, F-H) and 0.50 mm (E) anterior to Bregma. To illustrate the contrast within the basal forebrain area the mask was outlined on the same slice on D. FA, F. mean diffusivity, G. axial diffusivity and H. radial diffusivity maps (the outline itself is not part of the mask but depicts the first row of voxels outside of the mask). The mask was used for volumetric analysis of the basal forebrain and to extract DTI parameters for the basal forebrain and as a waypoint region for tractography streamlines.

between the control and lesioned groups. This revealed statistically significant increases in mean diffusivity (Fig. 5B) and radial diffusivity (Fig. 5D) in the lesioned group. No significant differences were observed in FA (Fig. 5A) and axial diffusivity (Fig. 5C), or in tract volume, streamline length or normalized streamline number (Table 2).

Finally, to determine whether the diffusion changes observed for the basal forebrain tracts occurred elsewhere, we performed tractography analysis on a cerebellar tract (see Tractography section), namely the inferior cerebellar peduncle (Figs. 6A, B). We reasoned that this tract should not be affected by the application of mu-p75-SAP, based on previous reports that cerebellar Purkinje neurons are unaffected by this toxin (Berger-Sweeney et al., 2001; Moreau et al., 2008). Our comparison revealed no differences in measures of streamline FA, mean diffusivity, axial diffusivity, or radial diffusivity (Figs. 6C–F), or in tract volume, streamline length or streamline number (Table 3) in the inferior cerebellar peduncle between test and control mice. This indicated that the changes in diffusion measures of the septo-hippocampal streamlines were unlikely to be due to nonspecific effects of the toxin.

Discussion

In this study we used a robust animal model of specific cholinergic lesion of the septo-hippocampal system, generating animals with a ~25% reduction in cholinergic neurons with no effect on the GABAergic neurons of the region. The cholinergic loss therefore replicates the cell loss and denervation of basal forebrain cholinergic neurons observed in Alzheimer's disease (Rossner, 1997). Through manual segmentation analysis we showed that the lesion did not cause atrophy of the basal forebrain. Therefore, the degeneration mimics the mild pathology of MCI or the prodromal stage of Alzheimer's disease rather than severe loss of basal forebrain cholinergic neurons seen in late-stage disease (Hall et al., 2008; Mufson et al., 2002).

In most studies to date, DTI has been used to assess white mater integrity; however, DTI-derived parameters can also be used to reliably quantify fiber-rich gray matter regions such as the thalamus (Unrath et al., 2008). We demonstrate here that DTI is able to distinguish differences between basal forebrain neurodegeneration and the unlesioned state. A total of four diffusion parameters, FA, mean diffusivity, axial diffusivity and radial diffusivity, showed a significant increase within the basal forebrain area and all of these measures significantly inversely correlated with the basal forebrain cholinergic neuron count. We observed an average 6.5% increase in the diffusion parameters (FA: +7.7%; mean diffusivity: +6.1%; axial diffusivity: +8.5%; radial diffusivity: +4.0%) of the basal forebrain in comparison to an average 25% loss of cholinergic neurons. However, this represents a minor loss of septo-hippocampal projection neurons and an even lesser percentage change relative to the entire tissue, in which the volume includes glial cells, axons and dendrites within the ROI. The ~6.5% change may therefore be proportional to the change in tissue density of the basal forebrain. As the FA parameter showed the greatest effect, we propose that this could provide a sensitive measure to determine the extent of tissue damage.

In general, increases in mean, axial and radial diffusivity are well-established features of white matter degeneration (Filippi and Agosta, 2011). However it has been shown that degeneration usually results in a decrease of FA in the affected regions (i.e. a less preferred direction of diffusion; Filippi and Agosta, 2011). In contrast we observed an increase in FA in the lesioned group compared to the

Table 1
MRI volumes of the whole brain and normalized MRI volumes of basal forebrain and hippocampus (normalized to the whole brain volume) of lesioned and control animals. No significant differences were found between groups. $n=6$ for control group, $n=4$ for lesioned group, mean ± SEM.

Structure	Control	Lesion	Significance (p value)
Whole brain (mm^3)	510.333 ± 5.800	509.960 ± 7.364	1.00
Basal forebrain ($*10^{-3}$ mm^3)	0.173 ± 0.006	0.177 ± 0.006	0.61
Hippocampus ($*10^{-3}$ mm)	4.827 ± 0.062	4.913 ± 0.097	0.61

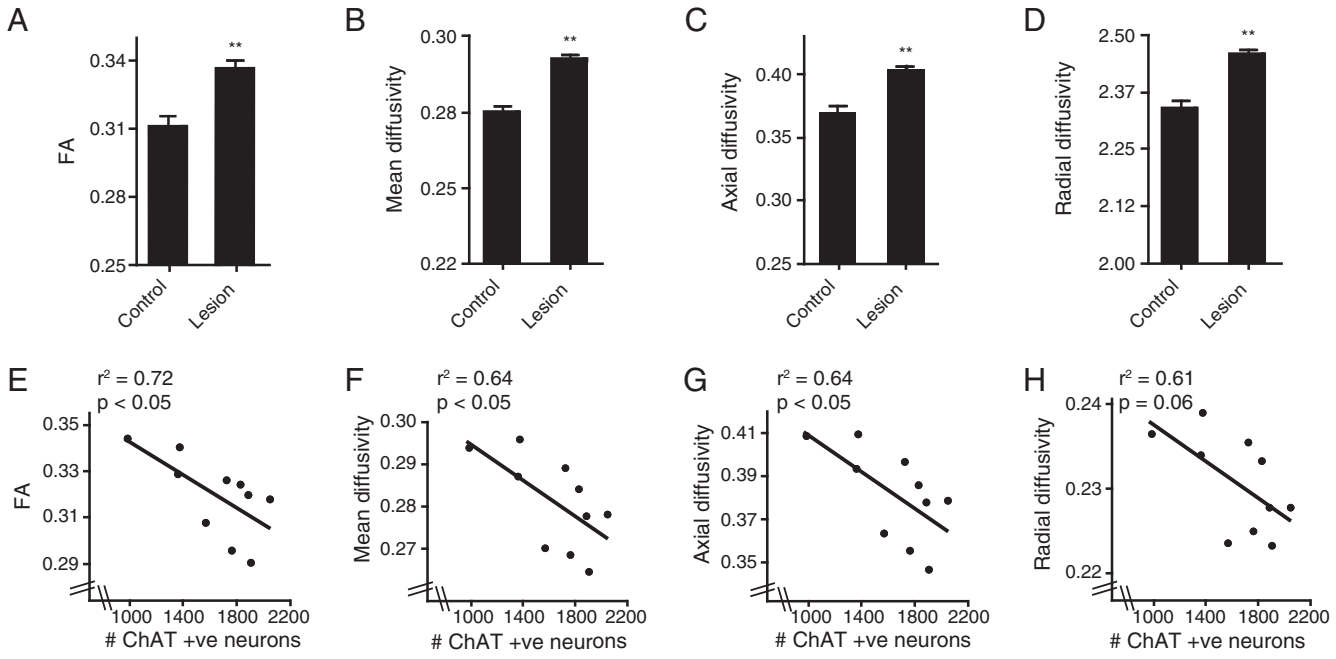

Fig. 3. The mean FA, mean diffusivity, axial diffusivity and radial diffusivity values of lesioned animals in the area of the basal forebrain mask inversely correlated to the cholinergic neuron number in the basal forebrain. A comparison of DTI parameters for lesioned and control animals revealed that A. FA (mean ± SEM), B. mean diffusivity (mean ± SEM), C. axial diffusivity (mean ± SEM) and D. radial diffusivity (mean ± SEM) values were significantly increased for the basal forebrain of lesioned compared to control animals. Correlation analysis of ChAT-positive neuron number (x-axis) to the previously mentioned DTI parameters (y-axis) of individual animals of mu-p75-SAP (lesion) and Rb-IgG-SAP (control) groups revealed a significant inverse correlation of E. FA, F. mean diffusivity and G. axial diffusivity parameters with ChAT-positive neuron number. $n = 6$ for control group, $n = 4$ for lesioned group, $^{**}p < 0.01$; unit for mean diffusivity, axial diffusivity and radial diffusivity is [10^{-3} mm^2/s].

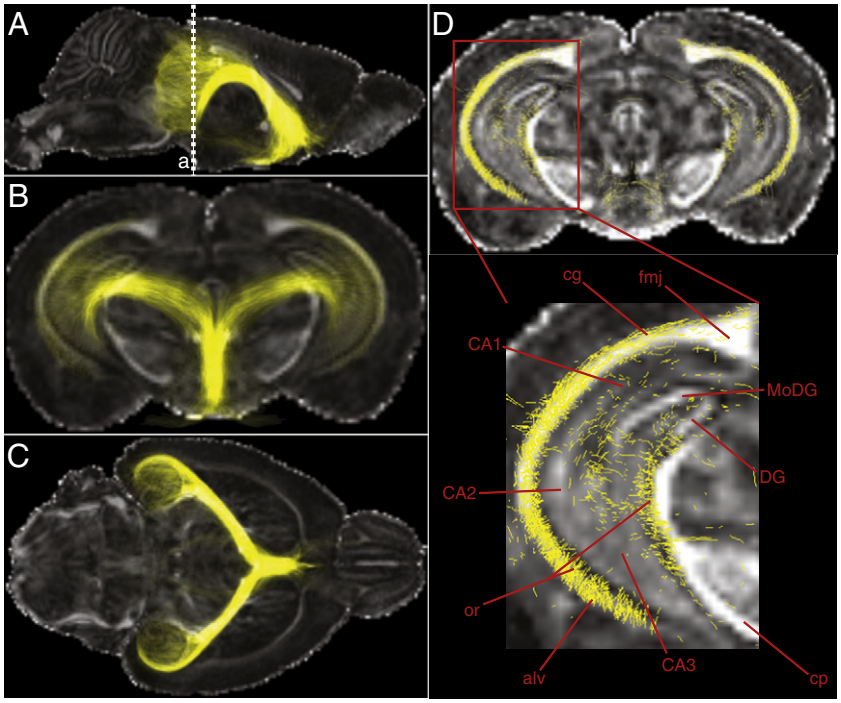

Fig. 4. Tractography streamlines connecting the basal forebrain and hippocampus. The basal forebrain mask shown in Fig. 3 was used as a waypoint region to generate a streamline profile of the basal forebrain and further delineated to only measure septo-hippocampal connections (yellow), shown in sagittal (A), coronal (B) and horizontal (C) planes. To achieve this, a hippocampus waypoint ROI at the level of (a) as indicated by the dashed line, was applied. D. A slice through the streamline profile is shown to validate the regions of the highest fiber density. Most streamlines were found to pass through the alveus (alv) and the oriens layer of the hippocampus (or) which are known to contain fimbria/fornix output from pyramidal neurons and the septal/diagonal band of Broca input to basal dendrites of pyramidal neurons, respectively. A very small proportion of streamlines were found to project to areas such as the cingulum, CA1–3 and other regions of the hippocampus. Additional abbreviations: cg, cingulum; cp, cerebellar peduncle; DG, dentate gyrus; fmj, forceps major of the corpus callosum; MoDG, molecular layer of the dentate gyrus.

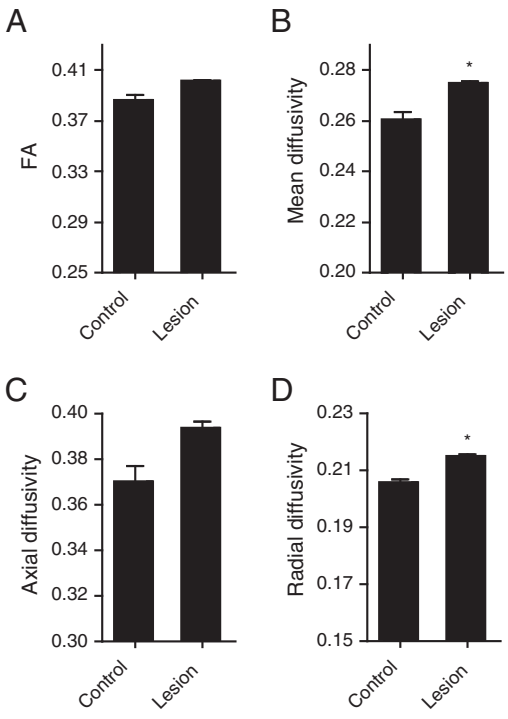

Fig. 5. Increased mean diffusivity and radial diffusivity of septo-hippocampal streamlines after lesion of the cholinergic basal forebrain. Diffusion parameters for the streamlines shown in Fig. 4 were analyzed, revealing that FA (A) and axial diffusivity (C) parameters were not significantly different between control and lesioned animals ($p = 0.17$ and $p = 0.07$, respectively), whereas mean diffusivity (B) and radial diffusivity (D) values showed significant increases in the lesioned animals. $n = 6$ for control group, $n = 4$ for lesioned group; unit for mean diffusivity, axial diffusivity and radial diffusivity is [10^{-3} mm^2/s]. *$p<0.05$.

control. One explanation of this may lie in the fact that the change in axial diffusivity (+8.5%) was larger than the change in radial diffusivity (+4.0%). These changes are likely to be due to a loss of isotropic (cholinergic) cells, which then leads to a greater contribution from residual anisotropic cells/axons in the basal forebrain. In addition, the observed changes are unlikely to occur as a result of a loss of crossing fibers in the basal forebrain, as comparison of principal eigenvector orientations for the basal forebrain area between control and lesioned animals revealed no difference (data not shown). The phenomenon of increased FA in pathological conditions has been previously documented (Jones, 2010; Tuch et al., 2005) and highlights the fact that interpretation of diffusion parameters must be carried out with reference to the nature of the pathology and the composition of the tissue being examined. Our study provides insight into how MRI parameters could change due to selective loss of a single neuron population, namely the basal forebrain cholinergic neurons, both in gray (basal forebrain) and white matter (septo-hippocampal tracts) areas.

The present study demonstrates that diffusion MR tractography has the potential to be a sensitive measure of cholinergic degeneration. Probabilistic tractography measures of projections between the basal forebrain nuclei and the hippocampus via the fimbria/fornix successfully detected changes in streamline characteristics induced by loss of cholinergic axons, revealing significant increases in streamline mean diffusivity and streamline radial diffusivity, as well as a trend toward significantly increased axial diffusivity ($p = 0.07$). A significant number of axonal tracts project from the basal forebrain through the fornix, of which the cholinergic axons that were affected by the lesion make up only a minor proportion. The actual volume occupied by cholinergic axons in the fimbria/fornix is even less, as cholinergic axons (a) are unmyelinated, and (b) have a significantly smaller axon diameter compared to, for example, myelinated GABAergic axons (Gartner et al., 2001) projecting via the same pathway. To confound the detection of cholinergic axons further, cholinergic axons are closely associated with myelinated axons in the fimbria/fornix, making it technically impossible for tractography to separate them. We were not surprised, therefore, to observe no changes in measures such as number of streamlines, tract volume or streamline length.

Of the factors that can influence diffusion anisotropy, intra-axonal organization appears to have the greatest influence (Pierpaoli et al., 1996). However, other features, such as the density of fiber and glial cell packing, degree of myelination, and individual fiber diameter may also play a role (Melhem et al., 2002). We observed significant increases in mean diffusivity and radial diffusivity, which suggest that subtle microscopic changes to a minor proportion of fiber tracts are detectable by tractography. Although the molecular changes remain undefined, axonal degeneration resulting in debris and/or changes to axonal organization and packing, may underpin the observed changes. In addition, a decrease in the proportion of unmyelinated cholinergic fibers relative to myelinated fibers (which are unaffected by the lesion) within the measured region may also contribute to the significant increases in mean diffusivity and radial diffusivity. Consistent with this idea, demyelination of the optic tract has been shown to result in decreased axial diffusivity with no change in radial diffusivity (Wu et al., 2007).

Although FA has been widely used as a measure to assess the integrity of brain connections (Kiuchi et al., 2009; Pievani et al., 2010; Teipel et al., 2010), we did not observe any trend towards significance in this parameter in our study. We observed significant increases in mean diffusivity and radial diffusivity, replicating significant increases in mean diffusivity and radial diffusivity in the fornix of Alzheimer's disease patients found by Oishi et al. (2011), as well as the increase in radial diffusivity in the fornix in MCI and Alzheimer's disease patients compared to healthy controls found by Pievani et al. (2010). Indeed, based on our work, the changes reported for the fornix may have been caused by degeneration of the cholinergic axons. In addition, significant changes in the integrity of tracts originating in the basal forebrain have been observed in Alzheimer's disease patients using tract-based spatial statistics (TBSS, Smith et al., 2006), where measures of tract integrity were determined based on FA (Teipel et al., 2010). TBSS (part of FSL; Smith et al., 2004) and the method employed by Oishi et al. (2011) utilize voxelwise cross-subject statistics to analyze local diffusion information, whereas we used a probabilistic tractography method to assess three-dimensional tract information, which might explain the difference in the observed parameter changes. However, we suggest that mean and radial diffusivities rather than FA (using either tractography or voxelwise analyses) may be the most sensitive parameters to reveal cholinergic axonal degeneration in the fornix.

In neurodegenerative conditions such as Alzheimer's disease, axonal dystrophy and retraction occur early and may be reversible (Burek and Oppenheim, 1996; Ypsilanti et al., 2008). In the current study, the death of cholinergic neurons was mediated through administration of the toxin mu-p75-SAP such that axonal degeneration occurred coincidental or subsequent to cell body loss. Nonetheless, our findings of significant changes to diffusion parameters in the septo-hippocampal streamlines serve as proof of principle that a moderate loss of cholinergic fibers within the fornix can result in changes to mean and radial diffusivity

Table 2
Septo-hippocampal connections remained unchanged for track volume, streamline length and normalized streamline number in lesioned animals. $n = 6$ for control group, $n = 4$ for lesioned group, mean ± SEM.

Parameter	Control	Lesion	Significance (p value)
Track volume (mm^3)	10.152 ± 0.677	11.115 ± 0.373	0.35
Streamline length (mm)	10.21 ± 0.07	10.12 ± 0.02	0.48
Normalized streamline number	1.22 ± 0.08	1.27 ± 0.06	1.00

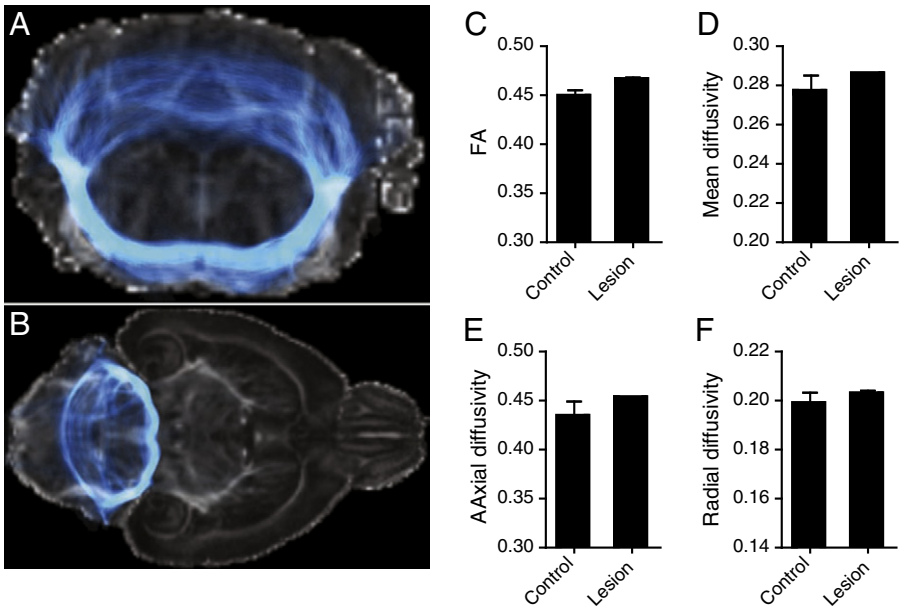

Fig. 6. Tractography of the inferior cerebellar peduncle, a white matter tract that should not be affected by the toxin-induced lesion or the surgery itself, shown in MRI space in coronal (A) and horizontal (B) planes. No changes in control vs. lesioned animals were observed for FA (C), mean diffusivity (D), axial diffusivity (E) or radial diffusivity (F). $n=6$ for control group, $n=4$ for lesioned group; unit for mean diffusivity, axial diffusivity and radial diffusivity is [10^{-3} mm^2/s].

parameters, and thus early changes associated with neurodegeneration may be observable even if the cell bodies are not yet lost. We therefore conclude that tractography shows promising sensitivity as a diagnostic tool for detecting pathological changes in the neuronal integrity of this fiber tract in humans, although further validation is still required.

Conclusions

Our study demonstrates that loss of basal forebrain cholinergic neurons is highly correlated to changes in water diffusion in the basal forebrain area. In addition, cholinergic neurodegeneration can be detected by analyzing diffusion parameters of the streamlines of the septo-hippocampal tracts in a mouse model. This study provides an important step forward in validating DTI and tractography as diagnostic imaging tools for the detection of subtle neurodegenerative events. Given that cholinergic basal forebrain degeneration is an early feature of Alzheimer's disease, our findings demonstrate the potential feasibility of combining conventional DTI with tractography as a non-invasive diagnostic tool to analyze both regional brain changes and variations in connectivity.

Acknowledgments

This project was funded by the Queensland State Government National and International Research Alliances Program. Adam S. Hamlin and Elizabeth J. Coulson were supported by National Health and Medical Research Council of Australia fellowships. Georg Kerbler was supported by an ANZ Trustees PhD Scholarship. We thank Zoran Boskovic and Sally Martin for assistance with experiments, Maree Smith, Ian Brereton, Andrew Whittaker and Dr Andrew Janke for helpful discussions, and Rowan Tweedale for editorial assistance. The authors acknowledge the facilities, scientific and technical assistance of the Queensland NMR Network, and National Imaging Facility Node at the Centre for Advanced Imaging, The University of Queensland, a facility funded by the University, Queensland State and Australian Commonwealth Governments.

Table 3
The toxin showed no effect on track volume, streamline length and normalized streamline number of the inferior cerebellar peduncle for lesioned animals compared to control animals. $n=6$ for control group, $n=4$ for lesioned group, mean ± SEM.

Parameter	Control	Lesion	Significance (p value)
Track volume (mm^3)	20.510 ± 0.932	19.876 ± 1.290	1.00
Streamline length (mm)	9.93 ± 0.19	10.12 ± 0.14	0.91
Normalized streamline number	109.34 ± 6.25	123.07 ± 5.92	0.29

References

Badea, A., Johnson, G.A., Jankowsky, J.L., 2010. Remote sites of structural atrophy predict later amyloid formation in a mouse model of Alzheimer's disease. Neuroimage 50, 416–427.
Berger-Sweeney, J., Stearns, N.A., Murg, S., Floerke-Nashner, L.R., Lappi, D.A., Baxter, M.G., 2001. Selective immunolesions of cholinergic neurons in mice: effects on neuranatomy, neurochemistry, and behavior. J. Neurosci. 21, 8164–8173.
Burek, M.J., Oppenheim, R.W., 1996. Programmed cell death in the developing nervous system. Brain Pathol. 6, 427–446.
Cole, A.E., Nicoll, R.A., 1984. Characterization of a slow cholinergic post-synaptic potential recorded in vitro from rat hippocampal pyramidal cells. J. Physiol. 352, 173–188.
Filippi, M., Agosta, F., 2011. Structural and functional network connectivity breakdown in Alzheimer's disease studied with magnetic resonance imaging techniques. J. Alzheimers Dis. 24, 455–474.
Franklin, K.J.B., Paxinos, G., 2007. The Mouse Brain in Stereotaxic Coordinates Third Edition. Academic Press, San Diego.
Gartner, U., Hartig, W., Brauer, K., Bruckner, G., Arendt, T., 2001. Immunofluorescence and immunoelectron microscopic evidence for differences in myelination of GABAergic and cholinergic septohippocampal fibres. Int. J. Dev. Neurosci. 19, 347–352.
George, S., Mufson, E.J., Leurgans, S., Shah, R.C., Ferrari, C., Detoledo-Morrell, L., 2009. MRI-based volumetric measurement of the substantia innominata in amnestic MCI and mild AD. Neurobiol. Aging 32, 1756–1764.
Grothe, M., Zaborszky, L., Atienza, M., Gil-Neciga, E., Rodriguez-Romero, R., Teipel, S.J., Amunts, K., Suarez-Gonzalez, A., Cantero, J.L., 2010. Reduction of basal forebrain cholinergic system parallels cognitive impairment in patients at high risk of developing Alzheimer's disease. Cereb. Cortex 20, 1685–1695.
Grothe, M., Heinsen, H., Teipel, S.J., 2011. Atrophy of the cholinergic basal forebrain over the adult age range and in early stages of Alzheimer's disease. Biol. Psychiatry 71, 805–813.
Hall, A.M., Moore, R.Y., Lopez, O.L., Kuller, L., Becker, J.T., 2008. Basal forebrain atrophy is a presymptomatic marker for Alzheimer's disease. Alzheimers Dement. 4, 271–279.
Harms, M.P., Kotyk, J.J., Merchant, K.M., 2006. Evaluation of white matter integrity in ex vivo brains of amyloid plaque-bearing APPsw transgenic mice using magnetic resonance diffusion tensor imaging. Exp. Neurol. 199, 408–415.

Hort, J., Laczo, J., Vyhnalek, M., Bojar, M., Bures, J., Vlcek, K., 2007. Spatial navigation deficit in amnestic mild cognitive impairment. Proc. Natl. Acad. Sci. U. S. A. 104, 4042–4047.
Jones, D.K., 2010. Challenges and limitations of quantifying brain connectivity in vivo with diffusion MRI. Imaging Med. 2, 341–355.
Jones, D.K., Horsfield, M.A., Simmons, A., 1999. Optimal strategies for measuring diffusion in anisotropic systems by magnetic resonance imaging. Magn. Reson. Med. 42, 515–525.
Kiuchi, K., Morikawa, M., Taoka, T., Nagashima, T., Yamauchi, T., Makinodan, M., Norimoto, K., Hashimoto, K., Kosaka, J., Inoue, Y., Inoue, M., Kichikawa, K., Kishimoto, T., 2009. Abnormalities of the uncinate fasciculus and posterior cingulate fasciculus in mild cognitive impairment and early Alzheimer's disease: a diffusion tensor tractography study. Brain Res. 1287, 184–191.
Kokjohn, T.A., Roher, A.E., 2009. Amyloid precursor protein transgenic mouse models and Alzheimer's disease: understanding the paradigms, limitations, and contributions. Alzheimers Dement. 5, 340–347.
Lau, J.C., Lerch, J.P., Sled, J.G., Henkelman, R.M., Evans, A.C., Bedell, B.J., 2008. Longitudinal neuroanatomical changes by deformation-based morphometry in a mouse model of Alzheimer's disease. Neuroimage 42, 19–27.
Maheswaran, S., Barjat, H., Rueckert, D., Bate, S.T., Howlett, D.R., Tilling, L., Smart, S.C., Pohlmann, A., Richardson, J.C., Hartkens, T., Hill, D.L., Upton, N., Hajnal, J.V., James, M.F., 2009. Longitudinal regional brain volume changes quantified in normal aging and Alzheimer's APP x PS1 mice using MRI. Brain Res. 1270, 19–32.
Mancuso, C., Siciliano, R., Barone, E., Butterfield, D.A., Preziosi, P., 2011. Pharmacologists and Alzheimer disease therapy: to boldly go where no scientist has gone before. Expert Opin. Investig. Drugs 20, 1243–1261.
Melhem, E.R., Mori, S., Mukundan, G., Kraut, M.A., Pomper, M.G., van Zijl, P.C., 2002. Diffusion tensor MR imaging of the brain and white matter tractography. Am. J. Roentgenol. 178, 3–16.
Mesulam, M.M., Mufson, E., Levey, A.I., Wainer, B.H., 1983. Cholinergic innervation of cortex by the basal forebrain: cytochemistry and cortical connectinos of the septal area, diagonal band nuclei, nucleus basalis (substantia innominata), and hypothalamus in the rhesus monkey. J. Comp. Neurol. 214, 170–197.
Moldrich, R.X., Pannek, K., Hoch, R., Rubenstein, J.L., Kurniawan, N.D., Richards, L.J., 2010. Comparative mouse brain tractography of diffusion magnetic resonance imaging. Neuroimage 51, 1027–1036.
Moreau, P.H., Cosquer, B., Jeltsch, H., Cassel, J.C., Mathis, C., 2008. Neuroanatomical and behavioral effects of a novel version of the cholinergic immunotoxin mu p75-saporin in mice. Hippocampus 18, 610–622.
Mueggler, T., Meyer-Luehmann, M., Rausch, M., Staufenbiel, M., Jucker, M., Rudin, M., 2004. Restricted diffusion in the brain of transgenic mice with cerebral amyloidosis. Eur. J. Neurosci. 20, 811–817.
Mufson, E., 2003. Human cholinergic basal forebrain: chemoanatomy and neurologic dysfunction. J. Chem. Neuroanat. 26, 233–242.
Mufson, E., Bothwell, M., Hersh, L.B., Kordower, J.H., 1989. Nerve growth factor receptor immunoreactive profiles in the normal, aged human basal forebrain: colocalization with cholinergic neurons. J. Comp. Neurol. 196–217.
Mufson, E.J., Ma, S.Y., Dills, J., Cochran, E.J., Leurgans, S., Wuu, J., Bennett, D.A., Jaffar, S., Gilmor, M.L., Levey, A.I., Kordower, J.H., 2002. Loss of basal forebrain $P75^{NTR}$ immunoreactivity in subjects with mild cognitive impairment and Alzheimer's disease. J. Comp. Neurol. 443, 136–153.
Muth, K., Schonmeyer, R., Matura, S., Haenschel, C., Schroder, J., Pantel, J., 2010. Mild cognitive impairment in the elderly is associated with volume loss of the cholinergic basal forebrain region. Biol. Psychiatry 67, 588–591.
Oishi, K., Akhter, K., Mielke, M., Ceritoglu, C., Zhang, J., Jiang, H., Li, X., Younes, L., Miller, M.I., van Zijl, P.C., Albert, M., Lyketsos, C.G., Mori, S., 2011. Multi-modal MRI analysis with disease-specific filtering: intial testing to predict mild cognitive impairment patients who convert to Alzheimer's disease. Front. Neurol. 2, 54.
Perry, T.A., Hodges, H., Gray, J.A., 2001. Behavioural, histological and immunocytochemical consequences following 192 IgG-saporin immunolesions of the basal forebrain cholinergic system. Brain Res. Bull. 54, 29–49.
Pierpaoli, C., Jezzard, P., Basser, P.J., Barnett, A., Di Chiro, G., 1996. Diffusion tensor MR imaging of the human brain. Radiology 201, 637–648.
Pievani, M., Agosta, F., Pagani, E., Canu, E., Sala, S., Absinta, M., Geroldi, C., Ganzola, R., Frisoni, G.B., Filippi, M., 2010. Assessment of white matter tract damage in mild cognitive impairment and Alzheimer's disease. Hum. Brain Mapp. 31, 1862–1875.
Rossner, S., 1997. Cholinergic immunolesions by 192-IgG-Saporin — a useful tool to stimulate pathogenic aspects of Alzheimer's disease. Int. J. Dev. Neurosci. 15, 835–850.
Smith, S.M., Jenkinson, M., Woolrich, M.W., Beckmann, C.F., Behrens, T.E.J., Johansen-Berg, H., Bannister, P.R., De Luca, M., Drobnjak, I., Flitney, D.E., Niazy, R., Saunders, J., Vickers, J., Zhang, Y., De Stefano, N., Brady, J.M., Matthews, P.M., 2004. Advances in functional and structural MR image analysis and implementation as FSL. Neuroimage 23, 208–219.
Smith, S.M., Jenkinson, M., Johansen-Berg, H., Rueckert, D., Nichols, T.E., Mackay, C.E., Watkins, K.E., Ciccarelli, O., Cader, M.Z., Matthews, P.M., Behrens, T.E.J., 2006. Tract-based spatial statistics: voxelwise analysis of multi-subject diffusion data. Neuroimage 31, 1487–1505.
Sun, S.W., Song, S.K., Lin, S.J., Holtzman, D.M., Merchant, K.M., Kotyk, J.J., 2005. Detection of age-dependent brain injury in a mouse model of brain amyloidosis associated with Alzheimer's disease using magnetic resonance diffusion tensor imaging. Exp. Neurol. 191, 77–85.
Teipel, S.J., Meindl, T., Grinberg, L., Grothe, M., Cantero, J.L., Reiser, M.F., Moller, H.J., Heinsen, H., Hampel, H., 2010. The cholinergic system in mild cognitive impairment and Alzheimer's disease: an in vivo MRI and DTI study. Hum. Brain Mapp. 32, 1349–1362.
Thiessen, J.D., Glazner, K.A., Nafez, S., Schellenberg, A.E., Buist, R., Martin, M., Albensi, B.C., 2010. Histochemical visualization and diffusion MRI at 7 Tesla in the TgCRND8 transgenic model of Alzheimer's disease. Brain Struct. Funct. 215, 29–36.
Tournier, J.D., Calamante, F., Connelly, A., 2012. MRtrix: diffusion tractography in crossing fiber regions. Int. J. Imaging Syst. Technol. 22, 53–66.
Tuch, D.S., Salat, D.H., Wisco, J.J., Zaleta, A.K., Hevelone, N.D., Rosas, H.D., 2005. Choice reaction time performance correlates with diffusion anisotropy in white matter pathways supporting visuospatial attention. Proc. Natl. Acad. Sci. U. S. A. 102, 12212–12217.
Unrath, A., Klose, U., Grodd, W., Ludolph, A.C., Kassubek, J., 2008. Directional colour encoding of the human thalamus by diffusion tensor imaging. Neurosci. Lett. 434, 322–329.
Wainer, B.H., Levey, A.I., Rye, D.B., Mesulam, M.M., Mufson, E.J., 1985. Cholinergic and non-cholinergic septohippocampal pathways. Neurosci. Lett. 54, 45–52.
Whitehouse, P.J., Price, D.L., Struble, R.G., Clark, A.W., Coyle, J.T., Delon, M.R., 1982. Alzheimer's disease and senile dementia: loss of neurons in the basal forebrain. Science 215, 1237–1239.
Wu, Q., Butzkueven, H., Gresle, M., Kirchhoff, F., Friedhuber, A., Yang, Q., Wang, H., Fang, K., Lei, H., Egan, G.F., Kilpatrick, T.J., 2007. MR diffusion changes correlate with ultra-structurally defined axonal degeneration in murine optic nerve. Neuroimage 37, 1138–1147.
Ypsilanti, A.R., Girao da Cruz, M.T., Burgess, A., Aubert, I., 2008. The length of hippocampal cholinergic fibers is reduced in the aging brain. Neurobiol. Aging 29, 1666–1679.

5.3 Discussion and implication of findings

The observed dMRI measures presented in this chapter were found to be correlated to an underlying, quantifiable biological event in the investigated animals. To our knowledge this is one of the first studies to successfully associate imaging measures with histological measures. By showing this relationship we provide further validity for using a technique such as dMRI for the assessment of neurodegenerative events in mice. In addition we give evidence for the way in which cholinergic neuronal degeneration could induce dMRI parameter changes, which could also be present in aging or in neurodegenerative disease in humans; however this requires further validation.

We also offer a novel imaging method for the assessment of neurodegenerative disease, which might be more sensitive than conventional structural MRI in detecting early structural damage. This study also forms the basis for follow-up investigations, which should be aimed at determining how additional pathological features such as amyloid plaques and NFT pathology as well as astrogliosis, in addition to cholinergic degeneration, influence dMRI parameters, in order to give a better estimate of the parameter changes to be expected when comparing human Alzheimer's disease subjects with controls.

In the current chapter we focussed on studying the septohippocampal connection originating from anterior basal forebrain areas; however as the results from our human studies suggest, the posterior basal forebrain connections might be affected even earlier in Alzheimer's disease. Therefore the next step would be to assess whether diffusion MRI can successfully measure changes in the connections between the basal forebrain and cortical regions.

Chapter 6: Development of a cytoarchitectonic map of the mouse cholinergic basal forebrain

6.1 Introduction

In the previous study it was highlighted that delineation of the mouse basal forebrain on structural MR images is difficult as there are no clearly visible anatomical boundaries. dMRI on the other hand, in particular fractional anisotropy images of mouse brains, reveal the basal forebrain as an area of high fibre bundle density (chapter 5), resulting from its efferent and afferent projections as well as fibres passing through this region. Fractional anisotropy values within the basal forebrain are therefore higher in comparison with other grey matter structures, and in some parts of the basal forebrain reach values comparable to those of white matter. Fractional anisotropy or colour-coded fractional anisotropy diffusion MR images, used in conjunction with the mouse brain atlas (Franklin and Paxinos, 2007), were therefore used to segment the basal forebrain in the previous chapter.

However the resulting segmentation is not ideal and starting/end-points of anterior/posterior boundaries are still difficult to delineate, as related fibre bundles extend beyond the cell body-defined boundaries of basal forebrain nuclei. Hence the aim of this study was to generate a map of the basal forebrain, which can be reliably used as a tool for imaging modalities such as MRI and PET, particularly in large animal cohorts, when manual structural segmentation is tedious.

In order to create a basal forebrain map in the greatest possible detail we used histological images to segment the basal forebrain into its traditionally demarcated nuclei (medial septum, vertical/horizontal/lateral diagonal band of Broca, nucleus basalis of Meynert). As cholinergic cells are located in all nuclei we decided to use ChAT as a marker to guide the segmentation process. To eliminate the need for immunohistochemistry and the inherent variation in staining intensity between sections/animals, we chose to use a transgenic mouse line expressing enhanced green fluorescent protein (eGFP) driven by the ChAT promoter: ChAT-eGFP (The Jackson Laboratory). Three adult male ChAT-eGFP mice at postnatal day 90 were used to generate the basal forebrain map.

6.2 Materials and Methods

Animals

Experimentally naïve male ChAT-eGFP mice were housed in groups of four and maintained on a 12 h light/dark cycle, with food and water provided ad libitum. All procedures were approved by the University of Queensland Animal Ethics Committee.

MRI acquisition and histological processing

Three twelve-week old male ChAT-eGFP mice were anaesthetized with sodium pentobarbital (100 mg/kg i.p.) and perfused transcardially with 4% paraformaldehyde in phosphate buffered saline (PBS). Brains were removed from the skulls and post-fixed overnight in the same fixative and then washed in PBS at 4°C for one day. Then brains were transferred into PBS 0.2% Magnevist and incubated for 4 days at 4°C. Next, the mouse brains were immersed in Fomblin oil (Y06/6 grade, Solvay) and images using a 3D gradient echo sequence according to the protocol of Ullmann et al. (2012) were acquired. In addition diffusion weighted MR images were acquired according to the protocol of Kerbler et al. (2012).

After MRI acquisition, brains were transferred into 20% sucrose solution and incubated overnight, after which 30 µm sections were cut through the extent of the basal forebrain using a sliding microtome (SM2000r, Leica). Sections were collected into PBS containing 0.1% sodium azide and stored at 4°C. Next, sections were transferred to 0.9% saline and mounted on Superfrost™ Plus glass slides, allowed to dry for 4 hours and then coverslipped with Dako® Fluorescence Mounting Medium and stored at 4°C. Images of sections were taken with a Zeiss Axio Imager Z2 and the basal forebrain was delineated using ITK-SNAP software (www.itksnap.org).

Segmentation of basal forebrain areas in histological sections

Compartments of the basal forebrain were traced on 2D images of sections (30 µm thickness) of each mouse using ITK-Snap (www.itksnap.org). There were no gaps between sections so the basal forebrain could be delineated with best possible detail. A contour line of each individual basal forebrain nucleus was drawn on each slice. We employed the nomenclature of the mouse brain atlas (Franklin and Paxinos, 2007) to

demarcate individual basal forebrain nuclei, with the exception that we employed the term lateral diagonal band of Broca (formerly called the magnocellular preoptic nucleus). The cholinergic neurons were easily identifiable on histological sections of mice and often arranged in cell aggregates. The borders of individual nuclei were drawn where the number of cells diminished toward surrounding regions.

Registration, stacking and generation of 3D basal forebrain maps

A MRI-guided histology reconstruction method (Yang et al., 2012) was adapted to stack the digitized sections into a histological volume and to register it to the MRI data (Figure 1). The method started with a series of 2D registrations of adjacent histological sections to stack them into an initial histological volume. The 3D MRI data of the same brain was co-registered to the initial histological volume. By transforming the MRI volume into the initial histological space and considering a linear shrinkage of histological volume, an initial estimation of the corresponding MR slice of each histological section was calculated. The histological sections were then registered to the corresponding MR slices, and an improved histological 3D volume was constructed, from which more accurate correspondence between histological sections and MR slices was established. By repeating this procedure, after several iterations, the method converged when there was no improvement in the 3D registration between the histological and MR volumes, yielding the final 3D reconstruction of histological volume in the same reference space as MR volume. The transform matrices of the 2D and 3D registrations were then applied to the manually segmented basal forebrain structure to form a 3D segmentation in the same reference space.

The 3D registrations between histological and MR volumes were performed in MIPAV (http://mipav.cit.nih.gov/). The 2D histology-histology and histology-MRI registrations were performed in MatLab(r) (MathWorks).

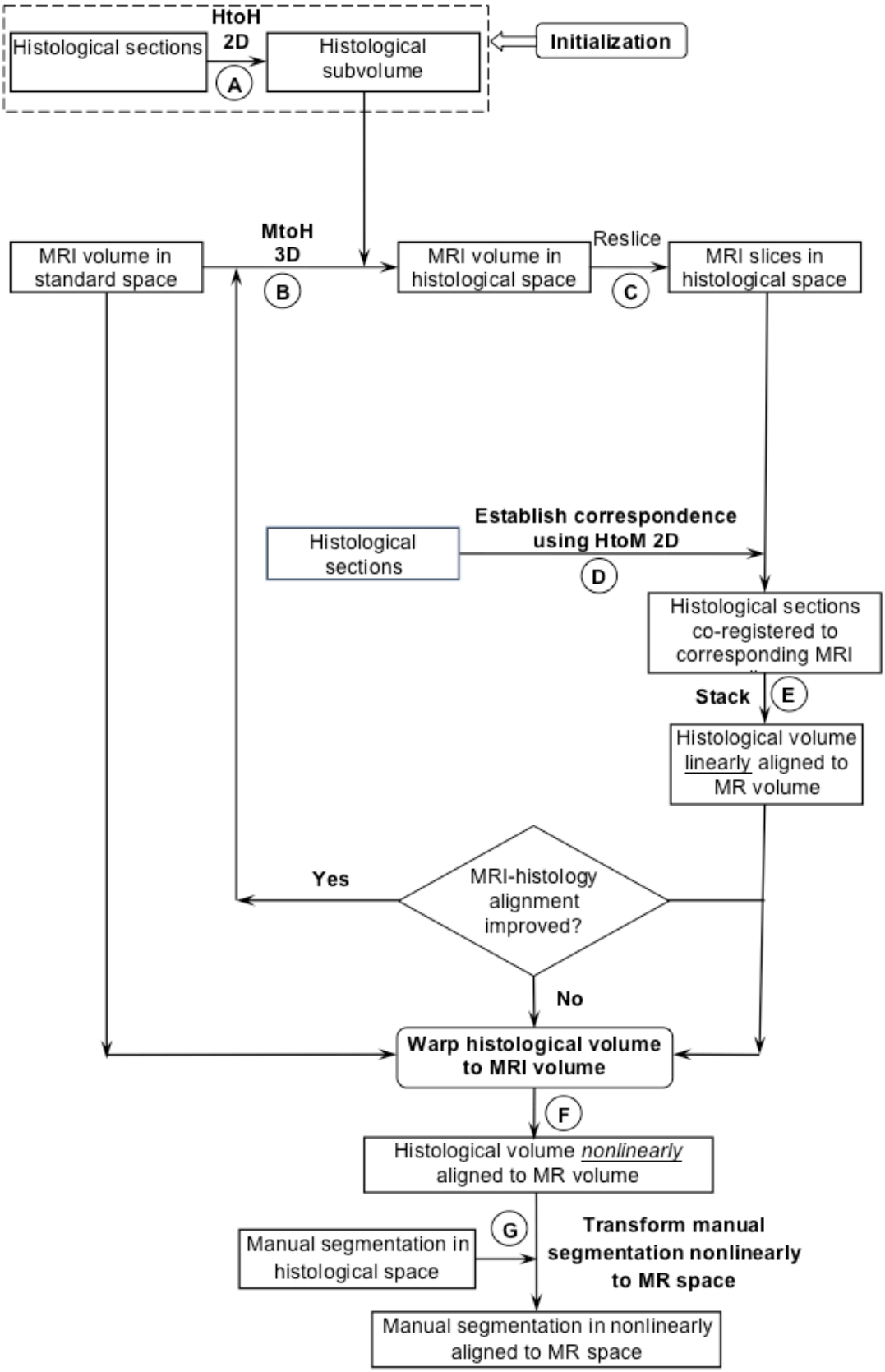

Figure 1: Iterative methods used to establish the correspondence between MR slices and histological sections.

Abbreviations: **HtoH** = histology to histology, **HtoM** = histology to MRI, **MtoH** = MRI to histology.

6.3 Results

Segmentation

The manual segmentation of basal forebrain structures over the anterior-posterior extent can be seen in Figure 2 at five different levels for mouse 2. Mouse brain sections from Bregma 2.10 mm to Bregma -2.92 mm were collected for segmentation purposes, with the final basal forebrain segmentation extending from Bregma 1.49 mm to Bregma -2.06 mm.

Vertical diagonal band of Broca

The vertical diagonal band of Broca appears first medially (Fig. 2; red/green, top row) at Bregma 1.49 mm and then extends dorsally and laterally over subsequent sections. The vertical diagonal band of Broca is then bordered ventrally by the horizontal diagonal band of Broca from Bregma 0.86 mm. On the following sections the medial septum and horizontal diagonal band of Broca areas take up increasingly more space, thereby reducing the vertical diagonal band of Broca area. The horizontal diagonal band of Broca then splits ventrolaterally from the vertical diagonal band of Broca and the vertical diagonal band of Broca finally diminishes at Bregma 0.38 mm.

Medial septum

The first cells belonging to the medial septum appear dorsal to the vertical diagonal band of Broca (Fig. 2; blue/yellow, top row) at about Bregma 1.20 mm at the level of the anterior commissure, and increasingly cells appear dorsal to the level of the anterior commissure over the following sections. In later sections (Fig. 2; blue/yellow, second row) the medial septum area also extends ventral to the anterior commissure. The medial septum is continuously bordered ventrally by the vertical diagonal band of Broca until the vertical diagonal band of Broca disappears and the medial septum then continues up to the point, where the anterior commissure crosses the midline at Bregma 0.14 mm.

Horizontal diagonal band of Broca

Cell aggregates representing the horizontal diagonal band of Broca commence ventrolateral to the vertical diagonal band of Broca from Bregma 0.86 mm and continue as far as Bregma -0.82 mm. Over the anterior-posterior extent, the horizontal diagonal band of Broca at first increases in size along the ventral surface of the brain (Fig. 2; teal/pink, second row) and then increasingly extends laterally, with the whole horizontal diagonal band of Broca structure deviating from the dorsally located vertical diagonal band of Broca and migrating laterally while at the same time declining in size (Fig. 2; teal/pink, third row). From Bregma 0.14 mm, cells of the horizontal diagonal band of Broca remain in the same location (Fig. 2; teal/pink, fourth row), mediolateral to the lateral diagonal band of Broca and ventral to the substantia innominata. The most posterior cells segmented as horizontal diagonal band of Broca were located at Bregma -0.82 mm (Fig. 2; teal/pink, fifth row).

Lateral diagonal band of Broca

Formerly known as the magnocellular preoptic nucleus, the lateral diagonal band of Broca is located lateral to the horizontal diagonal band of Broca throughout the brain (Fig. 2; white/blue, third to fifth row). The first cell aggregates belonging to the lateral diagonal band of Broca appear as early as Bregma 0.50 mm and extend to Bregma -1.06 mm. In the posterior parts, a few scattered cells of the nucleus basalis of Meynert (Fig. 2; brown/beige, fifth row) are located dorsally to the lateral diagonal band of Broca.

Nucleus basalis of Meynert

Cells belonging to the nucleus basalis of Meynert initially appear between the internal capsule and the globus pallidus at Bregma -0.34 mm, and with a small population also appearing dorsal to the lateral diagonal band of Broca and ventral to the ventral pallidum (Fig. 2; brown/beige, fifth row) at the same level. Whereas the latter cell population diminishes after a few slices, the former, more dorsally located population increases in number and spreads in all directions, thereby taking up larger areas within the internal capsule/globus pallidus areas (Fig. 2; brown/beige, fifth to sixth row) over the anterior-posterior extent of the structure. Cells that are part of the nucleus basalis of Meynert complex are more spread out than the other above mentioned nuclei. Cell numbers start progressively to decrease, as the optic tract starts moving from the ventral brain surface

towards the internal capsule area. After the most posterior parts of the diagonal band complex, the lateral diagonal band of Broca, have disappeared, the nucleus basalis of Meynert continues on and then diminishes as the most posteriorly located structure of the basal forebrain at Bregma -2.06 mm, when the fasciculus retroflexus starts to deviate from the habenular nucleus.

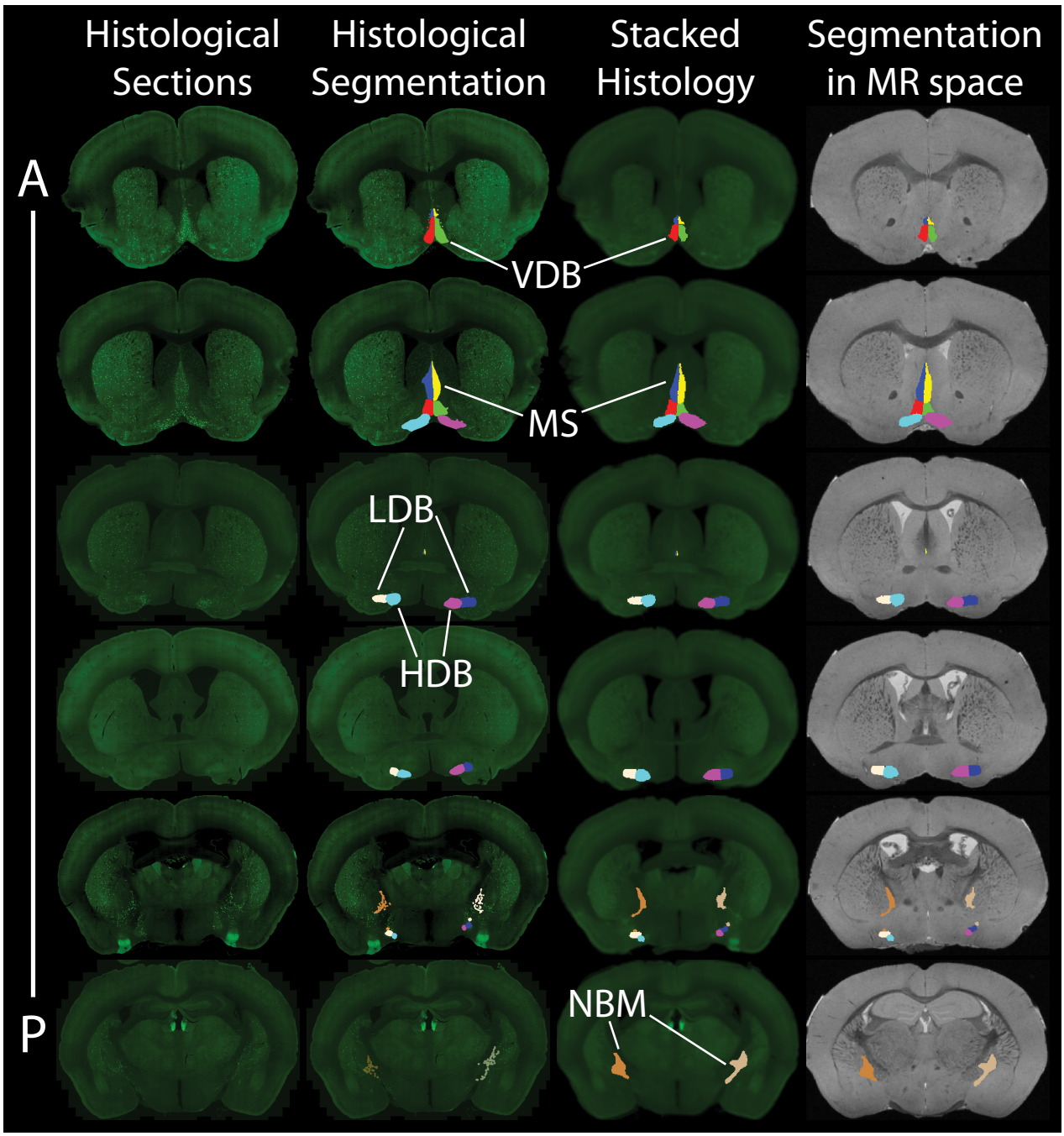

Figure 2: Representative images of the process of transferring the manual basal forebrain segmentation from histological images to the corresponding MRI space. The different steps are shown in columns in the processing order from left to right, and, different levels of the basal forebrain are shown in rows from anterior (A) to posterior (P). VDB = vertical diagonal band of Broca, MS = medial septum, LDB = lateral diagonal band of broca, HDB = horizontal diagonal band of broca, NBM = nucleus basalis of Meynert.

Histological volume measurements

After the 2D histological sections of each mouse were restacked using the MR-guided registration protocol, the volumes of each basal forebrain structure were calculated for all three mice. The individual measurements for each mouse can be seen in Table 1 together with the average volume measurements across all animals. These data also demonstrate the anatomical variability of each structure between animals, as well as between the left and right hemispheres. For example, mouse 2 displayed a larger horizontal diagonal band of Broca and lateral diagonal band of Broca as compared to mice 1 and 3. On the other hand, mice 1 and 3 showed larger vertical diagonal band of Broca volumes compared to mouse 2. There was no significant interhemispheric volume difference for any structure. Amongst the basal forebrain compartments, the horizontal diagonal band of Broca and nucleus basalis of Meynert had the largest volumes, whereas the lateral diagonal band of Broca was found to have the smallest volume.

Volume (mm^3)				
Structure	Mouse 1	Mouse 2	Mouse 3	Average
VDB left	0.1408	0.1009	0.1747	0.1388 ± 0.030
VDB right	0.1398	0.1049	0.1721	0.1388 ± 0.027
MS left	0.1321	0.1930	0.1418	0.1556 ± 0.027
MS right	0.1280	0.1969	0.1380	0.1543 ± 0.030
HDB left	0.1721	0.2602	0.1410	0.1911 ± 0.050
HDB right	0.1360	0.2755	0.1458	0.1858 ± 0.064
LDB left	0.0602	0.1352	0.0280	0.0745 ± 0.045
LDB right	0.0425	0.1307	0.0318	0.0683 ± 0.044
NBM left	0.1885	0.3375	0.2456	0.2572 ± 0.061
NBM right	0.2317	0.3196	0.2534	0.2682 ± 0.037

Table 1: Histological volumes of segmented structures of the basal forebrain in three adult (P90), male, ChAT-eGFP mice.

The structures are ordered according to their initial appearance in the brain from anterior (top) to posterior (bottom). Average volumes are expressed as mean ± standard deviation. Abbreviations: VDB = vertical diagonal band of Broca, MS = medial septum, HDB = horizontal diagonal band of Broca, LDB = lateral diagonal band of Broca, NBM = nucleus basalis of Meynert.

3D basal forebrain map

The final basal forebrain 3D map of mouse 2 is shown as a rendered surface (Fig. 3). From the images showing different angles of the final basal forebrain volume, the spatial distribution of the different structures and also the complex shape of the basal forebrain can be appreciated. Whereas medial septum and diagonal band of Broca areas merge into each other over the anterio-posterior extent of the basal forebrain, the 3D rendering clearly shows that the nucleus basalis of Meynert structure is not fully connected to the other structures (Fig. 3A-C). Furthermore the medial septum/diagonal band of Broca compartments together represent an overall band-like structure on the ventral surface of the mouse brain.

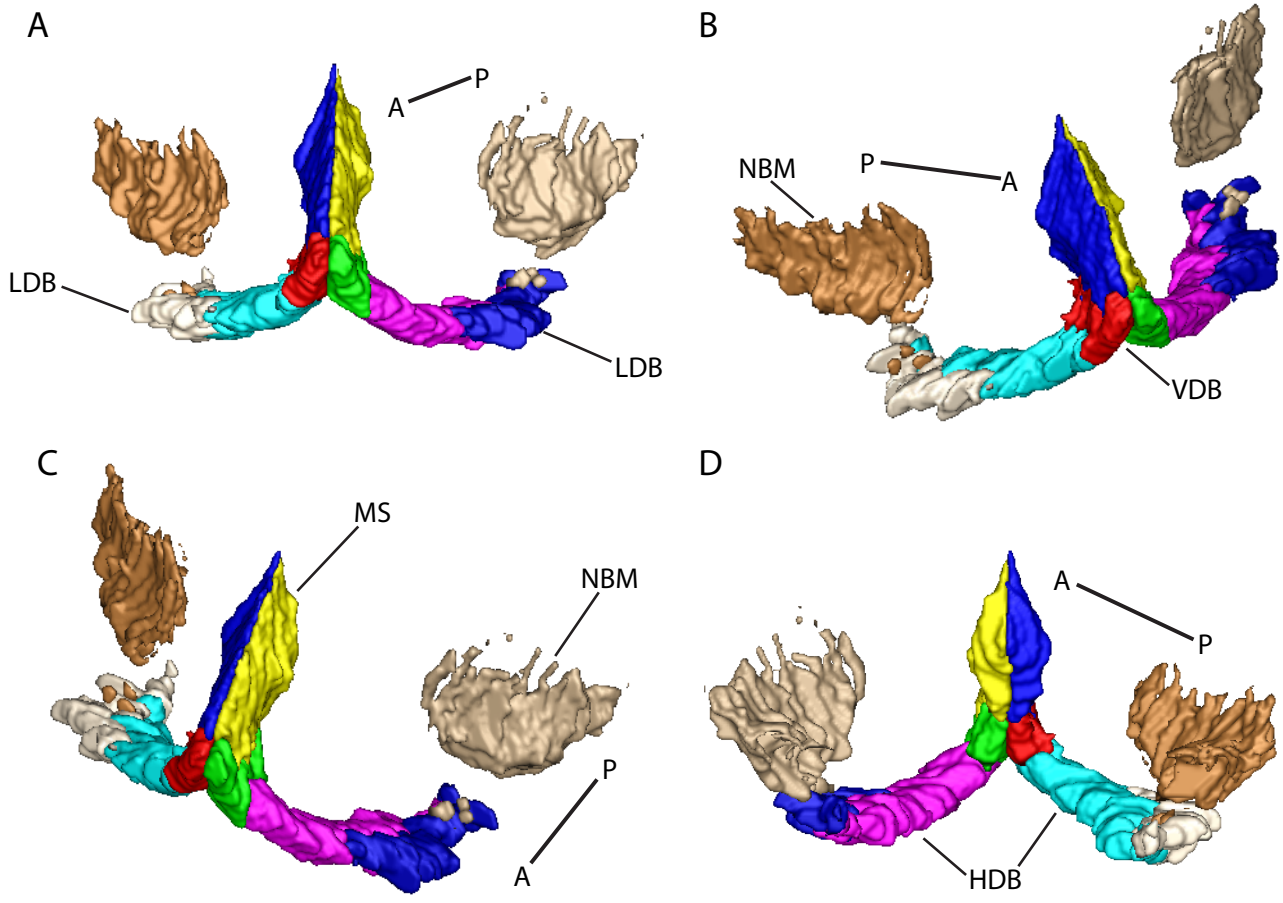

Figure 3: Surface rendering of 3D basal forebrain structures from mouse 2. The view angle is indicated by a A-P (anterior-posterior) axis. Abbreviations: VDB = vertical diagonal band of Broca, MS = medial septum, HDB = horizontal diagonal band of Broca, LDB = lateral diagonal band of Broca, NBM = nucleus basalis of Meynert.

6.4 Discussion and implication of findings

Here we present a map of the mouse basal forebrain created from histological segmentation, which can be applied for image analysis of large mouse cohorts using methods such as MRI and PET aimed at measuring particular features of the basal forebrain such as volume (MRI), retention of tracers (PET), or activity (functional MRI).

Furthermore the detailed segmentation introduced here will enable measures of the whole basal forebrain area in the left and right hemispheres, as well as individual nuclei.
The work introduced in this chapter is still in progress. So far three mice have been imaged at high resolution and subsequent histology of the basal forebrain sections has been completed. However, only one of the histological volumes has so far been registered to MRI space. Nevertheless the end result of the 3D basal forebrain maps in histological/MRI space can be seen from the single mouse for which the complete registration and stacking process was performed.

In the future the complete averaged histology as well as MRI volume of the three mice will be available and the final average basal forebrain MRI volume will be able to be applied to any MRI modality of interest. As the background strain of the ChAT-eGFP mice is the C57BL/6J mouse, the masks will be able to be applied to one of the most commonly used mouse strains in current research. The maps developed here will be particularly useful for the study of large cohorts of mice, where MRI study templates can be created with sufficient animal numbers.

Chapter 7: Conclusions and general discussion

7.1 Summary of findings and conclusions

The results presented in this thesis provide new insight into the pathophysiology of basal forebrain degeneration during the development of Alzheimer's disease and have contributed to our understanding of the pathological processes underlying this disease. It was shown for the first time that basal forebrain atrophy is associated with amyloid accumulation and tau aggregation in humans *in vivo*. Furthermore basal forebrain volume was correlated with overall cognitive decline in controls, amnestic mild cognitive impairment and Alzheimer's disease subjects and we demonstrated that basal forebrain volumetric reductions reflect impairment of navigation skills in Alzheimer's disease patients. In addition we introduced new ways of imaging basal forebrain dysfunction using a mouse model of basal forebrain degeneration, which have the potential to be translated into application in humans in the future.

The basal forebrain is divided into a number of different nuclei situated in the medioventral aspects of the brain and these nuclei project to almost the entire neocortex, the amygdala as well as the hippocampus, thereby creating a complex network of efferent connections. In healthy subjects, who show no signs of cognitive impairment but who have an amyloid burden comparable to that of Alzheimer's disease subjects, the volume of the posterior basal forebrain nucleus, which is affected early in Alzheimer's disease and its prodromal stages, was correlated to global amyloid load. As the posterior basal forebrain neurons project to a collection of structures, including the frontal cortex, parietal cortex and temporal lobe, which show heavy amyloid deposition during the course of Alzheimer's disease, the interaction seen in healthy subjects might represent the earliest neurodegenerative events occurring in the posterior basal forebrain neurons such as cellular shrinkage, axonal degeneration and synaptic dysfunction. However at this, possibly earliest, stage of Alzheimer's disease, cognitive and morphological reserves are sufficient to prevent any functional cognitive impairment.

Next it was shown that in amnestic mild cognitively impaired subjects with high amyloid burden and Alzheimer's disease subjects, the anterior basal forebrain volume rather than the posterior volume correlates with amyloid burden. As amyloid increases over time and exerts its toxic effect on the brain, including the basal forebrain neurons, thereby causing mild (amnestic mild cognitive impairment) to severe cognitive impairment (Alzheimer's

disease), it is reasonable to assume that volumetric changes in the anterior basal forebrain regions might become more pronounced.

In addition to correlations with amyloid burden, it was revealed that anterior and posterior basal forebrain volumes of control and Alzheimer's disease subjects were correlated to tau burden in brain regions known to be predominantly affected by NFT pathology and which are anatomically connected to the basal forebrain, in controls and Alzheimer's disease subjects. By measuring tau and amyloid burden in the same subjects and correlating these levels to basal forebrain volumes, it was demonstrated that the basal forebrain-tau correlation was stronger than the basal forebrain-amyloid interaction. Thus tau toxicity might be more detrimental to the function of basal forebrain neurons than amyloid. Consistent with this, tau levels have been shown to be correlated to cognitive decline, whereas amyloid levels are not (Villemagne et al., 2014).

Indeed, it was demonstrated herein that basal forebrain volumes correlate with cognitive scores and composite episodic memory scores. Moreover, it was discovered that basal forebrain volume is correlated to navigation performance specifically involving allocentric but not egocentric paradigms. In healthy subjects and amnestic mild cognitively impaired patients, the contribution of the basal forebrain degeneration appears to be indirect, and primarily mediated through modulation of the hippocampus. However in Alzheimer's disease patients, basal forebrain atrophy may have directly mediated the observed impairment in spatial navigation, independent of any hippocampal involvement. In particular, degeneration of the anterior basal forebrain, which sends projections to the hippocampus, was associated with both lower cognitive scores as well as navigation dysfunction in Alzheimer's disease.

Finally, it was demonstrated in mice that the integrity of the connections between the anterior basal forebrain and the hippocampus can be assessed by tractography. Lesion of a single neuronal type, namely cholinergic neurons, induced changes in diffusion parameters within the basal forebrain area, as well as causing changes to streamline parameters connecting the basal forebrain with the hippocampus. As the basal forebrain consists of many other cell types, this lesion did not affect the overall volume of the area. Hence this diffusion MRI technique could be a more sensitive method of detecting basal forebrain dysfunction in Alzheimer's disease compared with traditional structural MRI methods used elsewhere in this study. However this needs to be evaluated in human subjects.

The fact that basal forebrain integrity correlates with the major hallmarks of Alzheimer's disease pathology, namely deposition of amyloid and tau proteins as well as cognitive decline, demonstrating the potential of basal forebrain integrity measures for aiding the future diagnosis of subjects at risk of, or with, Alzheimer's disease.

7.2 General discussion

7.2.1 The basal forebrain selectively degenerates in Alzheimer's disease and is dysfunctional in its prodromal stage

The measurement of the basal forebrain volume using MRI in several independent patient cohorts from Australia (chapter 2; AIBL study; healthy controls n=141; amnestic mild cognitive impairment n=40; Alzheimer's disease n=38), the United States of America (chapter 2; ADNI study; healthy controls n=69; amnestic mild cognitive impairment n=127; Alzheimer's disease n=30) and Europe (chapter 4; healthy controls n=17; amnestic mild cognitive impairment n=27; Alzheimer's disease n=22), consistently revealed significant reductions of either the whole basal forebrain area and/or subregions (anterior, posterior) of the basal forebrain for both the amnestic mild cognitive impairment and Alzheimer's disease subject groups when compared to the control groups in each cohort (chapters 2, 4). This finding is in accordance with a number of other studies published during the time period of the thesis, which also used MRI to assess the basal forebrain volume. Although these studies employed various different methods of delineating the basal forebrain region, they similarly reported volumetric reductions in the basal forebrain area in amnestic mild cognitive impairment and Alzheimer's disease patients (George et al., 2011; Grothe et al., 2012; Grothe et al., 2011; Grothe et al., 2010; Teipel et al., 2005; Zhang et al., 2011).

With the exception of the European cohort, we found that the Alzheimer's disease groups had significantly smaller basal forebrain volumes. In the European cohort neither whole nor anterior/posterior basal forebrain volumes were significantly reduced in the Alzheimer's disease cohort, which might have been due to the slightly smaller subject number in that group compared with the amnestic mild cognitively impaired group, which did display significant atrophy. In comparison, in the AIBL study we found a clear reduction in basal forebrain volume in both the amnestic mild cognitive impairment and Alzheimer's disease subject groups; however this is perhaps not surprising as the masks used to calculate basal forebrain volumes of subjects were originally developed based on Alzheimer's disease-related atrophy (defined by comparing Alzheimer's disease and healthy control

subjects) in this cohort. On the other hand, in the American ADNI cohort, Alzheimer's disease subjects showed significant basal forebrain atrophy, whereas amnestic mild cognitively impaired subjects did not.

This finding in the ADNI cohort was confirmed by a recent study (George et al., 2011), based on manual segmentation of the substantia innominata of the basal forebrain in the same patient cohort, which demonstrated significant reductions in this basal forebrain nucleus in Alzheimer's disease but not amnestic mild cognitively impaired subjects. The fact that the ADNI analysis included a significantly larger amnestic mild cognitively impaired subject number than the European and the AIBL cohorts combined limits our conclusion of a consistent significant basal forebrain volumetric reduction in amnestic mild cognitively impaired subjects overall. One factor may be that a single clinic performed the diagnosis for all subjects in the AIBL and European cohorts, whereas data from ADNI subjects were derived from a large number of disparate clinics. Indeed amnestic mild cognitive impairment subject groups are in general considered to be heterogeneous in nature, with ~24% of subjects converting to a diagnosis of probable Alzheimer's disease and ~5% of subjects reverting to healthy control status over a 18 month time period in the present sample of the AIBL cohort. In line with this we consistently found a large range of basal forebrain volumes in the amnestic mild cognitive impairment group in all cohorts examined in this work (chapters 2, 4). This could reflect the presence of other dementias in this group as well as compensatory mechanisms occurring in the brains of amnestic mild cognitively impaired patients, where some subjects show greater morphological reserve than others (Guo et al., 2013). In fact all eight amnestic mild cognitively impaired subjects who subsequently converted to a clinical diagnosis of probable Alzheimer's disease (five amnestic mild cognitively impaired patients in the AIBL study and three amnestic mild cognitively impaired patients in the ADNI study) had reduced basal forebrain volumes and therefore reduced morphological and cognitive reserve, prior to conversion (chapter 2).

Evidence for compensatory metabolic events in basal forebrain neurons was recently demonstrated by measuring glucose uptake using PET (Kim et al., 2012). The authors of the study showed increased glucose uptake in the basal forebrain in mild cognitively impaired patients compared to controls. This in turn might reflect compensatory mechanisms masking the neuronal dysfunction and degeneration in these subjects, which, in Alzheimer's disease subjects, are then revealed by further degeneration that is reflected by increased atrophy. Indeed, when we calculated the annual rate of atrophy of basal forebrain and hippocampus (Fig. 7.1) in the AIBL study we found that Alzheimer's disease

subjects had a significantly higher rate of atrophy ($p<0.05$; determined by calculating the volumetric difference between time points and dividing by the follow-up time in years) compared to the healthy control groups (annual rates of atrophy: Alzheimer's disease 1.88%; amnestic mild cognitive impairment 0.71%; healthy controls PiB+ 0.58%; healthy controls PiB- 0.66%). Basal forebrain rates of atrophy were also similar to hippocampal rates of atrophy in the AIBL cohort (annual rates of atrophy: Alzheimer's disease 2.03%; amnestic mild cognitive impairment 1.59%; healthy controls PiB+ 0.51%; healthy controls PiB- 0.56%), with the hippocampal rate of atrophy also being significantly higher in the Alzheimer's disease subjects ($p<0.001$) and amnestic mild cognitive impairment group ($p<0.01$) as compared to healthy control groups. The absence of a significantly higher basal forebrain rate of atrophy in the mild cognitively impaired group might be due to the fact that basal forebrain volumetric measures generally display greater variance than, for example, hippocampal volume measures, but this does not exclude the possibility of higher basal forebrain atrophy being present in this group. Consistent with these findings, almost identical rates of atrophy for the basal forebrain and hippocampus were recently found by Grothe et al. (2012) in an independent patient cohort of healthy elderly and Alzheimer's disease subjects.

Overall the volumetric findings presented in this work showing significant and consistent basal forebrain volumetric atrophy in Alzheimer's disease, and to a lesser extent in amnestic mild cognitive impairment, is independent of global neocortical grey matter atrophy (chapter 2), is consistent with histological studies (chapter 1, section 1.4) showing no difference in cholinergic neuron numbers in mild cognitively impaired subjects, but significant reductions in Alzheimer's disease patients.

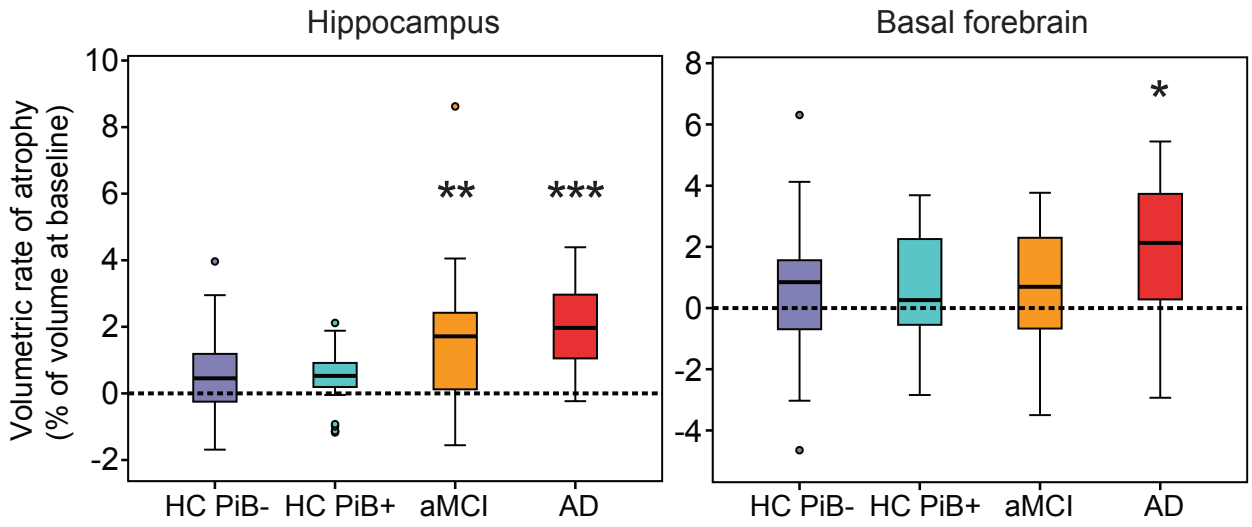

Figure 7.1: Annual rates of atrophy of hippocampus and basal forebrain volumes calculated over an ~18 months time frame.

The volumetric difference was calculated between two time points of the AIBL study (chapter 2) for each structure and divided by the follow-up time in years. The resulting annual rates of change for the subjects were then averaged across clinical groups. * $p<0.05$, ** $p<0.01$, *** $p<0.001$ compared to HC PiB+/HC PiB-. Whiskers represent min/max values except data points (circles) more than 1.5 interquartile ranges away from the 75th percentile.

7.2.2 Basal forebrain degeneration is correlated to Alzheimer's disease-related cognitive decline and mediates spatial navigation impairments

The current work revealed that basal forebrain volume is correlated to an impairment in cognitive ability in Alzheimer's disease. Correlations of whole, anterior and posterior basal forebrain volumes with various cognitive scores in different cohorts revealed significant associations between these modalities. For example in the AIBL study this was apparent when we found significant correlations between basal forebrain volumes (whole, anterior and posterior) and MMSE scores in the whole sample (whole $r=0.35$, $p<0.001$; anterior $r=0.33$, $p<0.001$; posterior $r=0.33$, $p<0.001$). In addition clinical dementia rating (CDR) scores were significantly correlated to basal forebrain volume (whole $r=0.41$, $p<0.001$; anterior $r=0.41$, $p<0.001$; posterior $r=0.36$, $p<0.001$) and CDR sum of boxes (SoB) scores also showed significant associations with basal forebrain volumes (whole $r=0.43$, $p<0.001$;

anterior r=0.39, p<0.001; posterior r=0.41, p<0.001) in the AIBL cohort. However the above interactions did not persist at an individual group level and were therefore partly driven by the differences between groups.

The influence of the basal forebrain on overall cognitive state of subjects is also indirect and occurs primarily through modulation of activity as well as neuronal plasticity of target projection areas such as neocortical regions and the hippocampus (chapter 1, Figure 1.1). Therefore early degeneration and atrophy of the basal forebrain in aging as well as predementia stages does not directly result in cognitive deficits. However the severe basal forebrain cell loss occurring at later stages of Alzheimer's disease has more direct ramifications on the cognitive state of patients. Nevertheless we recently replicated the above findings in the smaller independent European cohort, showing a significant correlation between anterior basal forebrain volume and CDR, CDR SoB as well as composite episodic memory score (chapter 3).

Moreover, we found that basal forebrain atrophy contributes to the functional impairment of subjects as measured by their ability to perform specific navigation tasks (chapter 4). Regression analyses in this study indicated that navigation performance in the whole cohort is only indirectly correlated to basal forebrain volume but that performance is strongly associated with hippocampal volume. In this case, the involvement of the basal forebrain in navigation performance in healthy subjects might occur predominantly through its contribution to modulating hippocampal function. However in Alzheimer's disease subjects, basal forebrain atrophy and therefore severe dysfunction of basal forebrain neurons was identified as solely mediating navigation impairments, independent of hippocampal contribution (chapter 4).

7.2.3 Basal forebrain atrophy is linked to amyloid and tau accumulation during the development of Alzheimer's disease

Reductions in basal forebrain volumes were shown to be associated with amyloid pathology measured by PiB-PET (chapter 2) as well as AV45 (florbetapir) PET (Grothe et al., 2014; Teipel et al., 2013) in Alzheimer's disease, amnestic mild cognitive impairment and control subjects. Interestingly, we found that while anterior basal forebrain volume correlated with neocortical amyloid burden in amnestic mild cognitively impaired and Alzheimer's disease patients, posterior basal forebrain volume was associated with amyloid burden in controls (chapter 2). This interaction of the basal forebrain with amyloid

accumulation is selective and independent of hippocampal and neocortical involvement, as neither hippocampal nor neocortical volumes were correlated to global amyloid load. Furthermore we found that there was no difference in the rate of basal forebrain atrophy of amyloid accumulators vs. non-accumulators (Fig. 7.2; as defined by Villain et al., 2012) within any of the subject groups over the 18 month time period in the AIBL study. Similarly, a recent study found no relationship between hippocampal rate of atrophy and amyloid accumulation (Jack et al., 2014). Another study demonstrated that there is no correlation between amyloid burden and the rate of brain atrophy or ventricular expansion (Josephs et al., 2008). However, we found a relationship between absolute amyloid burden and basal forebrain volume, and although amyloid-beta may not drive basal forebrain degeneration, degeneration could contribute to increasing amyloid-beta load within innervated brain areas.

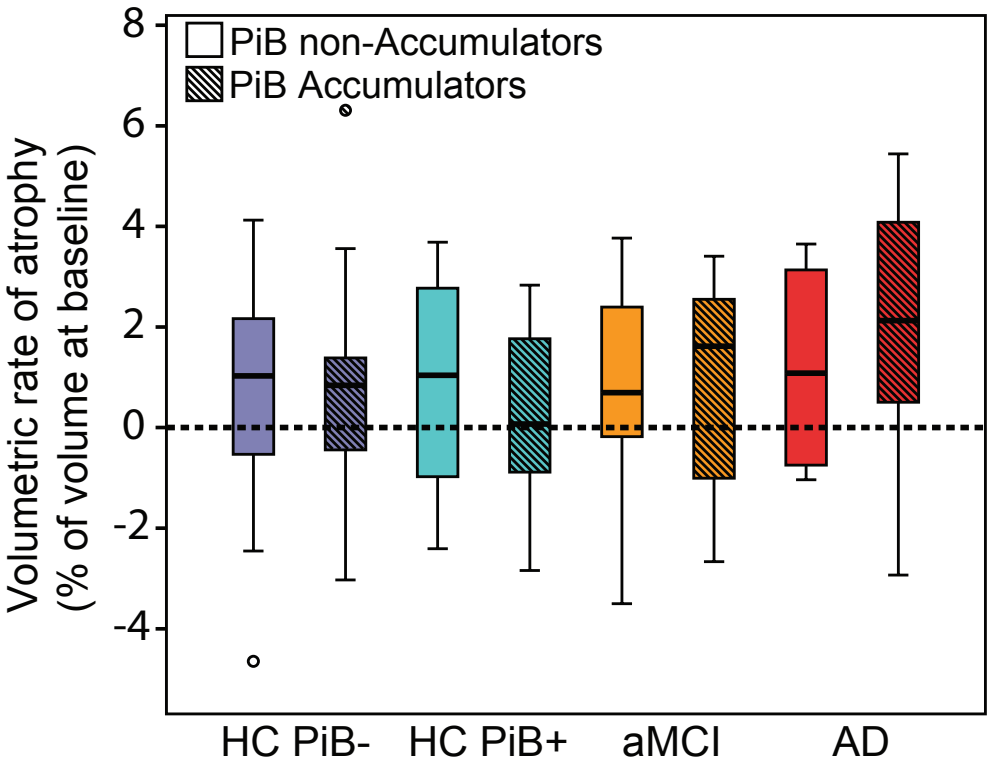

Figure 7.2: Basal forebrain annual rate of atrophy of subject groups that were subdivided into PiB accumulators and non-accumulators.

There was no effect of amyloid accumulation status on basal forebrain rate of atrophy in any of the clinical groups. Linear regression between rate of PiB retention over time (independent of accumulation status) and basal forebrain rate of atrophy in individual subject groups did not reveal any significant associations. Whiskers represent min/max values except data points (circles) more than 1.5 interquartile ranges away from the 75th percentile.

Our findings are equally consistent with accumulating levels of amyloid affecting basal forebrain neuronal terminals in their respective target areas (Auld et al., 2002; Yan and Feng, 2004). It has been suggested that amyloid oligomers have the potential to exert a wide range of effects on the function of basal forebrain neuronal networks, such as the depression of acetylcholine and muscarinic signalling, and enhancement of glutamate release (Auld et al., 2002). The correlations reported here might therefore represent the downstream consequences of some of the abovementioned processes.

Tau NFTs, on the other hand, which occur in brain regions that are innervated by basal forebrain neurons as well as within basal forebrain neurons themselves (Braak et al., 2006), were shown to exert a potentially stronger effect on basal forebrain neurons *in vivo* than that induced by amyloid accumulation (chapter 3). However the small sample size in the study limits the strength of our conclusions in this regard, and larger studies are required to verify our findings.

Nevertheless, we were able to show correlations of regional THK523/THK5105 retention with anterior and posterior basal forebrain volumes in two independent cohorts, as well as in the respective clinical groups. While anterior basal forebrain was correlated to THK523 retention in the hippocampus, orbitofrontal cortex and gyrus rectus in cohort 1, no significant correlations were found between anterior basal forebrain volume and THK5105 retention in cohort 2. In contrast, significant correlations were found between posterior basal forebrain volume and parietal as well as neocortical THK523 retention in cohort 1, and, parietal as well as neocortical THK5105 retention in cohort 2. In addition, significant correlations between basal forebrain volumes and THK523 retention were identified at the clinical group level in cohort 1, but these interactions were not replicated for THK5105 retention in cohort 2. Although the results of the analysis of both cohorts only partly overlaps, in both cohorts significant interactions were found.

These differences might be attributed to the minimal sample size in the THK5105 cohort as compared to the THK523 cohort or the different pharmacokinetic properties and binding profiles of the two tracers (section 3.4; Okamura et al., 2014; Okamura et al., 2013). Larger sample sizes and improved tau tracers currently under development will help to clarify the different interactions between global and regional tau burden and basal forebrain volumes. Despite these limitations we were able to identify significant correlations between basal forebrain volume and tau burden in various brain regions in two independent cohorts, employing two different PET tracers in control and Alzheimer's disease subjects. Thus we demonstrated that *in vivo* measures of tau burden also

correlates with another hallmark of Alzheimer's disease pathology, namely basal forebrain atrophy, in addition to previously identified interactions with atrophy of regions such as the hippocampus and temporal lobe (Okamura et al., 2014; Villemagne et al., 2014). Therefore the present findings further support the potential value usefulness of non-invasive evaluation of tau pathology *in vivo* in human populations for diagnostic and/or prognostic purposes.

The work presented herein provides evidence that amyloid and tau pathology, cognitive impairment and basal forebrain degeneration could be mechanistically linked. It is further proposed that amyloid might accumulate early in asymptomatic subjects but is not sufficient to cause the development of Alzheimer's disease. However parallel induction of tau pathology, potentially coupled to other secondary events (environmental and/or genetic), could be required to trigger basal forebrain and other brain regional degeneration, ultimately leading to cognitive decline. The application of a combination of both amyloid and tau imaging with structural MRI in large longitudinal studies, including amnestic mild cognitively impaired patient groups, will provide crucial insight into the interplay of these pathological features *in vivo* and their precise relationship to brain atrophy and cognitive impairment.

7.2.4 Basal forebrain measures and their potential as diagnostic tools of Alzheimer's disease

Measures of basal forebrain neuronal integrity have great potential as reliable biomarkers of Alzheimer's disease and other dementias. It is clear that basal forebrain volumes can be used to distinguish between Alzheimer's disease, amnestic mild cognitively impaired and control subjects. We found that amnestic mild cognitively impaired patients had basal forebrain volumes below a certain cut-off value prior to conversion to Alzheimer's disease. Subjects with a basal forebrain volume below this value were at a seven times higher risk of conversion to greater cognitive impairment than subjects with basal forebrain volumes in the range of the cognitively normal cluster (chapter 2). Furthermore diffusion MRI could in the future be used to measure disconnection and death of the cholinergic basal forebrain neuronal network prior to atrophy (Kerbler et al., 2012). However methods of evaluating basal forebrain integrity have only recently been developed (chapter 2; George et al., 2011; Kerbler et al., 2012) and before these methods could be considered for diagnostic application at the single subject level, significant validation, replication and standardization need to be performed. Nevertheless it has been demonstrated that basal

forebrain atrophy correlates with the major hallmarks of Alzheimer's disease pathology, namely amyloid accumulation, aggregation of tau and cognitive impairment.

Basal forebrain regions of interest (ROIs) such as the maximum probability masks developed in this work or the probabilistic maps developed by Zaborszky et al. (2008) should be used to assess volumetric integrity of the human basal forebrain as they most accurately represent the basal forebrain area. It was found that the maximum probability masks (which are partly based on the probabilistic maps) show a high overlap (85%; chapter 3) with the probabilistic maps developed through combined histological segmentation of the basal forebrain of 10 post-mortem brains (Zaborszky et al., 2008), verifying the anatomical precision of the maximum probability masks. The use of a probabilistic mask based on segmentation of a brain structure from several subjects' brains is crucial when measuring the volume of a highly variable brain region such as the basal forebrain, which does not have any visible anatomical boundaries on MR images. Therefore manual segmentation (George et al., 2011) of the basal forebrain should be avoided, as it is not a reliable way of determining the volume of this structure.

Using a mask created from histological segmentation of a single post-mortem brain (Grothe et al., 2011; Teipel et al., 2005) is equally flawed, as it does not give a reasonable estimate of the basal forebrain area in a population setting. For example, when the mask used by Teipel and colleagues (2005) was compared to the probabilistic ROI developed by Zaborszky et al. (2008), it was found that the Ch4 area of the former mask was about 20 times larger than that of the latter mask. The mask developed by Teipel et al. was also reported to include areas outside the basal forebrain such as the anterior commissure, large parts of the ventral globus pallidus and parts of the medioventral putamen, and analyses using this ROI could therefore lead to erroneous conclusions (Zaborszky et al., 2008). However, the masks developed by Zaborszky et al. (2008) are not yet publicly available. In a clinical setting with the aim of potential diagnosis of Alzheimer's disease, maximum probability masks would be particularly useful as they represent basal forebrain maps of Alzheimer's disease-specific change within anatomically verified regions of the basal forebrain.

Another reason basal forebrain atrophy should be incorporated into clinical setting is that, because basal forebrain volume correlates with the two pathological hallmarks of Alzheimer's disease, namely accumulation of amyloid and aggregation of tau (chapter 2; chapter 3) and is associated with cognitive impairment (chapter3; chapter 4), it is an excellent correlate of Alzheimer's disease, a critical attribute of a potential biomarker.

Basal forebrain volume measures might also have better predictive power than hippocampal volume measures or measures of global neocortical grey matter atrophy, as the latter do not correlate to amyloid burden.
In addition, basal forebrain neurons are amongst the first to develop tau pathology, seen in Braak stage I, whereas tau pathology is observed in the hippocampal formation only in Braak stage II (Braak et al., 2006). Although our results demonstrate that basal forebrain volume does correlate to tau burden in anatomically connected brain regions, it remains to be investigated whether the level of tau in the basal forebrain itself is correlated to basal forebrain volume. Assessment of glucose metabolism in the basal forebrain using FDG (fluorodeoxyglucose) PET was recently demonstrated to detect hypermetabolism in mild cognitively impaired patients compared to controls. This suggests that PET measures of tau burden in the basal forebrain could be of particular use for diagnosis of Alzheimer's disease due to the early presence of NFTs in this structure. However, the current spatiotemporal resolution of tau-PET imaging is not sufficient to measure tau burden in the basal forebrain due to the distance that positrons travel before annihilation. With advances in PET technology such as the development of new methods of spatial normalization, improvements in system geometry and the introduction of novel detectors, the sensitivity of PET systems will be enhanced (Kim et al., 2012; Lewellen, 2008; Peng and Levin, 2010), potentially enabling future studies to address the above issue.

It was reported herein that measuring diffusion MRI parameters of the basal forebrain area, as well as performing tractography of basal forebrain connections could be used to detect basal forebrain cholinergic degeneration in the absence of volumetric changes in mice, while being associated with histological measures (chapter 5). The changes in diffusion parameters in mice that had undergone lesioning of cholinergic neurons were comparable with the first results in human studies measuring similar parameter changes in either the basal forebrain area or the fornix in mild cognitively impaired and Alzheimer's disease patients as compared to controls (Oishi et al., 2011; Pievani et al., 2010), but in the latter studies there was no biological explanation for the findings. Therefore, our study demonstrates the potential sensitivity and feasibility of diffusion MRI to detect brain regional changes and alterations in connectivity of the basal forebrain specifically, before gross structural change can be detected. In the current study we assessed the septohippocampal connections; however tractography measurement of posterior basal forebrain projections, namely basalocortical connections, which appear to degenerate at the earliest stages of disease, might provide the most predictive clinical information. This method would also give a more complete picture of the integrity of the whole network of

basal forebrain connections. Furthermore tractography could be used to study pathophysiology namely the disconnection of basal forebrain neurons from their targets during the development of Alzheimer's disease. This is expected to occur much earlier in the disease, possibly in relation to amyloid deposition and tau aggregation. In addition, measuring local diffusion MRI parameters in the basal forebrain could provide a more sensitive method over volumetric assessment of the basal forebrain for the potential diagnosis of Alzheimer's disease. However this needs to be further evaluated in human subjects.

The methods of assessing basal forebrain integrity developed in this work using MRI are particularly useful because of their potential to be translated into future clinical application. These methods allow non-invasive assessment of the structural properties of pathological processes relevant for a neurological disorder involving basal forebrain dysfunction. If used early in the disease course, the analysis could help to identify those subjects who are at risk of developing significant basal forebrain dysfunction that could result in cognitive impairment and for whom early treatment with current acetyl cholinesterase drugs and future pharmacological agents would be most benificial (Knowles et al., 2013; Longo and Massa, 2013; Nguyen et al., 2014). Furthermore the human basal forebrain masks introduced here could be applied to study not only structural alterations, but also functional properties of the basal forebrain using, for example, functional MRI and PET.

This thesis has reported significant correlations between basal forebrain degeneration and hallmarks of Alzheimer's disease. However, it remains to be determined why basal forebrain neurons are particularly vulnerable to neurodegeneration. It is possible that long projection neurons have an increased susceptibility to protein deposits and it has been suggested that such neurons, which include basal forebrain neurons, might be the first to be affected in Alzheimer's disease, particularly when they are only sparsely myelinated, such as the cholinergic neurons (Braak and Del Tredici, 2011a; Braak et al., 2000; Gartner et al., 2001; Moceri et al., 2000).

Finally, this work provides a substantial contribution to the understanding of the process of degeneration of the basal forebrain network in Alzheimer's disease and its prodromal stages. The data that form this thesis and that obtained by others over the same time frame, now provide a significant body of evidence linking basal forebrain degeneration, tau aggregation, amyloid accumulation and cognitive impairment. Although cause and effects remain to be determined through both animal and longitudinal studies of clinical human cohorts, there is now strong justification to herald measures of basal forebrain dysfunction

as a key clinical attribute to be assessed for diagnostic purposes, and potentially for the purpose of individualizing the prescription of appropriate drugs.

References

Amaral, D.G., Kurz, J., 1985. An analysis of the origins of the cholinergic and noncholinergic septal projections to the hippocampal formation of the rat. The Journal of Comparative Neurology 240, 37-59.

Arendt, T., Bigl, V., Arendt, A., 1984. Neurone loss in the nucleus basalis of Meynert in Creutzfeldt-Jakob disease. Acta Neuropathologica 65, 85-88.

Arendt, T., Bigl, V., Arendt, A., Tennstedt, A., 1983. Loss of neurons in the nucleus basalis of Meynert in Alzheimer's disease, paralysis agitans and Korsakoff's Disease. Acta Neuropathologica 61, 101-108.

Armstrong, D.M., Saper, C.B., Levey, A.I., Wainer, B.H., Terry, R.D., 1983. Distribution of cholinergic neurons in rat brain: demonstrated by the immunocytochemical localization of choline acetyltransferase. The Journal of Comparative Neurology 216, 53-68.

Auld, D.S., Kornecook, T.J., Bastianetto, S., Quirion, R., 2002. Alzheimer's disease and the basal forebrain cholinergic system: relations to beta-amyloid peptides, cognition, and treatment strategies. Progress in Neurobiology 68, 209-245.

Barbelivien, A., Bertrand, N., Besret, L., Beley, A., MacKenzie, E.T., Dauphin, F., 1999a. Neurochemical stimulation of the rat substantia innominata increases cerebral blood flow (but not glucose use) through the parallel activation of cholinergic and non-cholinergic pathways. Brain Research 840, 115-124.

Barbelivien, A., Noel, C., MacKenzie, E.T., Dauphin, F., 1999b. Cerebrovascular evidence for a GABAergic modulation of the cholinergic vasodilatatory basalocortical system in the rat. Brain Research 834, 223-227.

Bartus, R.T., 2000. On neurodegenerative diseases, models, and treatment strategies: lessons learned and lessons forgotten a generation following the cholinergic hypothesis. Experimental Neurology 163, 495-529.

Bartus, R.T., Dean, R.L., 3rd, Beer, B., Lippa, A.S., 1982. The cholinergic hypothesis of geriatric memory dysfunction. Science 217, 408-414.

Baskerville, K.A., Kent, C., Personett, D., Lai, W.R., Park, P.J., Coleman, P., McKinney, M., 2008. Aging elevates metabolic gene expression in brain cholinergic neurons. Neurobiology of Aging 29, 1874-1893.

Baxter, M.G., Bucci, D.J., 2013. Selective immunotoxic lesions of basal forebrain cholinergic neurons: twenty years of research and new directions. Behavioral Neuroscience 127, 611-618.

Berger-Sweeney, J., Heckers, S., Mesulam, M.M., Wiley, R.G., Lappi, D.A., Sharma, M., 1994. Differential effects on spatial navigation of immunotoxin-induced cholinergic lesions of the medial septal area and nucleus basalis magnocellularis. Journal of Neuroscience 14, 4507-4519.
Bertram, L., Lill, C.M., Tanzi, R.E., 2010. The genetics of Alzheimer disease: back to the future. Neuron 68, 270-281.
Braak, H., Alafuzoff, I., Arzberger, T., Kretzschmar, H., Del Tredici, K., 2006. Staging of Alzheimer disease-associated neurofibrillary pathology using paraffin sections and immunocytochemistry. Acta Neuropathologica 112, 389-404.
Braak, H., Del Tredici, K., 2011a. Alzheimer's pathogenesis: is there neuron-to-neuron propagation? Acta Neuropathologica 121, 589-595.
Braak, H., Del Tredici, K., 2011b. The pathological process underlying Alzheimer's disease in individuals under thirty. Acta Neuropathologica 121, 171-181.
Braak, H., Del Tredici, K., Schultz, C., Braak, E., 2000. Vulnerability of select neuronal types to Alzheimer's disease. Annals of the New York Academy of Sciences 924, 53-61.
Bucci, D.J., Holland, P.C., Gallagher, M., 1998. Removal of cholinergic input to rat posterior parietal cortex disrupts incremental processing of conditioned stimuli. The Journal of Neuroscience 18, 8038-8046.
Burke, S.N., Barnes, C.A., 2006. Neural plasticity in the ageing brain. Nature reviews. Neuroscience 7, 30-40.
Burns, A., Whitehouse, P., Arendt, T., Forsti, H., 1997. Alzheimer's disease in senile dementia: loss of neurones in the basal forebrain. Whitehouse, P., Price, D., Struble, R., Clarke, A., Coyle, J. and Delong, M. Science (1982), 215, 1237-1239. International Journal of Geriatric Psychiatry 12, 7-10.
Butler, T., Blackmon, K., Zaborszky, L., Wang, X., DuBois, J., Carlson, C., Barr, W.B., French, J., Devinsky, O., Kuzniecky, R., Halgren, E., Thesen, T., 2012. Volume of the human septal forebrain region is a predictor of source memory accuracy. Journal of the International Neuropsychological Society 18, 157-161.
Carlsen, J., Zaborszky, L., Heimer, L., 1985. Cholinergic projections from the basal forebrain to the basolateral amygdaloid complex: a combined retrograde fluorescent and immunohistochemical study. The Journal of Comparative Neurology 234, 155-167.
Chudasama, Y., Dalley, J.W., Nathwani, F., Bouger, P., Robbins, T.W., 2004. Cholinergic modulation of visual attention and working memory: dissociable effects of basal forebrain 192-IgG-saporin lesions and intraprefrontal infusions of scopolamine. Learning & Memory 11, 78-86.

Citron, M., Westaway, D., Xia, W., Carlson, G., Diehl, T., Levesque, G., Johnson-Wood, K., Lee, M., Seubert, P., Davis, A., Kholodenko, D., Motter, R., Sherrington, R., Perry, B., Yao, H., Strome, R., Lieberburg, I., Rommens, J., Kim, S., Schenk, D., Fraser, P., St George Hyslop, P., Selkoe, D.J., 1997. Mutant presenilins of Alzheimer's disease increase production of 42-residue amyloid beta-protein in both transfected cells and transgenic mice. Nature Medicine 3, 67-72.

Contestabile, A., 2011. The history of the cholinergic hypothesis. Behavioural Brain Research 221, 334-340.

Coulson, E.J., 2006. Does the p75 neurotrophin receptor mediate Abeta-induced toxicity in Alzheimer's disease? Journal of Neurochemistry 98, 654-660.

Coulson, E.J., May, L.M., Sykes, A.M., Hamlin, A.S., 2009. The role of the p75 neurotrophin receptor in cholinergic dysfunction in Alzheimer's disease. The Neuroscientist 15, 317-323.

Cullinan, W.E., Zaborszky, L., 1991. Organization of ascending hypothalamic projections to the rostral forebrain with special reference to the innervation of cholinergic projection neurons. The Journal of Comparative Neurology 306, 631-667.

Davis, K.L., Mohs, R.C., Marin, D., Purohit, D.P., Perl, D.P., Lantz, M., Austin, G., Haroutunian, V., 1999. Cholinergic markers in elderly patients with early signs of Alzheimer disease. The journal of the American Medical Association 281, 1401-1406.

De Rosa, E., Desmond, J.E., Anderson, A.K., Pfefferbaum, A., Sullivan, E.V., 2004. The human basal forebrain integrates the old and the new. Neuron 41, 825-837.

DeKosky, S.T., Ikonomovic, M.D., Styren, S.D., Beckett, L., Wisniewski, S., Bennett, D.A., Cochran, E.J., Kordower, J.H., Mufson, E.J., 2002. Upregulation of choline acetyltransferase activity in hippocampus and frontal cortex of elderly subjects with mild cognitive impairment. Annals of Neurology 51, 145-155.

Dembrow, N.C., Chitwood, R.A., Johnston, D., 2010. Projection-specific neuromodulation of medial prefrontal cortex neurons. Journal of Neuroscience 30, 16922-16937.

Donat, C.K., Walter, B., Kayser, T., Deuther-Conrad, W., Schliebs, R., Nieber, K., Bauer, R., Hartig, W., Brust, P., 2010. Effects of lateral fluid percussion injury on cholinergic markers in the newborn piglet brain. International journal of developmental neuroscience : the official journal of the International Society for Developmental Neuroscience 28, 31-38.

Drachman, D.A., 2014. The amyloid hypothesis, time to move on: Amyloid is the downstream result, not cause, of Alzheimer's disease. Alzheimer's & dementia, 10.1016/j.alz.2013.11.003.

Fodero-Tavoletti, M.T., Okamura, N., Furumoto, S., Mulligan, R.S., Connor, A.R., McLean, C.A., Cao, D., Rigopoulos, A., Cartwright, G.A., O'Keefe, G., Gong, S., Adlard, P.A., Barnham, K.J., Rowe, C.C., Masters, C.L., Kudo, Y., Cappai, R., Yanai, K., Villemagne, V.L., 2011. 18F-THK523: a novel in vivo tau imaging ligand for Alzheimer's disease. Brain 134, 1089-1100.

Franklin, K.J.B., Paxinos, G., 2007. The Mouse Brain in Stereotaxic Coordinates Third Edition. Academic Press, San Diego.

Gartner, U., Hartig, W., Brauer, K., Bruckner, G., Arendt, T., 2001. Immunofluorescence and immunoelectron microscopic evidence for differences in myelination of GABAergic and cholinergic septohippocampal fibres. International Journal of Developmental Neuroscience 19, 347-352.

Gaykema, R.P., Luiten, P.G., Nyakas, C., Traber, J., 1990. Cortical projection patterns of the medial septum-diagonal band complex. The Journal of Comparative Neurology 293, 103-124.

Gaykema, R.P., Zaborszky, L., 1996. Direct catecholaminergic-cholinergic interactions in the basal forebrain. II. Substantia nigra-ventral tegmental area projections to cholinergic neurons. The Journal of Comparative Neurology 374, 555-577.

George, S., Mufson, E.J., Leurgans, S., Shah, R.C., Ferrari, C., deToledo-Morrell, L., 2011. MRI-based volumetric measurement of the substantia innominata in amnestic MCI and mild AD. Neurobiology of Aging 32, 1756-1764.

Geula, C., Bu, J., Nagykery, N., Scinto, L.F., Chan, J., Joseph, J., Parker, R., Wu, C.K., 2003. Loss of calbindin-D28k from aging human cholinergic basal forebrain: relation to neuronal loss. The Journal of Comparative Neurology 455, 249-259.

Gilmor, M.L., Erickson, J.D., Varoqui, H., Hersh, L.B., Bennett, D.A., Cochran, E.J., Mufson, E.J., Levey, A.I., 1999. Preservation of nucleus basalis neurons containing choline acetyltransferase and the vesicular acetylcholine transporter in the elderly with mild cognitive impairment and early Alzheimer's disease. The Journal of Comparative Neurology 411, 693-704.

Goedert, M., Jakes, R., 2005. Mutations causing neurodegenerative tauopathies. Biochimica et Biophysica Acta 1739, 240-250.

Gritti, I., Henny, P., Galloni, F., Mainville, L., Mariotti, M., Jones, B.E., 2006. Stereological estimates of the basal forebrain cell population in the rat, including neurons containing choline acetyltransferase, glutamic acid decarboxylase or phosphate-activated glutaminase and colocalizing vesicular glutamate transporters. Neuroscience 143, 1051-1064.

Gritti, I., Manns, I.D., Mainville, L., Jones, B.E., 2003. Parvalbumin, calbindin, or calretinin in cortically projecting and GABAergic, cholinergic, or glutamatergic basal forebrain neurons of the rat. The Journal of Comparative Neurology 458, 11-31.
Grothe, M., Heinsen, H., Teipel, S., 2012. Longitudinal measures of cholinergic forebrain atrophy in the transition from healthy aging to Alzheimer's disease. Neurobiology of Aging, doi: 10.1016/j.neurobiolaging.2012.10.018.
Grothe, M., Heinsen, H., Teipel, S.J., 2011. Atrophy of the cholinergic basal forebrain over the adult age range and in early stages of Alzheimer's disease. Biological Psychiatry 71, 805-813.
Grothe, M., Zaborszky, L., Atienza, M., Gil-Neciga, E., Rodriguez-Romero, R., Teipel, S.J., Amunts, K., Suarez-Gonzalez, A., Cantero, J.L., 2010. Reduction of basal forebrain cholinergic system parallels cognitive impairment in patients at high risk of developing Alzheimer's disease. Cerebral Cortex 20, 1685-1695.
Grothe, M.J., Ewers, M., Krause, B., Heinsen, H., Teipel, S.J., 2014. Basal forebrain atrophy and cortical amyloid deposition in nondemented elderly subjects. Alzheimer's & dementia, doi: 10.1016/j.alz.2013.09.011.
Gu, Z., Yakel, J.L., 2011. Timing-dependent septal cholinergic induction of dynamic hippocampal synaptic plasticity. Neuron 71, 155-165.
Guo, L.H., Alexopoulos, P., Wagenpfeil, S., Kurz, A., Perneczky, R., 2013. Brain size and the compensation of Alzheimer's disease symptoms: a longitudinal cohort study. Alzheimer's & dementia 9, 580-586.
Hajszan, T., Zaborszky, L., 2002. Direct catecholaminergic-cholinergic interactions in the basal forebrain. III. Adrenergic innervation of choline acetyltransferase-containing neurons in the rat. The Journal of Comparative Neurology 449, 141-157.
Hallanger, A.E., Wainer, B.H., 1988. Ascending projections from the pedunculopontine tegmental nucleus and the adjacent mesopontine tegmentum in the rat. The Journal of Comparative Neurology 274, 483-515.
Hamlin, A.S., Windels, F., Boskovic, Z., Sah, P., Coulson, E.J., 2013. Lesions of the basal forebrain cholinergic system in mice disrupt idiothetic navigation. PloS one 8, e53472.
Han, Y., Shi, Y.F., Xi, W., Zhou, R., Tan, Z.B., Wang, H., Li, X.M., Chen, Z., Feng, G., Luo, M., Huang, Z.L., Duan, S., Yu, Y.Q., 2014. Selective Activation of Cholinergic Basal Forebrain Neurons Induces Immediate Sleep-wake Transitions. Current biology 24, 693-698.
Hardy, J., Selkoe, D.J., 2002. The amyloid hypothesis of Alzheimer's disease: progress and problems on the road to therapeutics. Science 297, 353-356.

Hassani, O.K., Lee, M.G., Henny, P., Jones, B.E., 2009. Discharge profiles of identified GABAergic in comparison to cholinergic and putative glutamatergic basal forebrain neurons across the sleep-wake cycle. Journal of Neuroscience 29, 11828-11840.
Heimer, L., 2000. Basal forebrain in the context of schizophrenia. Brain Research Reviews 31, 205-235.
Heimer, L., de Olmos, J., Alheid, G.F., Zaborszky, L., 1991. "Perestroika" in the basal forebrain: opening the border between neurology and psychiatry. Progress in Brain Research 87, 109-165.
Henny, P., Jones, B.E., 2008. Projections from basal forebrain to prefrontal cortex comprise cholinergic, GABAergic and glutamatergic inputs to pyramidal cells or interneurons. The European Journal of Neuroscience 27, 654-670.
Hort, J., Andel, R., Mokrisova, I., Gazova, I., Amlerova, J., Valis, M., Coulson, E.J., Harrison, J., Windisch, M., Laczo, J., 2014. Effect of donepezil in Alzheimer disease can be measured by a computerized human analog of the morris water maze. Neuro-degenerative Diseases 13, 192-196.
Hur, E.E., Zaborszky, L., 2005. Vglut2 afferents to the medial prefrontal and primary somatosensory cortices: a combined retrograde tracing in situ hybridization study [corrected]. The Journal of Comparative Neurology 483, 351-373.
Ikonen, S., McMahan, R., Gallagher, M., Eichenbaum, H., Tanila, H., 2002. Cholinergic system regulation of spatial representation by the hippocampus. Hippocampus 12, 386-397.
Ikonomovic, M.D., Mufson, E.J., Wuu, J., Cochran, E.J., Bennett, D.A., DeKosky, S.T., 2003. Cholinergic plasticity in hippocampus of individuals with mild cognitive impairment: correlation with Alzheimer's neuropathology. Journal of Alzheimer's disease 5, 39-48.
Jack, C.R., Jr., Knopman, D.S., Jagust, W.J., Petersen, R.C., Weiner, M.W., Aisen, P.S., Shaw, L.M., Vemuri, P., Wiste, H.J., Weigand, S.D., Lesnick, T.G., Pankratz, V.S., Donohue, M.C., Trojanowski, J.Q., 2013. Tracking pathophysiological processes in Alzheimer's disease: an updated hypothetical model of dynamic biomarkers. Lancet Neurology 12, 207-216.
Jack, C.R., Jr., Wiste, H.J., Knopman, D.S., Vemuri, P., Mielke, M.M., Weigand, S.D., Senjem, M.L., Gunter, J.L., Lowe, V., Gregg, B.E., Pankratz, V.S., Petersen, R.C., 2014. Rates of beta-amyloid accumulation are independent of hippocampal neurodegeneration. Neurology, doi: 10.1212/WNL.0000000000000386.
Jellinger, K.A., 2000. Morphological substrates of mental dysfunction in Lewy body disease: an update. Journal of neural transmission. Supplementum 59, 185-212.

Jolkkonen, E., Miettinen, R., Pikkarainen, M., Pitkanen, A., 2002. Projections from the amygdaloid complex to the magnocellular cholinergic basal forebrain in rat. Neuroscience 111, 133-149.
Jones, B.E., 2004. Activity, modulation and role of basal forebrain cholinergic neurons innervating the cerebral cortex. Progress in Brain Research 145, 157-169.
Jones, B.E., Cuello, A.C., 1989. Afferents to the basal forebrain cholinergic cell area from pontomesencephalic--catecholamine, serotonin, and acetylcholine--neurons. Neuroscience 31, 37-61.
Josephs, K.A., Whitwell, J.L., Ahmed, Z., Shiung, M.M., Weigand, S.D., Knopman, D.S., Boeve, B.F., Parisi, J.E., Petersen, R.C., Dickson, D.W., Jack, C.R., Jr., 2008. Beta-amyloid burden is not associated with rates of brain atrophy. Annals of Neurology 63, 204-212.
Kerbler, G.M., Hamlin, A.S., Pannek, K., Kurniawan, N.D., Keller, M.D., Rose, S.E., Coulson, E.J., 2012. Diffusion-weighted magnetic resonance imaging detection of basal forebrain cholinergic degeneration in a mouse model. NeuroImage 66C, 133-141.
Khateb, A., Fort, P., Alonso, A., Jones, B.E., Muhlethaler, M., 1993. Pharmacological and immunohistochemical evidence for serotonergic modulation of cholinergic nucleus basalis neurons. The European Journal of Neuroscience 5, 541-547.
Kim, M.J., Lee, K.M., Son, Y.D., Jeon, H.A., Kim, Y.B., Cho, Z.H., 2012. Increased basal forebrain metabolism in mild cognitive impairment: an evidence for brain reserve in incipient dementia. Journal of Alzheimer's disease 32, 927-938.
Kiuchi, K., Morikawa, M., Taoka, T., Nagashima, T., Yamauchi, T., Makinodan, M., Norimoto, K., Hashimoto, K., Kosaka, J., Inoue, Y., Inoue, M., Kichikawa, K., Kishimoto, T., 2009. Abnormalities of the uncinate fasciculus and posterior cingulate fasciculus in mild cognitive impairment and early Alzheimer's disease: a diffusion tensor tractography study. Brain Research 1287, 184-191.
Klunk, W.E., Engler, H., Nordberg, A., Wang, Y., Blomqvist, G., Holt, D.P., Bergstrom, M., Savitcheva, I., Huang, G.F., Estrada, S., Ausen, B., Debnath, M.L., Barletta, J., Price, J.C., Sandell, J., Lopresti, B.J., Wall, A., Koivisto, P., Antoni, G., Mathis, C.A., Langstrom, B., 2004. Imaging brain amyloid in Alzheimer's disease with Pittsburgh Compound-B. Annals of Neurology 55, 306-319.
Knowles, J.K., Rajadas, J., Nguyen, T.V., Yang, T., LeMieux, M.C., Vander Griend, L., Ishikawa, C., Massa, S.M., Wyss-Coray, T., Longo, F.M., 2009. The p75 neurotrophin receptor promotes amyloid-beta(1-42)-induced neuritic dystrophy in vitro and in vivo. Journal of neuroscience 29, 10627-10637.

Knowles, J.K., Simmons, D.A., Nguyen, T.V., Vander Griend, L., Xie, Y., Zhang, H., Yang, T., Pollak, J., Chang, T., Arancio, O., Buckwalter, M.S., Wyss-Coray, T., Massa, S.M., Longo, F.M., 2013. Small molecule p75NTR ligand prevents cognitive deficits and neurite degeneration in an Alzheimer's mouse model. Neurobiology of Aging 34, 2052-2063.
Lamour, Y., Dutar, P., Jobert, A., 1984. Cortical projections of the nucleus of the diagonal band of Broca and of the substantia innominata in the rat: an anatomical study using the anterograde transport of a conjugate of wheat germ agglutinin and horseradish peroxidase. Neuroscience 12, 395-408.
Lehmann, O., Grottick, A.J., Cassel, J.C., Higgins, G.A., 2003. A double dissociation between serial reaction time and radial maze performance in rats subjected to 192 IgG-saporin lesions of the nucleus basalis and/or the septal region. The European Journal of Neuroscience 18, 651-666.
Lewellen, T.K., 2008. Recent developments in PET detector technology. Physics in Medicine and Biology 53, R287-317.
Longo, F.M., Massa, S.M., 2013. Small-molecule modulation of neurotrophin receptors: a strategy for the treatment of neurological disease. Nature Reviews Drug Discovery 12, 507-525.
Lowes-Hummel, P., Gertz, H.J., Ferszt, R., Cervos-Navarro, J., 1989. The basal nucleus of Meynert revised: the nerve cell number decreases with age. Archives of Gerontology and Geriatrics 8, 21-27.
Luiten, P.G., Gaykema, R.P., Traber, J., Spencer, D.G., Jr., 1987. Cortical projection patterns of magnocellular basal nucleus subdivisions as revealed by anterogradely transported Phaseolus vulgaris leucoagglutinin. Brain Research 413, 229-250.
Mancuso, C., Siciliano, R., Barone, E., Butterfield, D.A., Preziosi, P., 2011. Pharmacologists and Alzheimer disease therapy: to boldly go where no scientist has gone before. Expert Opinion on Investigational Drugs 20, 1243-1261.
Mann, D.M., Yates, P.O., Marcyniuk, B., 1984. Changes in nerve cells of the nucleus basalis of Meynert in Alzheimer's disease and their relationship to ageing and to the accumulation of lipofuscin pigment. Mechanisms of Ageing and Development 25, 189-204.
Markowska, A.L., Wenk, G.L., Olton, D.S., 1990. Nucleus basalis magnocellularis and memory: differential effects of two neurotoxins. Behavioral and Neural Biology 54, 13-26.
Marrosu, F., Portas, C., Mascia, M.S., Casu, M.A., Fa, M., Giagheddu, M., Imperato, A., Gessa, G.L., 1995. Microdialysis measurement of cortical and hippocampal acetylcholine release during sleep-wake cycle in freely moving cats. Brain Research 671, 329-332.

Martinez, A., Lahiri, D.K., Giacobini, E., Greig, N.H., 2009. Advances in Alzheimer therapy: understanding pharmacological approaches to the disease. Current Alzheimer Research 6, 83-85.
Martinez-Murillo, R., Villalba, R., Montero-Caballero, M.I., Rodrigo, J., 1989. Cholinergic somata and terminals in the rat substantia nigra: an immunocytochemical study with optical and electron microscopic techniques. The Journal of Comparative Neurology 281, 397-415.
Masters, C.L., Beyreuther, K., 1991. Alzheimer's disease: molecular basis of structural lesions. Brain Pathology 1, 226-227.
McGeer, P.L., McGeer, E.G., Suzuki, J., Dolman, C.E., Nagai, T., 1984. Aging, Alzheimer's disease, and the cholinergic system of the basal forebrain. Neurology 34, 741-745.
McKinney, M., Jacksonville, M.C., 2005. Brain cholinergic vulnerability: relevance to behavior and disease. Biochemical Pharmacology 70, 1115-1124.
Mesulam, M.M., Hersh, L.B., Mash, D.C., Geula, C., 1992. Differential cholinergic innervation within functional subdivisions of the human cerebral cortex: a choline acetyltransferase study. Journal of Comparative Neurology 318, 316-328.
Mesulam, M.M., Mufson, E., Levey, A.I., Wainer, B.H., 1983a. Cholinergic innervation of cortex by the basal forebrain: cytochemistry and cortical connectinos of the septal area, diagonal band nuclei, nucleus basalis (substantia innominata), and hypothalamus in the rhesus monkey. Journal of Comparative Neurology 214, 170-197.
Mesulam, M.M., Mufson, E., Wainer, B.H., Levey, A.I., 1983b. Central cholinergic pathways in the rat: an overview based on an alternative nomenclature. Neuroscience 10, 16.
Moceri, V.M., Kukull, W.A., Emanuel, I., van Belle, G., Larson, E.B., 2000. Early-life risk factors and the development of Alzheimer's disease. Neurology 54, 415-420.
Moreau, P.H., Cosquer, B., Jeltsch, H., Cassel, J.C., Mathis, C., 2008. Neuroanatomical and behavioral effects of a novel version of the cholinergic immunotoxin mu p75-saporin in mice. Hippocampus 18, 610-622.
Mori, S., Zhang, J., 2006. Principles of diffusion tensor imaging and its applications to basic neuroscience research. Neuron 51, 527-539.
Morrison, J.H., Hof, P.R., 1997. Life and death of neurons in the aging brain. Science 278, 412-419.

Mrzljak, L., Pappy, M., Leranth, C., Goldman-Rakic, P.S., 1995. Cholinergic synaptic circuitry in the macaque prefrontal cortex. The Journal of Comparative Neurology 357, 603-617.
Mufson, E., 2003. Human cholinergic basal forebrain: chemoanatomy and neurologic dysfunction. Journal of Chemical Neuroanatomy 26, 233-242.
Mufson, E., Ma, S.Y., Cochran, E.J., Bennett, D.A., Beckett, L.A., Jaffar, S., Saragovi, H.U., Kordower, J.H., 2000. Loss of nucleus basalis neurons containing TrkA immunoreactivity in individuals with mild cognitive impairment and early Alzheimer's disease. The Journal of Comparative Neurology 427, 12-19.
Mufson, E.J., Counts, S.E., Perez, S.E., Ginsberg, S.D., 2008. Cholinergic system during the progression of Alzheimer's disease: therapeutic implications. Expert Review of Neurotherapeutics 8, 1703-1718.
Mufson, E.J., Ma, S.Y., Dills, J., Cochran, E.J., Leurgans, S., Wuu, J., Bennett, D.A., Jaffar, S., Gilmor, M.L., Levey, A.I., Kordower, J.H., 2002. Loss of basal forebrain $P75^{NTR}$ immunoreactivity in subjects with mild cognitive impairment and Alzheimer's disease. Journal of Comparative Neurology 443, 136-153.
Mufson, E.J., Ward, S., Binder, L., 2014. Prefibrillar tau oligomers in mild cognitive impairment and Alzheimer's disease. Neuro-degenerative diseases 13, 151-153.
Nadasdy, Z., Varsanyi, P., Zaborszky, L., 2010. Clustering of large cell populations: method and application to the basal forebrain cholinergic system. Journal of Neuroscience Methods 194, 46-55.
Nardone, R., Bergmann, J., Tezzon, F., Ladurner, G., Golaszewski, S., 2008. Cholinergic dysfunction in subcortical ischaemic vascular dementia: a transcranial magnetic stimulation study. Journal of Neural Transmission 115, 737-743.
Nguyen, T.V., Shen, L., Vander Griend, L., Quach, L.N., Belichenko, N.P., Saw, N., Yang, T., Shamloo, M., Wyss-Coray, T., Massa, S.M., Longo, F.M., 2014. Small Molecule p75NTR Ligands Reduce Pathological Phosphorylation and Misfolding of Tau, Inflammatory Changes, Cholinergic Degeneration, and Cognitive Deficits in AbetaPPL/S Transgenic Mice. Journal of Alzheimer's disease, doi: 10.3233/JAD-140036.
Nyakas, C., Luiten, P.G., Spencer, D.G., Traber, J., 1987. Detailed projection patterns of septal and diagonal band efferents to the hippocampus in the rat with emphasis on innervation of CA1 and dentate gyrus. Brain Research Bulletin 18, 533-545.
Okamura, N., Furumoto, S., Fodero-Tavoletti, M.T., Mulligan, R.S., Harada, R., Yates, P., Pejoska, S., Kudo, Y., Masters, C.L., Yanai, K., Rowe, C.C., Villemagne, V.L., 2014. Non-

invasive assessment of Alzheimer's disease neurofibrillary pathology using 18F-THK5105 PET. Brain 137, 1762-1771.
Okamura, N., Furumoto, S., Harada, R., Tago, T., Yoshikawa, T., Fodero-Tavoletti, M., Mulligan, R.S., Villemagne, V.L., Akatsu, H., Yamamoto, T., Arai, H., Iwata, R., Yanai, K., Kudo, Y., 2013. Novel 18F-labeled arylquinoline derivatives for noninvasive imaging of tau pathology in Alzheimer's disease. Journal of Nuclear Medicine 54, 1420-1427.
Page, K.J., Everitt, B.J., Robbins, T.W., Marston, H.M., Wilkinson, L.S., 1991. Dissociable effects on spatial maze and passive avoidance acquisition and retention following AMPA- and ibotenic acid-induced excitotoxic lesions of the basal forebrain in rats: differential dependence on cholinergic neuronal loss. Neuroscience 43, 457-472.
Pang, K.C., Jiao, X., Sinha, S., Beck, K.D., Servatius, R.J., 2011. Damage of GABAergic neurons in the medial septum impairs spatial working memory and extinction of active avoidance: effects on proactive interference. Hippocampus 21, 835-846.
Pang, K.C., Nocera, R., 1999. Interactions between 192-IgG saporin and intraseptal cholinergic and GABAergic drugs: role of cholinergic medial septal neurons in spatial working memory. Behavioral Neuroscience 113, 265-275.
Parikh, V., Kozak, R., Martinez, V., Sarter, M., 2007. Prefrontal acetylcholine release controls cue detection on multiple timescales. Neuron 56, 141-154.
Peng, B.H., Levin, C.S., 2010. Recent development in PET instrumentation. Current Pharmaceutical Biotechnology 11, 555-571.
Pepeu, G., Giovannini, M.G., 2009. Cholinesterase inhibitors and beyond. Current Alzheimer Research 6, 86-96.
Perry, E.K., Tomlinson, B.E., Blessed, G., Bergmann, K., Gibson, P.H., Perry, R.H., 1978. Correlation of cholinergic abnormalities with senile plaques and mental test scores in senile dementia. British Medical Journal 2, 1457-1459.
Pievani, M., Agosta, F., Pagani, E., Canu, E., Sala, S., Absinta, M., Geroldi, C., Ganzola, R., Frisoni, G.B., Filippi, M., 2010. Assessment of white matter tract damage in mild cognitive impairment and Alzheimer's disease. Human Brain Mapping 31, 1862-1875.
Radley, J.J., Gosselink, K.L., Sawchenko, P.E., 2009. A discrete GABAergic relay mediates medial prefrontal cortical inhibition of the neuroendocrine stress response. Journal of Neuroscience 29, 7330-7340.
Raschetti, R., Albanese, E., Vanacore, N., Maggini, M., 2007. Cholinesterase inhibitors in mild cognitive impairment: a systematic review of randomised trials. PLoS Medicine 4, e338.

Riedel, A., Hartig, W., Seeger, G., Gartner, U., Brauer, K., Arendt, T., 2002. Principles of rat subcortical forebrain organization: a study using histological techniques and multiple fluorescence labeling. Journal of Chemical Neuroanatomy 23, 75-104.
Robbins, T.W., Everitt, B.J., Ryan, C.N., Marston, H.M., Jones, G.H., Page, K.J., 1989. Comparative effects of quisqualic and ibotenic acid-induced lesions of the substantia innominata and globus pallidus on the acquisition of a conditional visual discrimination: differential effects on cholinergic mechanisms. Neuroscience 28, 337-352.
Roman, G.C., 2005. Cholinergic dysfunction in vascular dementia. Current Psychiatry Reports 7, 18-26.
Roman, G.C., Kalaria, R.N., 2006. Vascular determinants of cholinergic deficits in Alzheimer disease and vascular dementia. Neurobiology of Aging 27, 1769-1785.
Rye, D.B., Wainer, B.H., Mesulam, M.M., Mufson, E.J., Saper, C.B., 1984. Cortical projections arising from the basal forebrain: a study of cholinergic and noncholinergic components employing combined retrograde tracing and immunohistochemical localization of choline acetyltransferase. Neuroscience 13, 627-643.
Sakurai, T., Nagata, R., Yamanaka, A., Kawamura, H., Tsujino, N., Muraki, Y., Kageyama, H., Kunita, S., Takahashi, S., Goto, K., Koyama, Y., Shioda, S., Yanagisawa, M., 2005. Input of orexin/hypocretin neurons revealed by a genetically encoded tracer in mice. Neuron 46, 297-308.
Salmond, C.H., Chatfield, D.A., Menon, D.K., Pickard, J.D., Sahakian, B.J., 2005. Cognitive sequelae of head injury: involvement of basal forebrain and associated structures. Brain 128, 189-200.
Sato, A., Sato, Y., Uchida, S., 2004. Activation of the intracerebral cholinergic nerve fibers originating in the basal forebrain increases regional cerebral blood flow in the rat's cortex and hippocampus. Neuroscience Letters 361, 90-93.
Schliebs, R., Arendt, T., 2006. The significance of the cholinergic system in the brain during aging and in Alzheimer's disease. Journal of neural transmission 113, 1625-1644.
Schliebs, R., Arendt, T., 2011. The cholinergic system in aging and neuronal degeneration. Behavioural Brain Research 221, 555-563.
Schwab, C., Yu, S., Wong, W., McGeer, E.G., McGeer, P.L., 2013. GAD65, GAD67, and GABAT immunostaining in human brain and apparent GAD65 loss in Alzheimer's disease. Journal of Alzheimer's Disease 33, 1073-1088.
Schwaber, J.S., Rogers, W.T., Satoh, K., Fibiger, H.C., 1987. Distribution and organization of cholinergic neurons in the rat forebrain demonstrated by computer-aided data

acquisition and three-dimensional reconstruction. The Journal of Comparative Neurology 263, 309-325.
Semba, K., 2000. Multiple output pathways of the basal forebrain: organization, chemical heterogeneity, and roles in vigilance. Behavioural Brain Research 115, 117-141.
Semba, K., Reiner, P.B., McGeer, E.G., Fibiger, H.C., 1988. Brainstem afferents to the magnocellular basal forebrain studied by axonal transport, immunohistochemistry, and electrophysiology in the rat. The Journal of Comparative Neurology 267, 433-453.
Snyder, H.M., Carrillo, M.C., Grodstein, F., Henriksen, K., Jeromin, A., Lovestone, S., Mielke, M.M., O'Bryant, S., Sarasa, M., Sjogren, M., Soares, H., Teeling, J., Trushina, E., Ward, M., West, T., Bain, L.J., Shineman, D.W., Weiner, M., Fillit, H.M., 2014. Developing novel blood-based biomarkers for Alzheimer's disease. Alzheimer's & dementia 10, 109-114.
Sofroniew, M.V., Eckenstein, F., Thoenen, H., Cuello, A.C., 1982. Topography of choline acetyltransferase-containing neurons in the forebrain of the rat. Neuroscience Letters 33, 7-12.
Sofroniew, M.V., Pearson, R.C., Powell, T.P., 1987. The cholinergic nuclei of the basal forebrain of the rat: normal structure, development and experimentally induced degeneration. Brain Research 411, 310-331.
Sotthibundhu, A., Sykes, A.M., Fox, B., Underwood, C.K., Thangnipon, W., Coulson, E.J., 2008. Beta-amyloid(1-42) induces neuronal death through the p75 neurotrophin receptor. Journal of neuroscience 28, 3941-3946.
Stanfield, B.B., Cowan, W.M., 1982. The sprouting of septal afferents to the dentate gyrus after lesions of the entorhinal cortex in adult rats. Brain research 232, 162-170.
Sui, X., Liu, J., Yang, X., 2014. Cerebrospinal fluid biomarkers of Alzheimer's disease. Neuroscience Bulletin 30, 233-242.
Szutowicz, A., Bielarczyk, H., Gul, S., Ronowska, A., Pawelczyk, T., Jankowska-Kulawy, A., 2006. Phenotype-dependent susceptibility of cholinergic neuroblastoma cells to neurotoxic inputs. Metabolic brain disease 21, 149-161.
Teipel, S., Heinsen, H., Amaro, E., Jr., Grinberg, L.T., Krause, B., Grothe, M., 2013. Cholinergic basal forebrain atrophy predicts amyloid burden in Alzheimer's disease. Neurobiology of Aging, doi: 10.1016/j.neurobiolaging.2013.09.029.
Teipel, S.J., Flatz, W.H., Heinsen, H., Bokde, A.L., Schoenberg, S.O., Stockel, S., Dietrich, O., Reiser, M.F., Moller, H.J., Hampel, H., 2005. Measurement of basal forebrain atrophy in Alzheimer's disease using MRI. Brain 128, 2626-2644.

Teipel, S.J., Meindl, T., Grinberg, L., Grothe, M., Cantero, J.L., Reiser, M.F., Moller, H.J., Heinsen, H., Hampel, H., 2010. The cholinergic system in mild cognitive impairment and Alzheimer's disease: An in vivo MRI and DTI study. Human Brain Mapping 32, 1349-1362.
Terry, A.V., Jr., Buccafusco, J.J., 2003. The cholinergic hypothesis of age and Alzheimer's disease-related cognitive deficits: recent challenges and their implications for novel drug development. The Journal of Pharmacology and Experimental Therapeutics 306, 821-827.
Tiraboschi, P., Hansen, L.A., Alford, M., Masliah, E., Thal, L.J., Corey-Bloom, J., 2000. The decline in synapses and cholinergic activity is asynchronous in Alzheimer's disease. Neurology 55, 1278-1283.
Torres, E.M., Perry, T.A., Blockland, A., Wilkinson, L.S., Wiley, R.G., Lappi, D.A., Dunnet, S.B., 1994. Behavioural, histochemical and biochemical consequences of selective immunolesions in discrete regions of the basal forebrain cholinergic system. Neuroscience 63, 95-122.
Ullmann, J.F., Keller, M.D., Watson, C., Janke, A.L., Kurniawan, N.D., Yang, Z., Richards, K., Paxinos, G., Egan, G.F., Petrou, S., Bartlett, P., Galloway, G.J., Reutens, D.C., 2012. Segmentation of the C57BL/6J mouse cerebellum in magnetic resonance images. NeuroImage 62, 1408-1414.
Unal, C.T., Golowasch, J.P., Zaborszky, L., 2012. Adult mouse basal forebrain harbors two distinct cholinergic populations defined by their electrophysiology. Frontiers in Behavioral Neuroscience 6, 21.
Vana, L., Kanaan, N.M., Ugwu, I.C., Wuu, J., Mufson, E.J., Binder, L.I., 2011. Progression of tau pathology in cholinergic Basal forebrain neurons in mild cognitive impairment and Alzheimer's disease. The American Journal of Pathology 179, 2533-2550.
Vertes, R.P., 1988. Brainstem afferents to the basal forebrain in the rat. Neuroscience 24, 907-935.
Villain, N., Chetelat, G., Grassiot, B., Bourgeat, P., Jones, G., Ellis, K.A., Ames, D., Martins, R.N., Eustache, F., Salvado, O., Masters, C.L., Rowe, C.C., Villemagne, V.L., 2012. Regional dynamics of amyloid-beta deposition in healthy elderly, mild cognitive impairment and Alzheimer's disease: a voxelwise PiB-PET longitudinal study. Brain 135, 2126-2139.
Villemagne, V.L., Furumoto, S., Fodero-Tavoletti, M.T., Mulligan, R.S., Hodges, J., Harada, R., Yates, P., Piguet, O., Pejoska, S., Dore, V., Yanai, K., Masters, C.L., Kudo, Y., Rowe, C.C., Okamura, N., 2014. In vivo evaluation of a novel tau imaging tracer for Alzheimer's disease. European Journal of Nuclear Medicine and Molecular Imaging, doi: 10.1007/s00259-013-2681-7.

Villemagne, V.L., Pike, K.E., Chetelat, G., Ellis, K.A., Mulligan, R.S., Bourgeat, P., Ackermann, U., Jones, G., Szoeke, C., Salvado, O., Martins, R., O'Keefe, G., Mathis, C.A., Klunk, W.E., Ames, D., Masters, C.L., Rowe, C.C., 2011. Longitudinal assessment of Abeta and cognition in aging and Alzheimer disease. Annals of Neurology 69, 181-192.
Wainer, B.H., Levey, A.I., Rye, D.B., Mesulam, M.M., Mufson, E.J., 1985. Cholinergic and non-cholinergic septohippocampal pathways. Neuroscience Letters 54, 45-52.
Wenk, G.L., Stoehr, J.D., Quintana, G., Mobley, S., Wiley, R.G., 1994. Behavioral, biochemical, histological, and electrophysiological effects of 192 IgG-saporin injections into the basal forebrain of rats. Journal of Neuroscience 14, 5986-5995.
Whitehouse, P.J., Hedreen, J.C., White, C.L., 3rd, Price, D.L., 1983. Basal forebrain neurons in the dementia of Parkinson disease. Annals of Neurology 13, 243-248.
Whitehouse, P.J., Price, D.L., Clark, A.W., Coyle, J.T., DeLong, M.R., 1981. Alzheimer disease: evidence for selective loss of cholinergic neurons in the nucleus basalis. Annals of Neurology 10, 122-126.
Wolf, D., Grothe, M., Fischer, F.U., Heinsen, H., Kilimann, I., Teipel, S., Fellgiebel, A., 2014. Association of basal forebrain volumes and cognition in normal aging. Neuropsychologia 53, 54-63.
Woolf, N.J., Eckenstein, F., Butcher, L.L., 1984. Cholinergic systems in the rat brain: I. projections to the limbic telencephalon. Brain Research Bulletin 13, 751-784.
Woolf, N.J., Hernit, M.C., Butcher, L.L., 1986. Cholinergic and non-cholinergic projections from the rat basal forebrain revealed by combined choline acetyltransferase and Phaseolus vulgaris leucoagglutinin immunohistochemistry. Neuroscience Letters 66, 281-286.
Yan, Z., Feng, J., 2004. Alzheimer's disease: interactions between cholinergic functions and beta-amyloid. Current Alzheimer Research 1, 241-248.
Yang, Z., Richards, K., Kurniawan, N.D., Petrou, S., Reutens, D.C., 2012. MRI-guided volume reconstruction of mouse brain from histological sections. Journal of Neuroscience Methods 211, 210-217.
Yoder, R.M., Pang, K.C., 2005. Involvement of GABAergic and cholinergic medial septal neurons in hippocampal theta rhythm. Hippocampus 15, 381-392.
Zaborszky, L., Buhl, D.L., Pobalashingham, S., Bjaalie, J.G., Nadasdy, Z., 2005. Three-dimensional chemoarchitecture of the basal forebrain: spatially specific association of cholinergic and calcium binding protein-containing neurons. Neuroscience 136, 697-713.
Zaborszky, L., Carlsen, J., Brashear, H.R., Heimer, L., 1986. Cholinergic and GABAergic afferents to the olfactory bulb in the rat with special emphasis on the projection neurons in

the nucleus of the horizontal limb of the diagonal band. The Journal of Comparative Neurology 243, 488-509.
Zaborszky, L., Csordas, A., Mosca, K., Kim, J., Gielow, M.R., Vadasz, C., Nadasdy, Z., 2013. Neurons in the Basal Forebrain Project to the Cortex in a Complex Topographic Organization that Reflects Corticocortical Connectivity Patterns: An Experimental Study Based on Retrograde Tracing and 3D Reconstruction. Cerebral Cortex.
Zaborszky, L., Cullinan, W.E., Luine, V.N., 1993. Catecholaminergic-cholinergic interaction in the basal forebrain. Progress in Brain Research 98, 31-49.
Zaborszky, L., Duque, A., 2003. Sleep-wake mechanisms and basal forebrain circuitry. Frontiers in Bioscience 8, d1146-1169.
Zaborszky, L., Gaykema, R.P., Swanson, D.J., Cullinan, W.E., 1997. Cortical input to the basal forebrain. Neuroscience 79, 1051-1078.
Zaborszky, L., Hoemke, L., Mohlberg, H., Schleicher, A., Amunts, K., Zilles, K., 2008. Stereotaxic probabilistic maps of the magnocellular cell groups in human basal forebrain. NeuroImage 42, 1127-1141.
Zaborszky, L., Leranth, C., Heimer, L., 1984. Ultrastructural evidence of amygdalofugal axons terminating on cholinergic cells of the rostral forebrain. Neuroscience Letters 52, 219-225.
Zaborszky, L., Pang, K., Somogyi, J., Nadasdy, Z., Kallo, I., 1999. The basal forebrain corticopetal system revisited. Annals of the New York Academy of Sciences 877, 339-367.
Zhang, H., Trollor, J.N., Wen, W., Zhu, W., Crawford, J.D., Kochan, N.A., Slavin, M.J., Brodaty, H., Reppermund, S., Kang, K., Mather, K.A., Sachdev, P.S., 2011. Grey matter atrophy of basal forebrain and hippocampus in mild cognitive impairment. Journal of Neurology, Neurosurgery, and Psychiatry 82, 487-493.